DOCTOR OF PHILOSOPHY

An investigation of microstrip antennas and their feeder structures.

Richards, Owen

Award date:
1988

Awarding institution:
Bangor University

AN INVESTIGATION OF MICROSTRIP ANTENNAS AND THEIR FEEDER STRUCTURES.

by

Owen Richards

A thesis submitted to the University of Wales

in candidature for the degree of

Doctor of Philosophy.

School of Electronic Engineering Science,

University College of North Wales,

Bangor.

June 1988

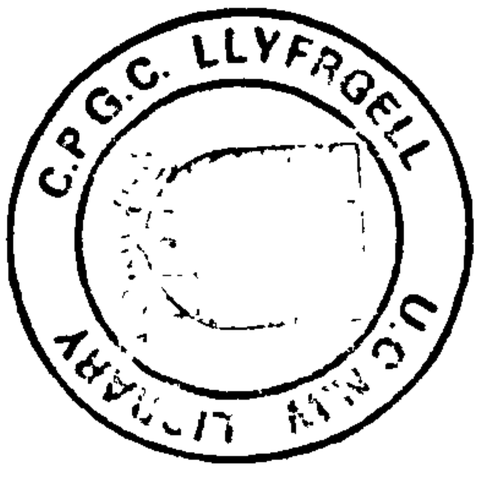

ACKNOWLEDGEMENTS

I would like to thank my supervisor, Mr. B. Easter, for his invaluable advice and encouragement. I would also like to express my sincere gratitude to Professor I.M. Stephenson for his guidance and support.

I wish to thank Professor J.J. O' Reilly, for the opportunity of carrying out this work in the School of Electronic Engineering Science.

The financial support of the Science and Engineering Research Council in this work, is also gratefully acknowledged. I would also like to thank the various members of the academic, technical and administrative staff of the School for their assistance during the course of this work.

ABSTRACT

For a typical microstrip antenna placing the radiating elements and feed lines on one side of the substrate realises the advantages of planar fabrication. It can be shown that the currents in many parts of the feeder circuit have magnitudes comparable with those in the radiators and make a significant contribution to the total radiation.

In this thesis the radiation from both the radiators and the feed lines will be examined. The radiation from microstrip was calculated from the current distribution. This method allows the calculation of the radiation from the nominal radiators and the feed circuits. Theoretical and experimental results verifying this approach will be given for examples of relatively low Q resonators on thick, low permittivity substrates required for efficient antennas.

Unwanted radiation from the feed circuit could be reduced by the use of coaxial lines below ground or a multiple-layer strip line assembly, but such complications are unattractive. Reduction in unwanted feed line radiation has been investigated by the use of a balanced line feeder, combined with a suitable balun.

INDEX

			Page
ACKNOWLEDGEMENTS.			(iv)
ABSTRACT.			(v)
CHAPTER 1.		**MICROSTRIP ANTENNAS.**	1
	1.1	Radiating Elements.	3
	1.2	Patch Antennas.	3
	1.3	Array Configuration.	4
	1.3.1	Linear Arrays.	6
	1.3.2	Travelling wave antennas.	6
	1.4	The series feed.	6
	1.5	The corporate feed.	11
	1.6	General features of planar antennas.	11
REFERENCES FOR CHAPTER 1.			14
CHAPTER 2.		**CALCULATION OF RESONATOR RADIATION**	16
	2.1	Radiation from Microstrip Structures.	17
	2.2	Narrow Microstrip Lines.	19
	2.3	Radiation from a Medium Width Microstrip Resonator.	27
	2.4	Radiation from aperture fields.	30
	2.5	Conclusions.	34
REFERENCES FOR CHAPTER 2.			36

			Page
CHAPTER	**3.**	**FEED LINES FOR MICROSTRIP ANTENNAS.**	37
	3.1	Theoretical evaluation of feed line radiation.	37
	3.2	Radiation from a linear feed.	42
	3.3	Feed line radiation from corporate feed antennas.	43
	3.4	Methods of reducing feeder radiation.	45
	3.5	Balanced line feeders.	46
	3.5.1	Dipole radiating elements.	49
	3.6	Evaluation of balanced line radiation.	51
	3.7	Estimation of feeder loss.	58
	3.8	Losses in coupled lines.	60
	3.9	Conclusions.	60
REFERENCES FOR CHAPTER 3.			61
CHAPTER	**4.**	**MEASUREMENT OF RESONATOR LOSS**	63
	4.1	Q factor.	64
	4.2	Q Factor Measurements.	65
	4.2.1	Resonator Radiation Measurements.	69
	4.2.2	Radiation Measurements on a single dipole.	73
	4.3	Stripline Discontinuities.	73
	4.3.1	Coupled line discontinuities.	75
	4.4	Antenna Substrates.	75
	4.4.1	Measurement of Conductivity.	76
	4.4.2	Measurement of dielectric loss.	76
	4.5	Conclusions.	77
REFERENCES FOR CHAPTER 4.			78

			Page
CHAPTER	**5.**	**ANTENNA DESIGN AND TESTING.**	79
	5.1	Antenna Arrays.	79
	5.2	Antenna Measurements.	82
	5.3	Microstrip fed linear arrays	85
	5.3.1	10 element microstrip fed array	90
	5.3.2	Cross Polar Radiation.	94
	5.4	Corporate fed Microstrip Antennas.	94
	5.5	Balanced line fed Antennas.	98
	5.5.1	12 element antenna array.	107
	5.5.2	24 element antenna array.	112
	5.6	Centre Fed Balanced line Antennas.	112
	5.7	Conclusions.	119
REFERENCES FOR CHAPTER 5.			120
CHAPTER	**6.**	**BALUN DESIGN AND TESTING.**	121
	6.1	Hybrid ring baluns.	121
	6.2	Microstrip to Slotline Balun.	123
	6.2.1	Marchand Balun.	126
	6.3	The Slot line to Balanced line transition	130
	6.4	Improvements in Balun Design.	130
	6.5	Conclusions.	134
REFERENCES FOR CHAPTER 6.			137
CHAPTER	**7.**	**CONCLUSIONS**	138
APPENDIX 1.			140
APPENDIX 2.			153
APPENDIX 3.			156

CHAPTER 1.

1. Microstrip Antennas.

Conventional wire antennas consist of suitably disposed conductors which radiate electromagnetic energy. When the antenna is excited, a current distribution exists over the conductor surface, dependent on the conductor geometry. If the current distribution is known to a fair approximation, the radiation from the antenna can be determined. A common practical antenna is the centre-fed halfwavelength dipole which has an approximately sinusoidal current distribution, and produces a maximum of radiation in the plane normal to the axis.

Much expertise on conventional wire antenna has been accumulated over the last 100 years, and it is well appreciated that conductors of a variety of cross sections may be employed. It was natural to consider antennas fabricated from planar conductors supported by a dielectric substrate, once the manufacturing process for printed circuit boards had become established. Interest in the fabrication of microwave circuits using planar techniques, arose in the 1950's.

Initially microstrip line-above-ground transmission lines were proposed, but were of limited application because of high attenuation due to dielectric loss and lack of understanding of the propagation characteristics. In order to overcome these problems, the "triplate" transmission line, often referred to as "strip-line" received greater attention, and was widely used in the manufacture of lower frequency microwave circuits. The triplate transmission line consisted of a flat conducting strip located in a symmetrical position between two parallel ground planes. The guided wave is close to the ideal t.e.m form, and is fully enclosed and shielded.

The availability of better materials, improved understanding of the open microstrip propagation characteristics, and the need for a circuit media compatible with evolving solid state devices caused a renewal of interest in microstrip techniques. For circuit applications, unwanted radiation remained a practical limitation, but could be kept within acceptable limits by the use of thin, high permittivity substrates and effective shielding.

Conversely, the use of thicker substrates of lower permittivity enhances the radiation from a given circuit configuration and operating frequency, and the possibility of using the microstrip circuit as the basis of an antenna structure attracted attention. The first practical microstrip antennas were developed in the early 1970's by Howell [1] and Munson [2]. Various types of flat profile printed antenna have been developed such as the microstrip antenna, the triplate slot antenna, the cavity backed printed antenna, and the printed dipole antenna. Compared with waveguide antennas these new types of printed antenna have some advantages in weight, thickness and cost, but still involve complex manufacture.

A continuing attraction of the microstrip circuit and microstrip antennas is that the conducting elements together with the feed lines, can be printed onto one surface of a single substrate directly backed by a ground plane, which can be conformally mounted. The supporting substrate should have as low a value of permittivity as possible, while maintaining good thermal and mechanical properties. For example, foam has a value of permittivity close to that of free space, but does not have the required thermal and mechanical properties.

1.1 Radiating Elements.

The radiation from microstrip line and discontinuities was first calculated by Lewin [3], who showed that this radiation is most apparent in microstrip circuits involving resonant structures. Using this analysis the effect of radiation on the overall Q factor of common microstrip circuit elements such as the open-circuit half-wavelength resonator, can be described as a function of resonator dimensions, operating frequency, relative dielectric constant and thickness of substrate. At microwave frequencies the radiation loss dominated the conductor loss for thick, low permittivity substrates. Thus, the open-circuit half-wavelength microstrip resonator can be used as an efficient microstrip antenna when fabricated on a thick, low permittivity substrate. Since, microstrip circuits and discontinuities radiate, it is obvious that the feeder network to the microstrip antenna elements will also radiate.

In order to increase the radiation efficiency of an open-circuit half-wavelength microstrip resonator, the width of the resonator was increased to form a resonant, rectangular patch.

1.2 Patch Antennas.

The rectangular patch antenna was one of the earliest microstrip antenna to be developed, the structure and operation being related to that of resonators used in circuit design. The antenna consists of an isolated area of rectangular conductor on the upper surface of the microstrip substrate, of arbitrary width, with a length dimension comparable to one half-wavelength in the microstrip, fig 1.1(a). Munson [2] and Howell [1] modelled the patch antenna as a cavity with high impedance walls at the sides, with radiation occurring from the open circuit discontinuity at each end of the resonator.

Further developments by Munson included the idea of wrapping a long rectangular antenna around the body of a vehicle or missile. The open circuit ends of the microstrip are considered to be thin slot radiators, described by Harrington [4], and joined by a low impedance, half-wavelength transmission line. The circular patch antenna fig 1.1(b) requires only a single feed line to achieve circularly polarised radiated fields. Other patch antennas utilising triangular and pentagonal shapes have been fabricated fig 1.1(c). But these patches are difficult to analyse. The fields inside these patches can only be determined by the use of numerical techniques since boundary conditions cannot be imposed in a simple fashion.

All these patch antennas can be designed to operate in a dual-frequency mode by stacking the patches one above the other with a dielectric layer between the two radiators, and a dielectric substrate between the bottom radiator and the ground plane. Caver [5] stacked two resonant patches closely spaced. The larger radiator acts as a partial ground plane for the smaller radiator, which is resonant at a higher frequency.

1.3 Array Configuration.

As with conventional wire antennas, characteristics such has high gain, beam scanning, or steering capability are only possible when discrete radiators are combined to form arrays. Microstrip antennas are ideally suited for conformal array's, since for phased array configurations they have the advantage that all ancillary electronics can be incorporated into one integrated board. During the 1970's series-fed arrays were developed using new low loss substrates for fixed beam communications and radar applications due to their lightweight, flat profile shape and simple construction, which outweighed the reduced performance obtained when compared with conventional antenna. Arrays of resonators with integrated printed phase shifters for beam steering were developed during this period.

(a)

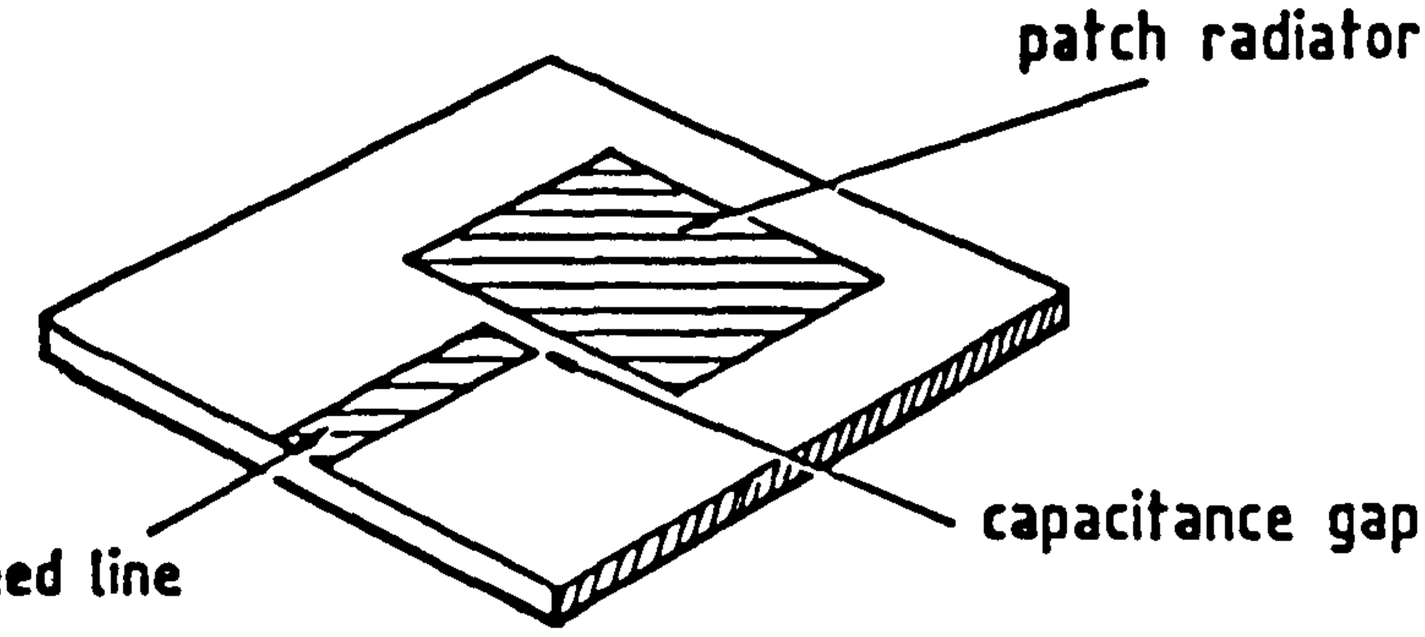

Patch antenna with capacitance feed.

(b)

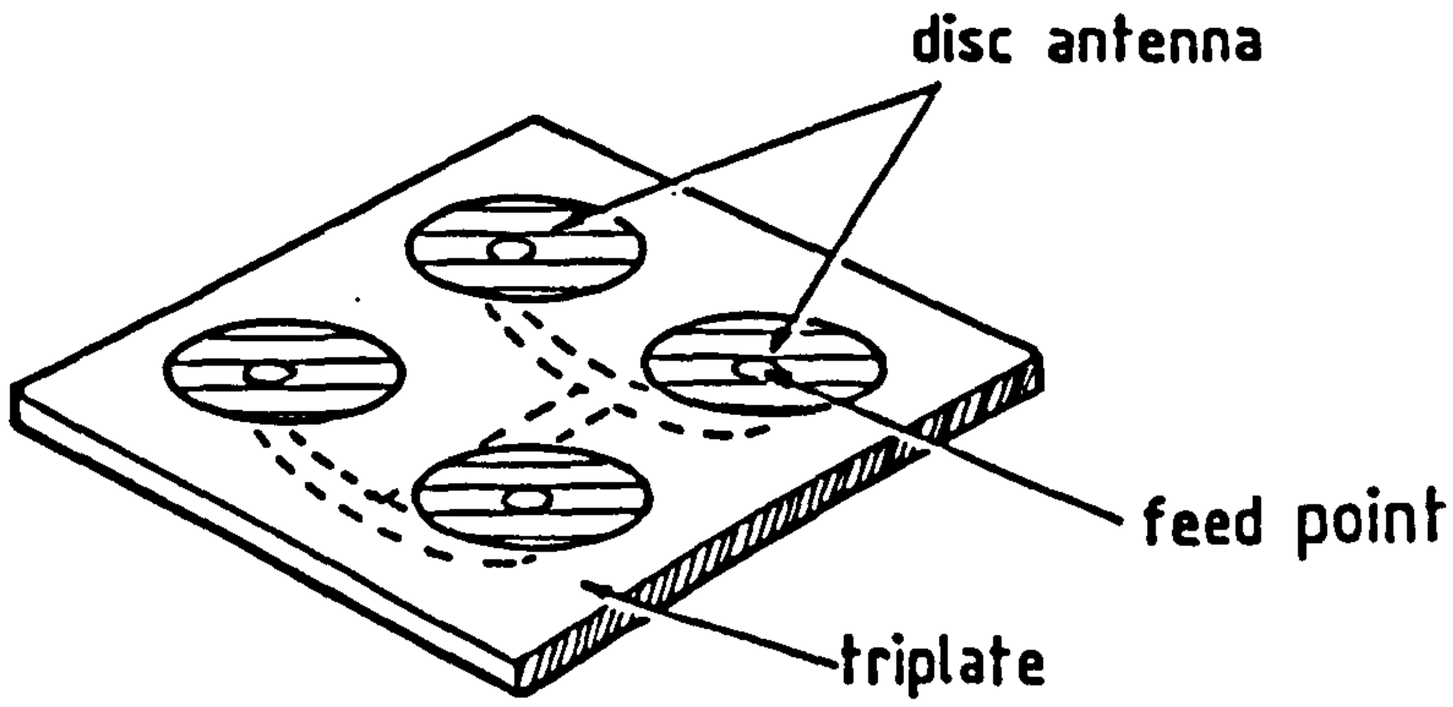

Circular patch antenna.

(c)

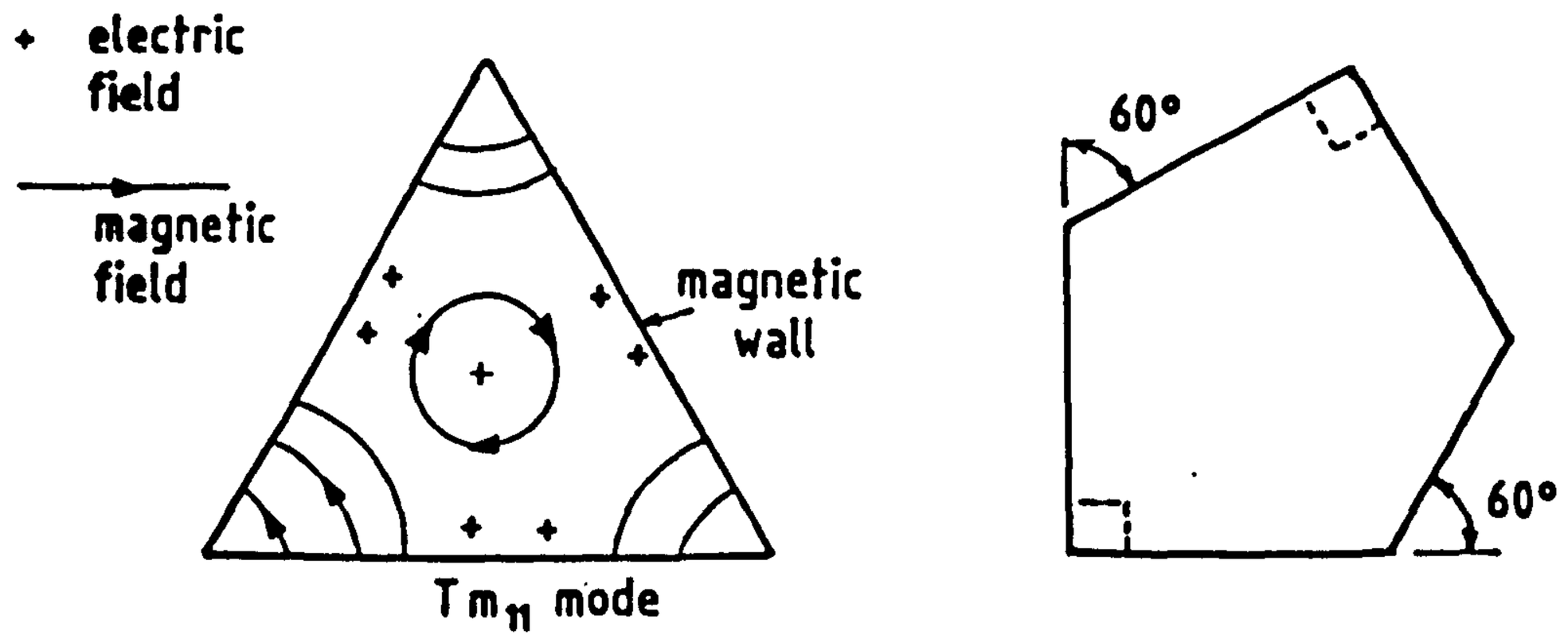

Figure 1.1. Triangular and pentagonal patch antenna.

1.3.1 Linear Arrays

A linear array consists of elements located at finite distances along a straight line. These linear array elements can be distributed over the surface of the substrate to form a linear planar array.

For microstrip, two types of transmission line array are feasible, the travelling wave antenna where the end of the line is terminated in a resistive match, and the standing wave antenna where the microstrip line is terminated in an open or short circuit. A standing wave antenna usually radiates a broadside beam, while travelling wave antennas can be designed to radiate a beam in any direction from backfire to endfire.

1.3.2 Travelling Wave Antennas.

A series fed microstrip patch antenna has been described by Derneryd [6], which consists of an array of cascaded patch elements interconnected by high impedance lines. If widely scanned beams are required then halfwave elements are unsuitable due to the deep null in the radiation pattern near the ground plane.

1.4 The Series Feed

The simplest form of feed system for a linear array is series feeding in which the radiating elements are periodically attached to a transmission line, fig 1.2. The loading of this transmission line is determined by the radiating element used. The spacing between the radiating elements is chosen, so as to produce the required phase distribution across the radiating elements. Thus, as the source frequency changes a progressive phase shift down the array results, which causes the main beam direction to change.

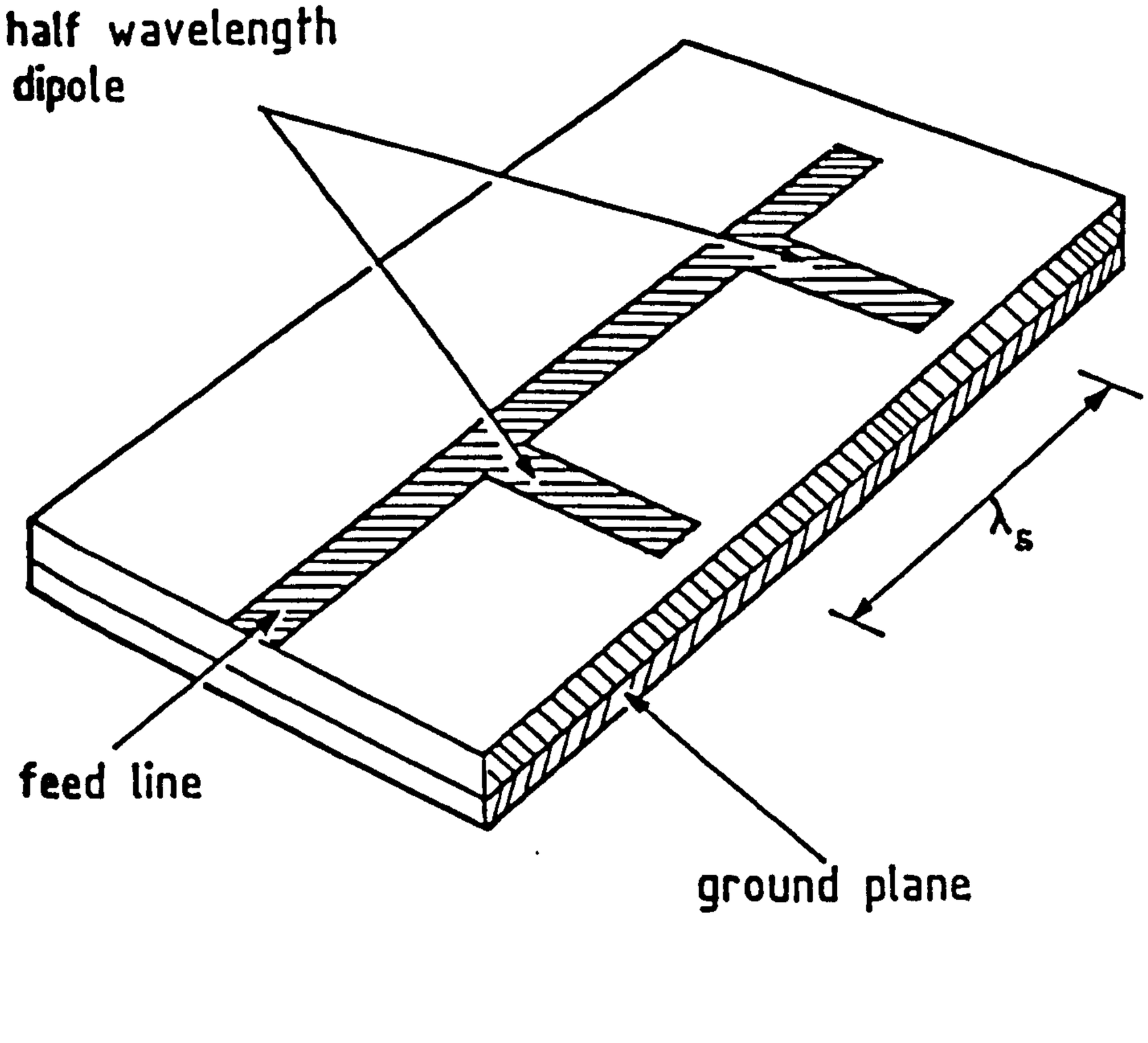

Figure 1.2. Microstrip antenna with coplanar feed.

In order to achieve a broadside directed beam the elements must all be in phase, which implies that the radiating elements are spaced at λ_g intervals. A broadside directed beam can also be obtained by offsetting the antenna elements on either side of the feed line and feeding each alternative element in antiphase, at $\lambda_g/2$ intervals.

For a linear array it can be seen that the mismatch of consecutive radiating elements returns to the input in phase, and for a long array produces a high input V.S.W.R. For this reason most standing wave arrays operate a few degress off broadside. If the radiating elements are spaced at quarterwave length intervals and alternate pairs of elements fed in antiphase, this squint in the broadside pattern can be suppressed. If the losses in the feeder are significant some improvement in the efficiency of the antenna can be obtained by centre feeding the array.

Series feeding of resonator arrays is possible by capacitive coupling of the resonator to the feed line as described by Cashen [7]. The coupling to each resonator is controlled by the distance of the element from the line, fig 1.3(a). In the resonant form the elements are placed at voltage maxima on the line, and the element spacing in either case is one strip-wavelength.

By rotating the resonators by 90^{o} and directly coupling one end to the feed line, a comb array, is formed, fig 1.3(b). The resonators or stubs are spaced at one wavelength intervals along the feed line, so as to radiate in phase. The radiation conductance across the feed line is directly governed by the stub width. The power radiated per unit wavelength can be increased by placing halfwave-length spaced stubs on alternate sides of the feed line, fig 1.3(c).

The resonant array is advantageous in that no matched load is required, but is counter balanced by higher values of stub loss, and the bandwidth of the array decreases steeply as the number of stubs increases. James [8] proposed that the beam scan of the comb array could be increased by placing slits in the resonators, fig 1.3(d). However, the close spacing of the resonant elements suggests that undesirable coupling between resonant elements may be set up within the array.

A particular problem with centre feeding the antenna is that each half-section of the array has a different squint angle which will severely limit the bandwidth obtained for this arrangement. The bandwidth of the end-fed array is limited by the degradation of the sidelobes by the feed system, and the transmitted power falls off as the beam scans away from the desired direction.

Beam squint with frequency is a particular disadvantage of travelling wave arrays. In principle this squint can be eliminated by equalising the path length between the input and each radiating element. Such an arrangement is the series compensated feed system proposed by Rodgers [9]. By ensuring that there is an equal path length to each radiating element and tapering the power distribution down the feeder structure.

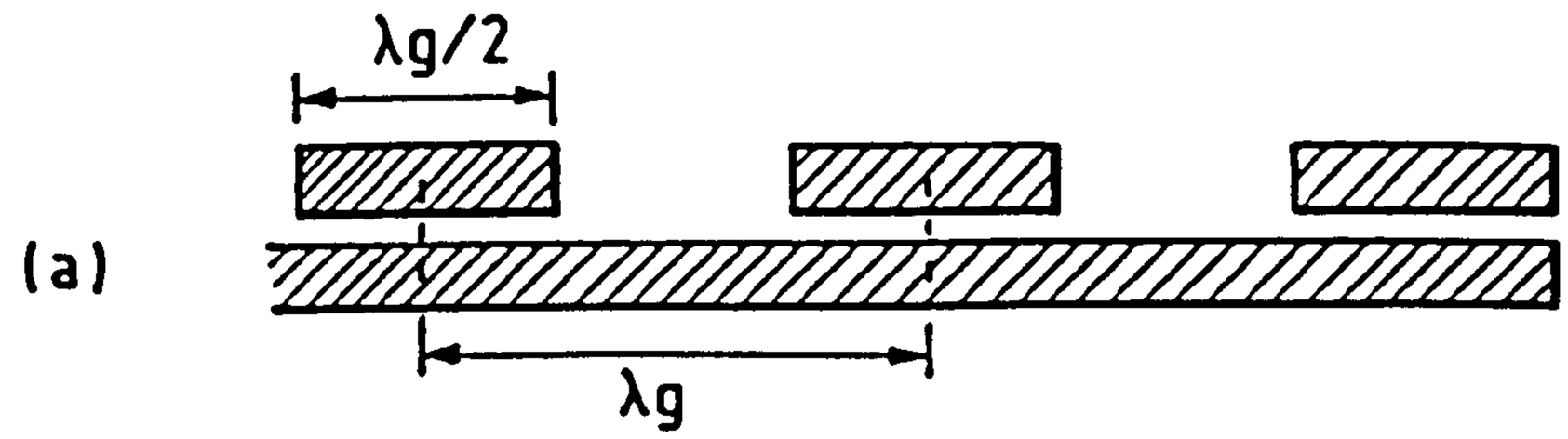

Figure 1.3. Series fed antenna.

1.5 The Corporate feed.

The corporate feed system is a feed arrangement in which the power is split between n output ports with a pre-determined power and phase distribution. This may take the form of a series of multiple power splitters.

By using two-way power splitters combined with broadband impedance transformers etc, this feed is capable of wide band operation, limited mainly by the matching to the radiating elements. The corporate feed array in planar form will occupy a large area and cannot be stacked to form a three dimensional array.

An example of a novel corporate feed system is outlined by Williams [10, 11] using a diagonally connected array of microstrip elements, fig 1.4 . This technique allows for a compact packing density on low permittivity substrates (ε_r=2.55) . This allows the antenna elements to be spaced at $\lambda_o/2$ intervals, while feeding the elements with λ_g feed line sections to produce a co-phase array. Side lobe radiation control is accomplished by centre feeding the array.

1.6 General features of planar antennas.

In many applications the advantages of microstrip antenna far outweigh their disadvantages, so that they could be used to replace conventional antenna. Some of the principle advantages of microstrip antenna compared to conventional antenna are :

a) They are lightweight, low volume, low profile planar configurations which can be made conformal.

b) The fabrication costs are low and the structures produced are amenable to mass production using p.c.b production techniques

c) They may be mounted on missiles, rockets and satellites.

d) Linear polarisation and circular polarisations is possible.

e) Dual frequency antennas may be made and no cavity backing is required.

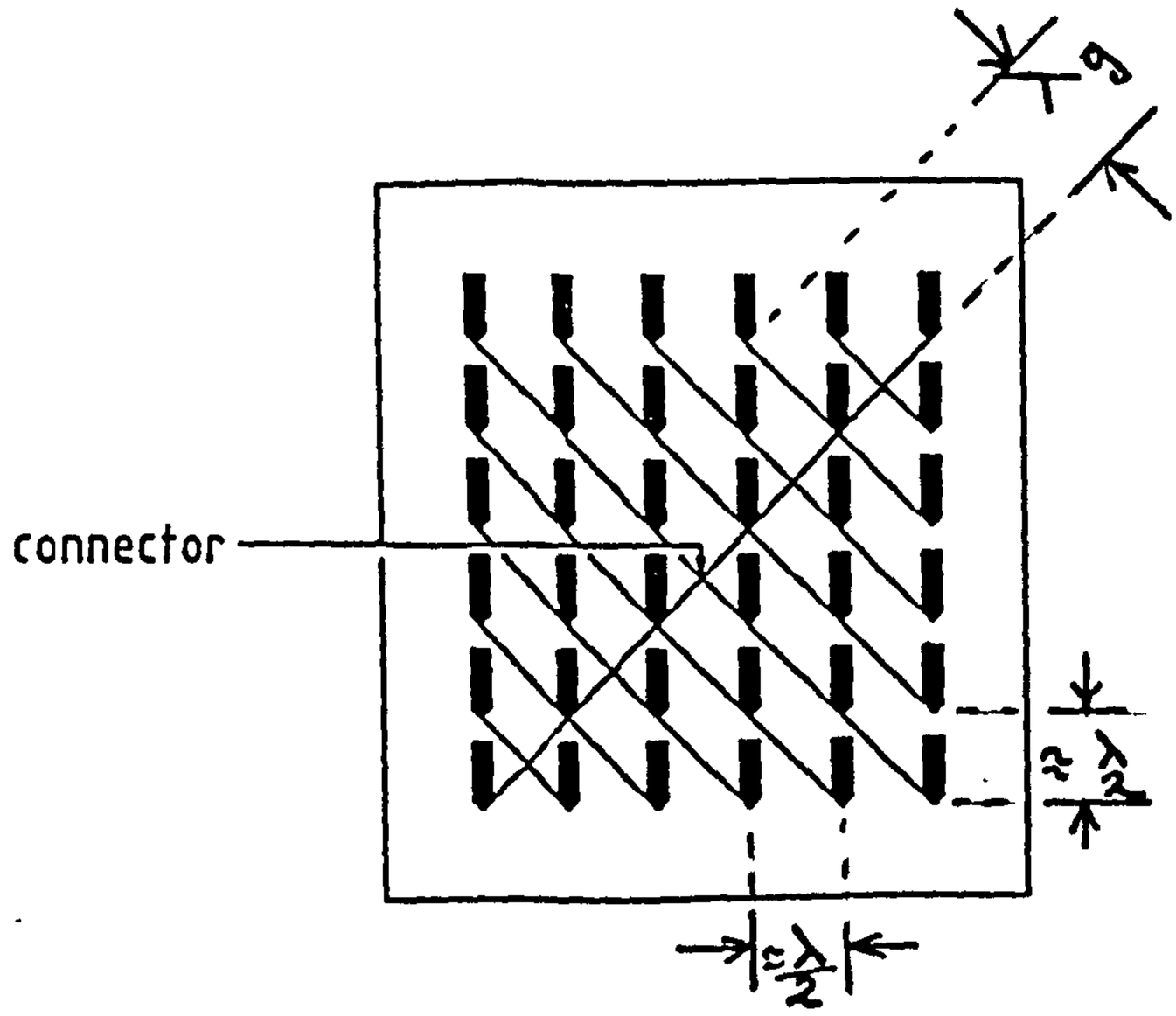

$\lambda_g \approx .7\lambda$

Figure 1.4. Cross-fed antenna by Williams.

f) The microstrip antenna is compatible with modular design and solid state devices can be added directly to the antenna substrate board. The feed lines and matching networks can be fabricated simultaneously with the antenna structure.

However, microstrip antenna also have some disadvantages :

a) There are practical limitations on the maximum gain obtainable by microstrip antenna due to feeder losses.

b) There is poor isolation between the feed and the radiating elements, with the radiation from the feeder affecting the desired radiation pattern.

c) These antenna have a narrow bandwidth.

d) These antenna have poor endfire radiation performance, and there is a possibility that surface waves can be generated.

f) These antennas have low power handling capability.

Some system applications for which microstrip antennas have been developed include :

a) Satellite communication

b) Doppler radars and radio altimeters.

c) Command and control with missile telemetry.

d) Feed elements in complex antennas.

e) Satellite navigation receiver, etc

REFERENCES FOR CHAPTER 1.

[1] Howell,

Microstrip Antenna. IEEE trans.Vol AP-23, page 90 - 93, 1975 .

[2] Munson R.E.,

Conformal Microstrip Antenna, IEEE trans. Vol AP-22, page 74-78, 1974

[3] Lewin L.,

Radiation from discontinuities in strip-line.

IEEE Monograph No 358 E, Feb. 1960

[4] Harrington R.F.,

Time Harmonic Electromagnetic fields, New York,

McGraw Hill, page 276 , 1961 .

[5] Caver K.R. & Mink J.W.,

Microstrip Array Technology, IEEE trans. Vol AP - 29,

page 1-25, 1981.

[6] Derneryd A.G.,

Linearly Polarised Microstrip Antenna's,

IEEE trans AP-24, page 846 - 851, 1976.

[7] Cashen E.R., Frost R., Young D.E,

Improvements relating to aerial arrangements.

British Provisional Patent (E.M.I. ltd).

Specification 1294024 .

[8] James J.R. & Wilson,

Microstrip antennas and arrays, Pt 1 & 2

IEE J. MOA 1, page 165-181, 1977.

[9] Rogers A.,

Wideband squint less linear arrays,

Marconi Rev. 35, page 221 - 243 , 1973 .

[10] Williams J.C.

Cross-fed printed aerials, Proc 7th European Microwave Conf. Copenhagen, page 292 - 296, 1977 .

[11] Williams J.C.

A 36 Ghz printed planar array,
Electronic Lett., 14 page 136 - 137 . 1978 .

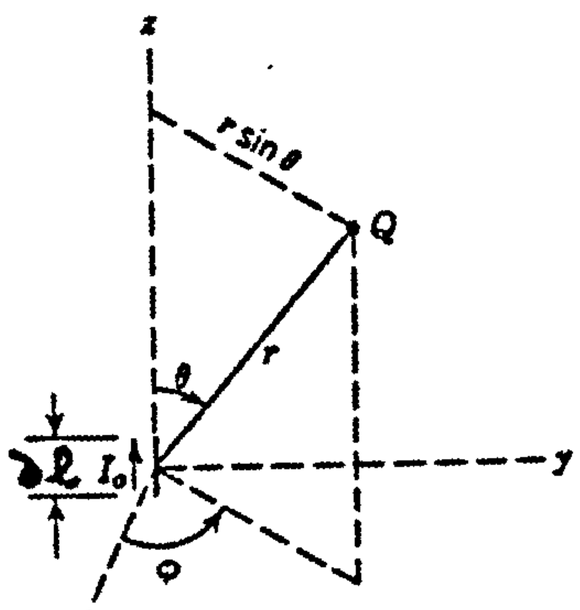

Fig (a) . Hertzian dipole.

CHAPTER 2.

2. Calculation of Resonator Radiation.

The simplest radiating current element, that can be considered is the short oscillating electric dipole consisting of a filament of elemental length ∂l carrying a complex time varying current I_o. From the retarded vector potential, using spherical polar co-ordinates it can be shown that [1] : fig (a)

$$H_\phi = \frac{I_o\, \partial l}{4\pi}\, e^{-jkr}\left[\frac{jk}{r} + \frac{1}{r^2}\right] \sin\theta \qquad (2.1)$$

$$E_r = \frac{I_o\, \partial l}{4\pi}\, e^{-jkr}\left[\frac{2\eta}{r^2} + \frac{2}{j\omega\varepsilon r^3}\right] \cos\Theta \qquad (2.2)$$

$$E_\theta = \frac{I_o\, \partial l}{4\pi}\, e^{-jkr}\left[\frac{j\omega\mu}{r} + \frac{1}{j\omega\varepsilon r^3} + \frac{\eta}{r^2}\right] \sin\theta \qquad (2.3)$$

where

$$\eta = \sqrt{\frac{\upsilon}{\varepsilon}} \;\approx\; 120\pi \;; \quad E_\varphi = H_r = H_\Theta = 0 \qquad (2.4)$$

and

∂l is elemental length. $\partial l = a\,dz$

λ is the free space wavelength. ; $i(t) = Re(I_o\, e^{jwt})$

$\frac{1}{\sqrt{2}}|I_0|$ is the r.m.s current.

In the far field as r -> ∞ only the "1/r" terms are significant and approximate locally to a uniform plane wave. At great distances from the source, any portion of a spherical wave surface is essentially a plane wave, with E_Θ and H_φ are in time phase, related by η .

$$H_\phi = \frac{jk\, I_o\, \partial l}{4\pi r}\, e^{-jkr} \sin\Theta \qquad (2.5)$$

$$E_0 = \frac{j\omega\,\mu\; I_o}{4\pi r}\, \partial l\; e^{-jkr} \sin\Theta \qquad (2.6)$$

E_Θ and H_ϕ are in time phase, related by η, and at right angles to each other and the direction of propagation. The Poynting vector is then completely in the radial direction The time average P_r for a short dipole, calculated from the peak values of E_Θ and H_ϕ using Poyntings theorem :-

$$P_{av} = \frac{1}{2} \int_S \mathrm{Re} \left(\bar{E} \times \bar{H}^* \right) . \bar{d}s \qquad (2.7)$$

and

$$P_{av} = \eta \pi \left| \frac{I}{3^o} \right|^2 \left| \frac{\partial l}{\bar{\lambda}} \right|^2 \approx 40 \pi^2 |I_o|^2 \left| \frac{\partial l}{\bar{\lambda}} \right|^2 \quad \text{(watts)} \qquad (2.8)$$

This power corresponds to an effective radiation resistance given by :-

$$R_{rad} = \frac{2 P_{av}}{|\bar{I}_0|^2} = 80 \pi^2 \left| \frac{\partial l}{\bar{\lambda}} \right|^2 \quad (\Omega) \qquad (2.9)$$

2.1 Radiation from Microstrip Structures.

Any physical circuit or antenna structure carrying current may be modelled as a distribution of elements. In principle the electromagnetic field of such an antenna may be calculated. In practice precise knowledge of the current distribution may not be available, however an approximate current distribution can often be assumed. Interest is usually centred on calculating the far field radiation and in these circumstances the following assumptions may be justified in order to simplify the calculation of radiated power from the antenna, fig 2.1 :-

a) Differences in radius vector to different points of the radiator are absolutely unimportant in their relative effect on magnitude.

b) All field components decreasing with distance faster than 1/r are completely negligible compared with those decreasing as 1/r.

c) Differences in radius vector r" relative to r' for the purpose of finding phase difference are taken as $r'\cos\psi$, where r' is the radius to the radiating element from the origin, ψ the angle between r' and r, r is the radius from the origin to the distant point $P(r,\Theta,\varphi)$ at which the field is calculated.

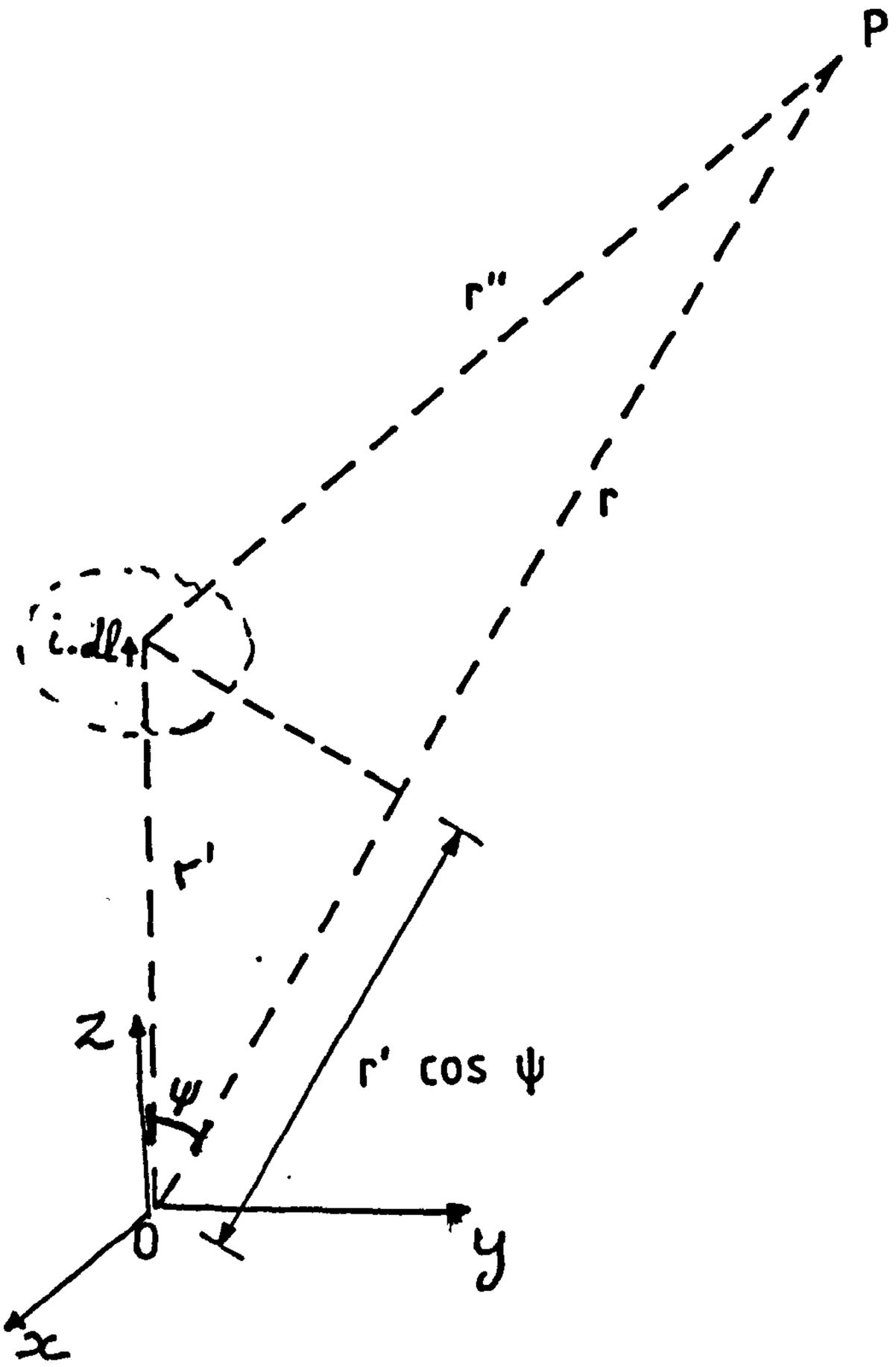

Figure 2.1. Coordinates for calculation of radiation.

for a current element on the z axis

Ramo S., Whinnery J.R., Duzer T.V.,
Fields and waves in communication electronics, second edition,
page 588, 1984 .

The calculation of power radiated from the system follows a systematic application of the Poynting vector as described by Schelkunoff [2]. The radiated field in any direction (Θ,φ) may be determined in terms of a radiation vector $d\bar{N}$ for any current element $\bar{J}\,dV$ as

$$\bar{N} = \int_v \bar{J}\, e^{(jkr'\cos\psi)}\, dV \qquad (A.m) \qquad (2.10)$$

where $k = 2\pi/\lambda_0$ and $\cos\psi$ for an element with angular co-ordinates (Θ',φ') is given by (page 589, reference 1) :

$$\cos\psi = \cos(\theta)\cos(\theta') + \sin(\theta)\sin(\theta')\cos(\phi - \phi') \qquad (2.11)$$

This integral is taken over all the current elements in the system. The components $N\Theta, N\varphi$ of the radiation vector are then used to evaluate the total average power radiated over a hemisphere above the ground plane (page 588, reference 1):

$$P_r = \frac{\eta}{8\lambda_0^2} \int_0^{\pi} \int_0^{2\pi} \left[|N_\theta|^2 + |N_\phi|^2\right] \sin(\theta)\, \partial\theta\, \partial\phi \qquad (2.12)$$

2.2 Narrow Microstrip lines

For microstrip circuit applications the effect of unwanted radiation can be reduced to acceptable levels by the use of thin, high permittivity substrates and appropriate shielding. This radiation is most apparent in microstrip circuits, involving resonant structures, due to the relatively high currents set up in the resonator. In particular the open circuit halfwave resonator has a standing wave pattern which enhances the radiation from the microstrip line. This resonator is easy to fabricate and is often used as a radiating element in antenna arrays.

Lewin [3] gave the first analysis of radiation from microstrip lines and discontinuities in microstrip circuits, by modelling the strip current across narrow width microstrip lines as a single current filament, with an 'effective polarisation current' to account for the effect of the substrate permittivity on the resonator.

This analysis can be used to calculate the far field radiation from an open circuit half-wavelength resonator by utilising the following simplifications :-

1) The dimension of the cross section of the microstrip is small compared to the free space wavelength. Quasi-T.E.M propagation can be assumed and dispersion neglected.

2) It follows that if the width of the strip is small when compared to the free space wavelength, then the current distribution across the microstrip line can be assumed to be concentrated along the centre line of the strip.

3) Similarly the dielectric polarisation current is considered to be concentrated on a plane normal to the ground plane and containing the axis of the strip. The radiation from components of polarisation current normal to this plane is considered to be negligible.

4) Sinusoidal distribution of current along the strip is assumed. End effects are thereby neglected, but may taken into account by the use of an effective length ($\lambda_g/2$), rather than the physical length of the resonator.

$$I = I_m \cos(k'z) \qquad (2.13)$$

where

$$k' = \frac{2\pi}{\lambda_g} \qquad (2.14)$$

*

From the two filaments corresponding to y = +h and y = -h

$$\bar{N}_s = \int_{-\frac{\lambda}{2^g}}^{\frac{\lambda}{2^g}} I_m \cos(k'z)\, e^{(jkz\cos\theta + jkh\sin(\theta)\sin(\varphi))}\, \bar{a}_z\, dz$$

$$+$$

$$-\int_{-\frac{\lambda}{2^g}}^{\frac{\lambda}{2^g}} I_m \cos(k'z)\, e^{(jkz\cos\theta - jkh\sin(\theta)\sin(\varphi))}\, \bar{a}_z\, dz$$

For the system shown in fig 2.2 the strip currents will give rise to elements :

$$I_z\, dz = I_m \cos(k'z)\, dz \qquad (2.15)$$

for $-\frac{\lambda_g}{2} < z < \frac{\lambda_g}{2}$

$$k' = \frac{2\pi}{\lambda_g}$$

$$x' = 0 \quad ; \quad y' = h$$

and from the image in the ground plane:

$$I_z\, dz = -I_m \cos(k'z)dz \qquad (2.16)$$

$$x' = 0 \quad ; \quad y' = -h$$

Substituting into equation (2.10) *

$$\bar{N}_s = 2j\, I_m \sin(kh \sin\theta \sin\phi) \int_{-\frac{\lambda}{4}g}^{\frac{\lambda}{4}g} \cos(k'z)\, \exp(jkz\cos\theta)\bar{a}_z dz \qquad (2.17)$$

$$x = 0\ ,\ y = 0$$

Roberts [4] integrated this equation to obtain a closed form expression for the radiation $\bar{N}_s$ due to the strip current :-

$$\bar{N}_s = \frac{4\, j \sqrt{\varepsilon_e}\, I_m \sin(kh \sin\theta \sin\phi)}{k\,(\varepsilon_e - \cos^2\theta)} \cos\left\{\cos(\theta)\left[\frac{\pi}{2\sqrt{\varepsilon_e}}\right]\right\} \bar{a}_x \qquad (2.18)$$

(A.m)

$\bar{a}_z$ is a unit vector in the z direction.

Since the current in the radiating system flows only along one axis :-

$$\bar{N}_\theta = -N_s \sin\theta \quad ; \quad N_\phi = 0 \qquad (2.19)$$

where, ε_e is the effective dielectric constant { $\varepsilon_e = (\lambda_o/\lambda_g)^2$} .

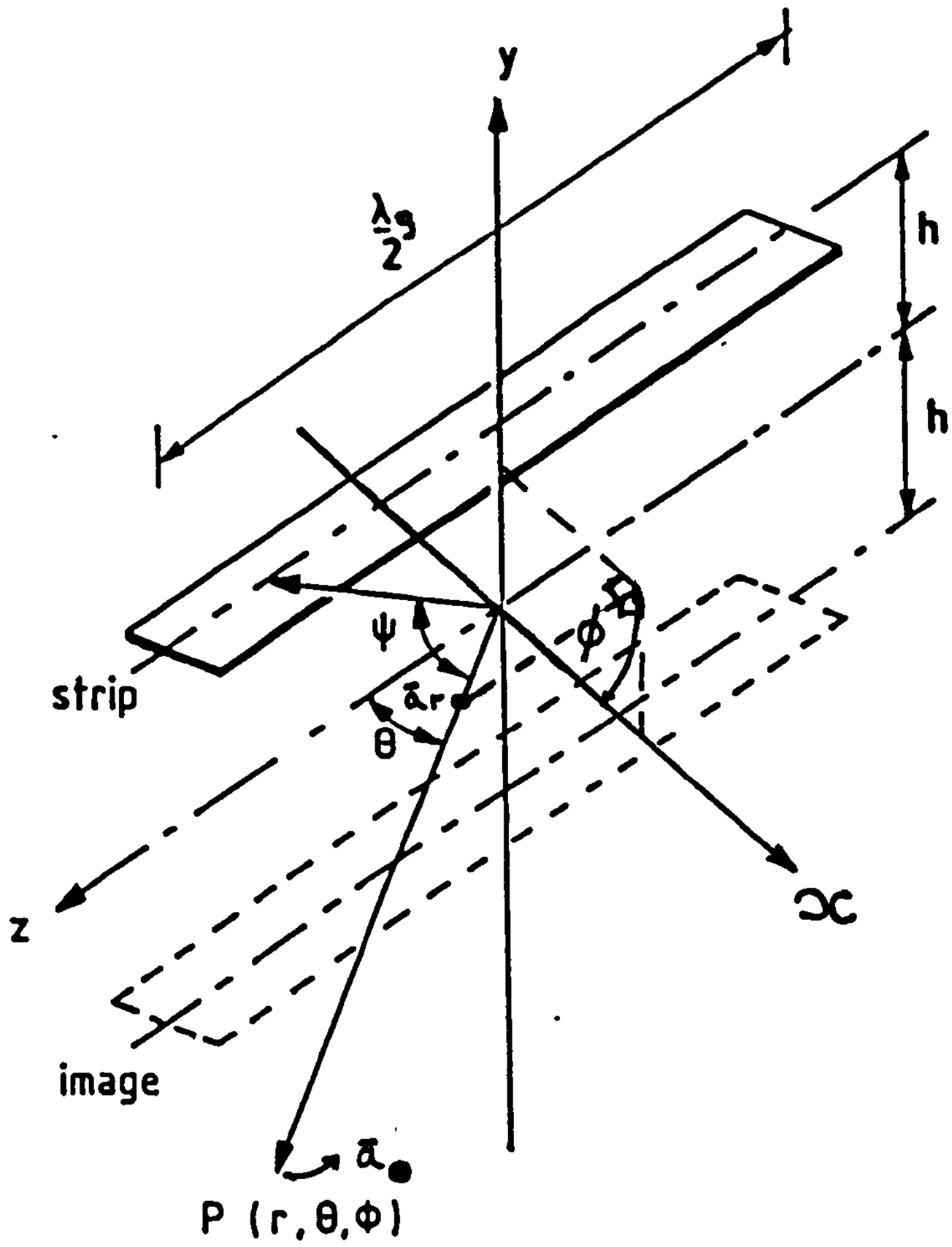

Figure 2.2. Resonant antenna coordinates for radiated field calculation.

If it can be assumed that all the electric flux lines eventually pass through the dielectric giving rise to polarisation currents, the dielectric polarisation currents for the system can be derived :-

$$i = 2h\,j\omega\,C \left\{ \frac{\varepsilon_r - 1}{\varepsilon_r} \right\} V \qquad (A) \qquad (2.20)$$

where,

i = polarisation current x $\frac{2h}{\text{unit length of strip.}}$

$$\delta I = -j\omega\, C\, \partial z\, V$$

Therefore

$$i = -2h \left\{ \frac{\varepsilon_r - 1}{\varepsilon_r} \right\} \frac{\partial I}{\partial z} \qquad (A) \qquad (2.21)$$

So, that the dielectric polarisation current has current elements given by :-

$$i_y\, dz = -2h \left\{ \frac{\varepsilon_r - 1}{\varepsilon_r} \right\} I_m\, k'\, \sin(k'z)\, dz \qquad (2.22)$$

And, substituting into equation (2.10) :

$$\bar{N}_\rho = -2h \left\{ \frac{\varepsilon_r - 1}{\varepsilon_r} \right\} Im\, k' \int_{-\frac{\lambda}{4}^g}^{\frac{\lambda}{4}^g} \sin(k'z)\, \exp(jkz\cos\theta)\, \bar{a}_y\, dz \qquad (2.23)$$

(A.m)

a_z is a unit vector in the z direction.

Roberts then showed that the radiation, N_p due to the dielectric polarisation current (with its image) is given by :-

$$\bar{N}_p = -4j\, h\, I_m \sqrt{\varepsilon_e} \frac{\left\{ \frac{(\varepsilon_r - 1)}{\varepsilon_r} \right\}}{(\varepsilon_e - \cos^2\theta)} \cos(\theta)\, \cos\left[\pi \frac{\cos\theta}{2\sqrt{\varepsilon_e}} \right] \bar{a}_y \qquad (2.24)$$

(A.m)

where,

$\tilde{a}_y$ is a unit vector in the y direction.

ε_e is the effective dielectric constant $\{\varepsilon_e = (\lambda_o/\lambda_g)^2\}$

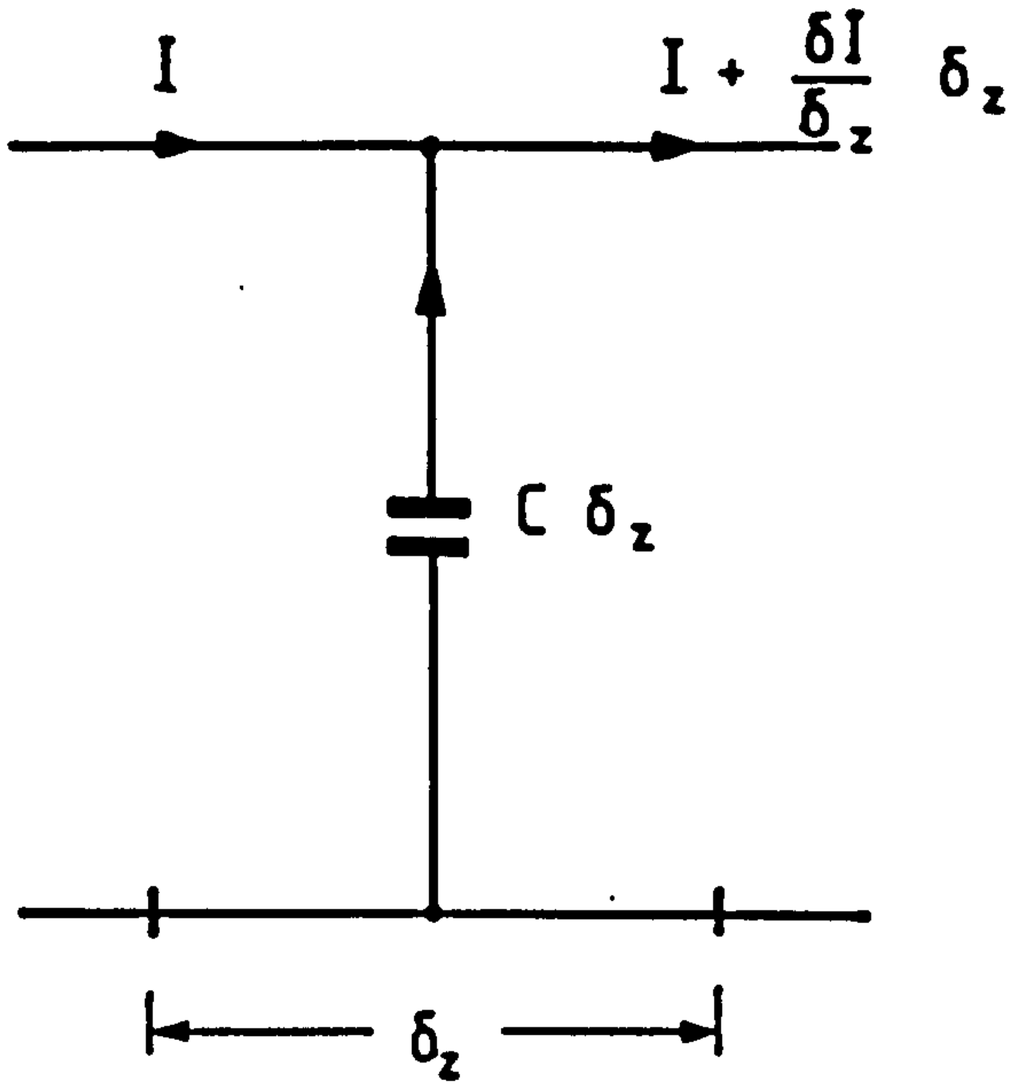

Figure 2.3. Polarisation currents.

The components of $\overline{N}_p$ in the directions Θ and φ are given by :-

$$\overline{N}_\Theta = N_p \cos\Theta \sin\varphi \ \overline{a}_\Theta \quad ; \quad \overline{N}_\varphi = N_p \cos\varphi \ \overline{a}_\varphi \qquad (2.25)$$

It is possible to calculate the power radiated by the strip, and polarisation currents by substituting the values of N_Θ, N_φ into the following equation to give the total power radiated into the half-hemisphere above the ground plane, for $-\pi/2 < \varphi < \pi/2$:

$$\int_0^{\pi} \int_{-\frac{\pi}{2}}^{\frac{\pi}{2}} \left\{ |N_\theta|^2 + |N_\phi|^2 \right\} \sin\theta . \partial\theta . \partial\phi_{(W)} \qquad (2.26)$$

This integral was evaluated using a numerical programme based on Simpsons rule for double integrals. This theoretical study can be further simplified and a simple closed form formula derived for the radiation loss. For higher values of dielectric constant the following approximations are made :

$\{(\varepsilon_r - 1)/\varepsilon_r\} \approx 1$ and $\sin(k'z) = k'z$, $z < \lambda_g/4$

Easter [10] showed that the radiation from the resonator could be approximated by a small loop antenna in the plane containing the strip axis and its image which has a current area product of $h \lambda_g I_m \frac{2}{\pi}$ $(A m^2)$. It follows that the power radiated above the ground plane is given by

$$P_r = \frac{\eta k^4}{24\pi} * (\text{current-area product})^2 \quad (w) \qquad (2.28)$$

The radiated power fraction [10] is given by :-

$$\frac{P_r}{P_i} = \frac{64 \eta \pi h^2}{3 \varepsilon_e Z_o \lambda_o^2} \qquad (2.29)$$

where, $Pi = \frac{1}{8} |I_m|^2 Z_o$ is the power incident at each end of the resonator.

From equation 2.29 it can be seen that the radiated power from the resonator is a complex function of the substrate height, strip width and permittivity of the substrate, fig 2.4 . By increasing the substrate height the radiation from the strip is increased. While increasing the substrate permittivity reduces the radiated power. A computer programme (appendix 1) based on the above expressions was written so as to calculate the total power radiated by a resonator of known substrate height and permittivity. The validity of this programme is confirmed by experimental measurements in chapter 4

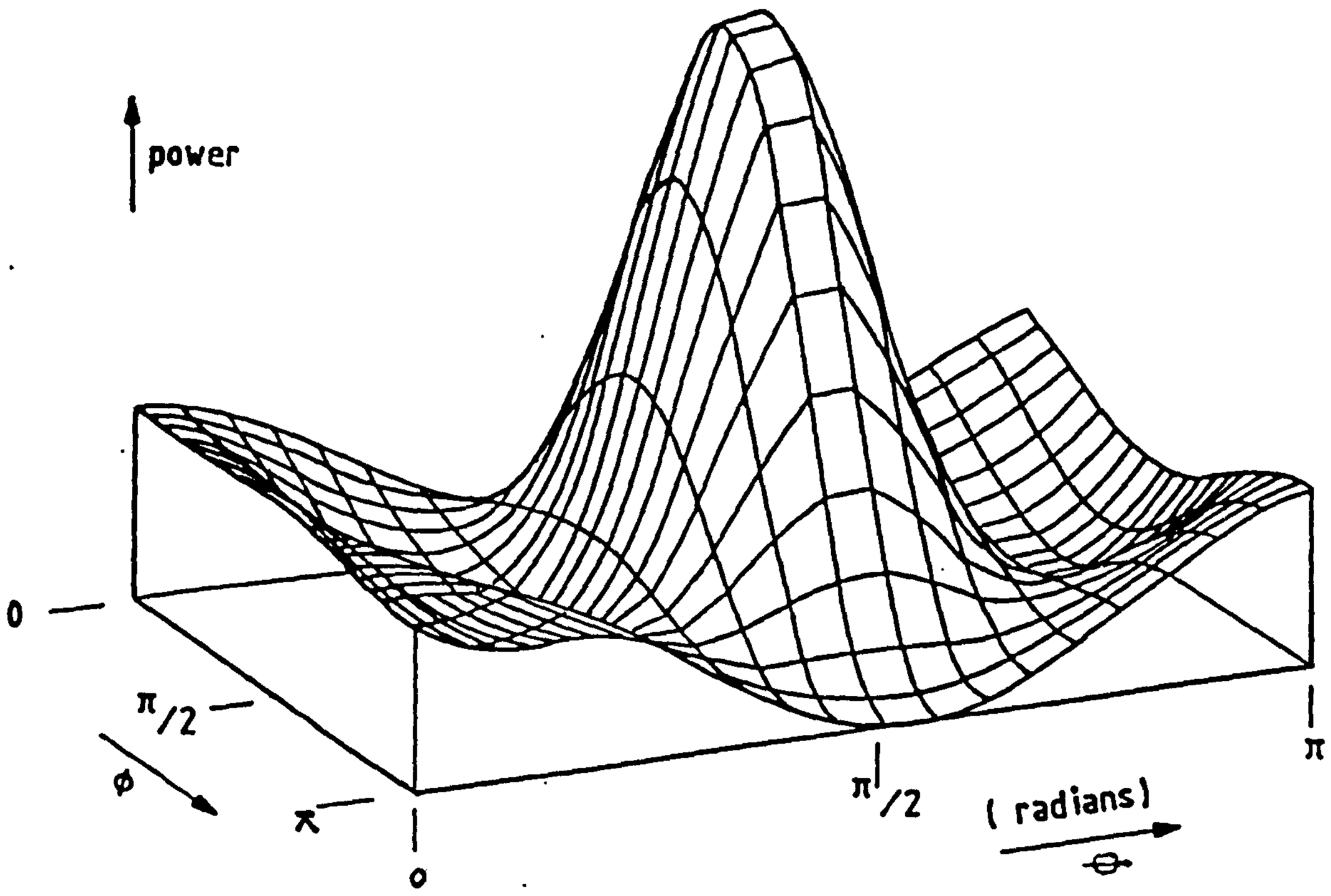

Figure 2.4. Polar distribution of radiated power from a λ/2 O.C. resonator.

Since the radiated power P_r and the incident power P_i can be calculated, the radiation efficiency can be determined for the half-wavelength resonator.
Graphs were then plotted of the antenna efficiency as a function of line width, substrate height and permittivity.

Fig 2.5 shows the calculated radiation efficiency of the resonator as a function of the effective dielectric constant for λ_o=3cm, $z_o = 50\Omega$ and h =1.6mm.

Fig 2.6 shows the calculated radiation efficiency as a function of characteristic impedance for a substrate of permittivity 2.55 and a thickness of 1.6mm.

2.3 Radiation from a Medium Width Microstrip Resonator.

To produce theoretical predictions applicable to all microstrip configurations, the analysis must allow for the spreading of radiation sources as the strip width increases. For medium width microstrip lines where the line width is greater than $\lambda/16$, the simplifying assumptions outlined by Lewin, are no longer valid, since the current distribution across the strip cannot be assumed to be concentrated along the centre line of the strip. The differences in radius vector to different parts of the radiator is no longer unimportant since it affect the magnitude of the far field radiation.

For a non-rigorous approximation in order to calculate the far field radiation the current distribution can be split into two symmetrical line charges spaced, either side of the centre line of the strip. The far field Poynting vector due to the two line charges can then be calculated using systematic approximations outlined by Schelkunoff. A more exact numerical technique using the moment method was developed by Agrawal [5] et al, who represented the antenna as a fine wire grid immersed in a dielectric medium.

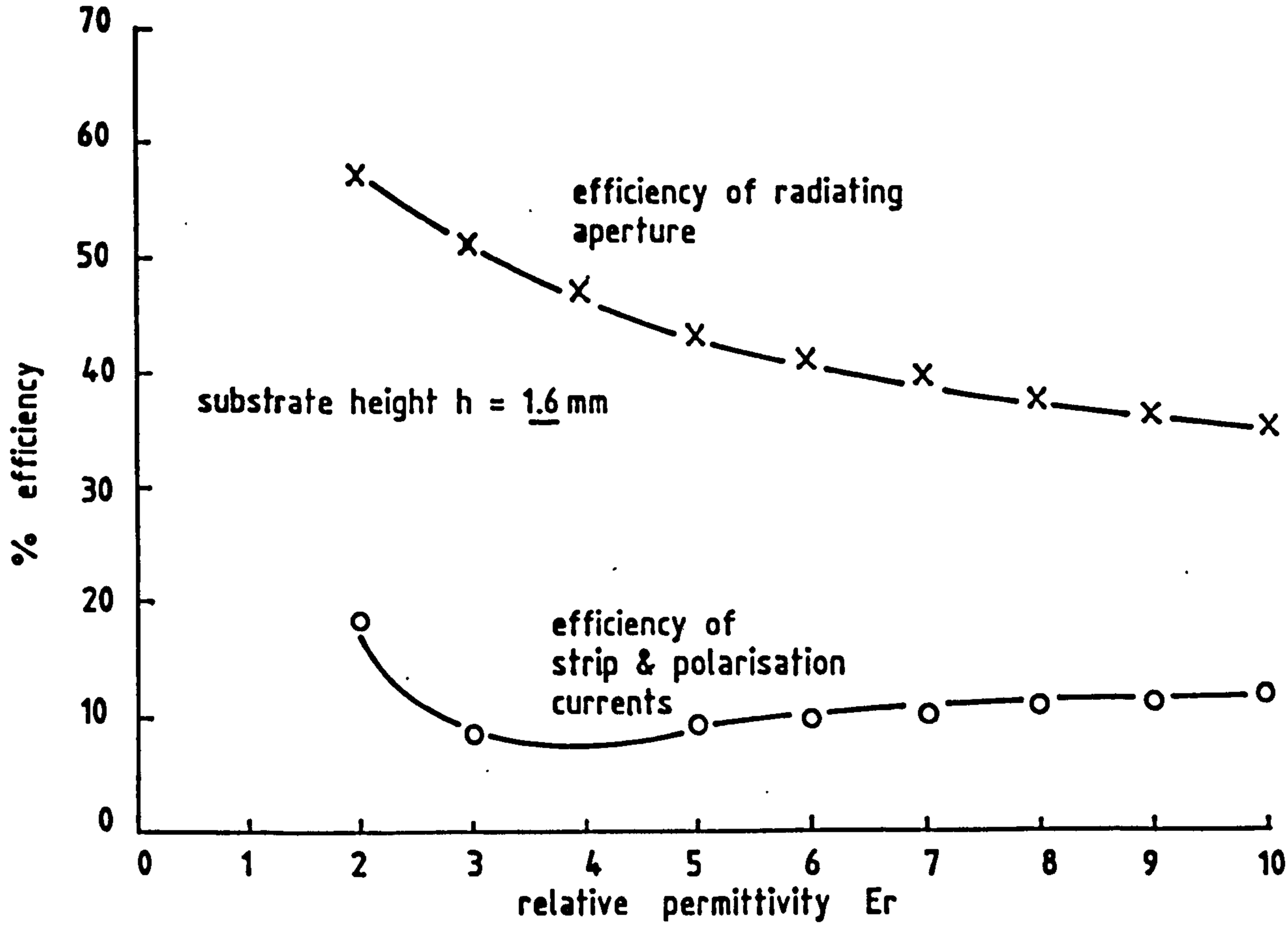

Figure 2.5. Radiation efficiency against relative permittivity Er.
Strip width W = 4 mm , Zo = 100.

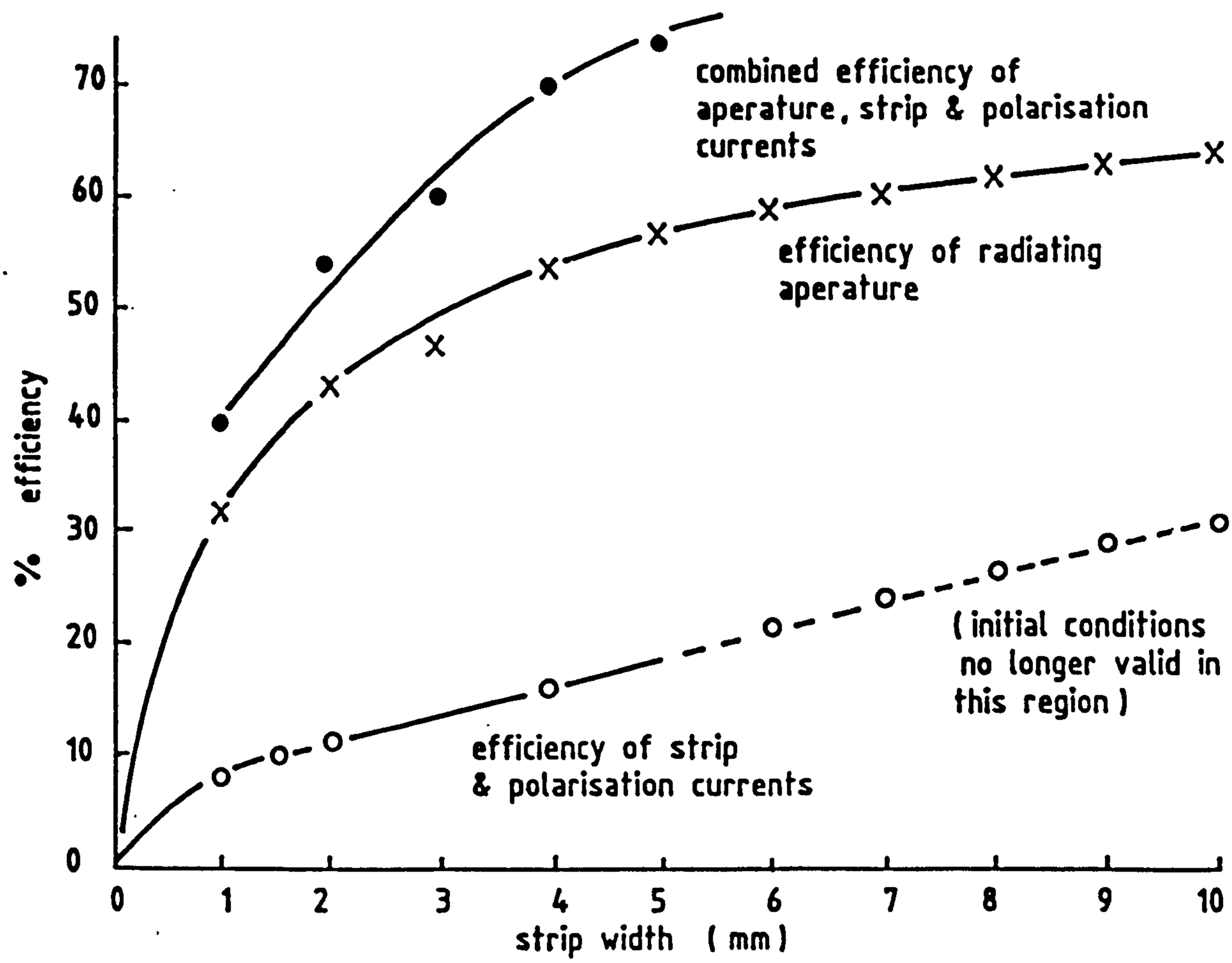

Figure 2.6. The radiation efficiency of a single resonator :-

Relative permittivity Er = 2.55

Substrate height h = 1.6 mm.

Richmonds reaction formulation is then used to evaluate the piecewise sinusoidal current as a set of n overlapping dipoles to give a set of n simultaneous equations.

Solving these n unknown equations leads to the segment currents and hence gain, input impedance, efficiency and far field radiation. This approach However, is tedious to implement and requires considerable computational time.

2.4 Radiation calculated from the aperture field.

For wire antennas it is natural to assume a current distribution over the antenna, and to consider the current elements as the source of radiation. For other types of antenna such as the electromagnetic horn antenna it is more natural to think of the antenna as an aperture and to consider the aperture fields as radiation sources using Huygens principle.

Thus a knowledge of the field distribution over the aperture should yield the far field radiation by summing the contributions of the huygen sources distributed over the aperture. While, for microstrip antennas there are fields and currents on the surface of the conductor, together with a polarisation current contained within the substrate. However, if the microstrip line is relatively wide it can be considered as a conventional aperture. Since, the aperture gain is large, the relative effect of the neglected fields outside the aperture is small, and can be neglected. Kompa [6] has pointed out that a very wide open circuited microstrip line, will tend to behave as a semi-infinite dielectric loaded waveguide with radiation occurring from the narrow slot aperture formed by the fringing field between the conducting sheet and the ground plane at the open circuit discontinuity.

Munson [7] modelled the rectangular patch antenna as two electrically thin slots spaced $\lambda/2$ apart excited in phase, and radiating into the half-space above the ground plane, fig 2.7 . The electric fields in the slots can be resolved into vertical and horizontal components, with the horizontal component extending a length equal to the ground plane spacing, from the edge of the slot. The far field radiation is then obtained by summing the radiation fields in the horizontal and vertical directions. The admittance of a thin slot aperture in a ground plane was derived by Harrington [8], who showed that for $a/\lambda < .1$:

$$G_L \approx \frac{\pi}{\lambda \eta}\left[1 - \frac{(ka)^2}{24}\right] \quad (\Omega^{-1}.m^{-1}) \qquad (2.30)$$

$$B_L \approx \frac{3.135 - 2\log(ka)}{\lambda \eta} \quad (\Omega^{-1}.m^{-1}) \qquad (2.31)$$

where,

k is the wave number, G_l is the radiation conductance/ unit length of the slot aperture.

and a is the slot height, B_l is the radiation susceptance/ unit length of the slot aperture.

In most microstrip applications, the conductance simplifies to :-

$$G_L \approx \frac{\pi}{\lambda \eta} \quad (\Omega^{-1}.m^{-1}) \qquad (2.32)$$

Thus, the resistance of the slot is given by :-

$$r_a = \frac{120}{L} \quad (\Omega) \qquad (2.33)$$

where, L is in wavelengths.

r_a is the resistance of the slot aperture.

Since, the electric field in the slot can be resolved into vertical and horizontal components, Derneyd [9] like Munson [7] assumed that the horizontal component extends a length equal to the height of the substrate above the ground plane, fig 2.8 . A far-field approximation for the radiation from the two slots spaced $\lambda/2$ apart, gives only a φ directed component of the electric field.

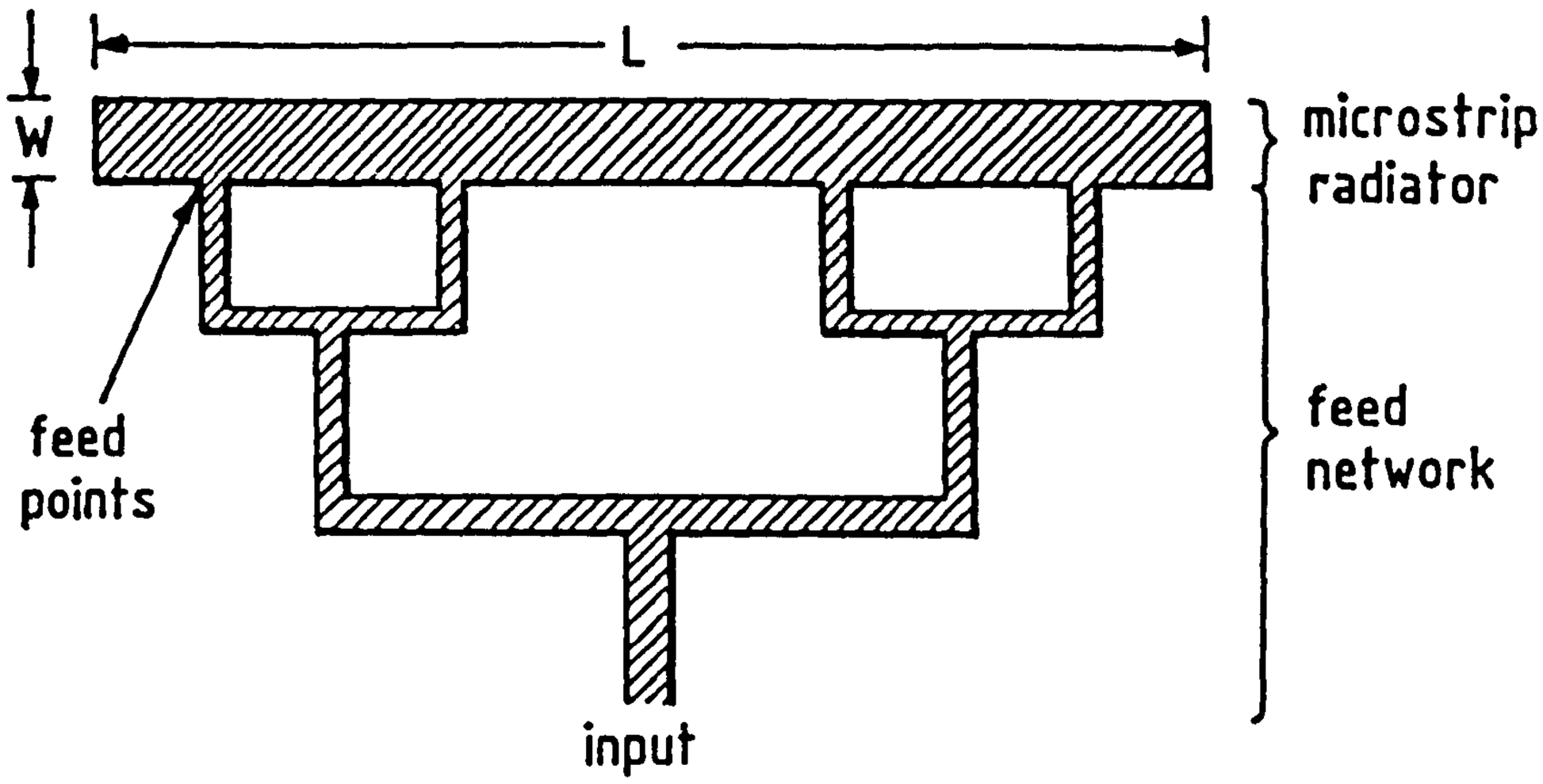

Figure 2.7. Microstrip patch antenna.

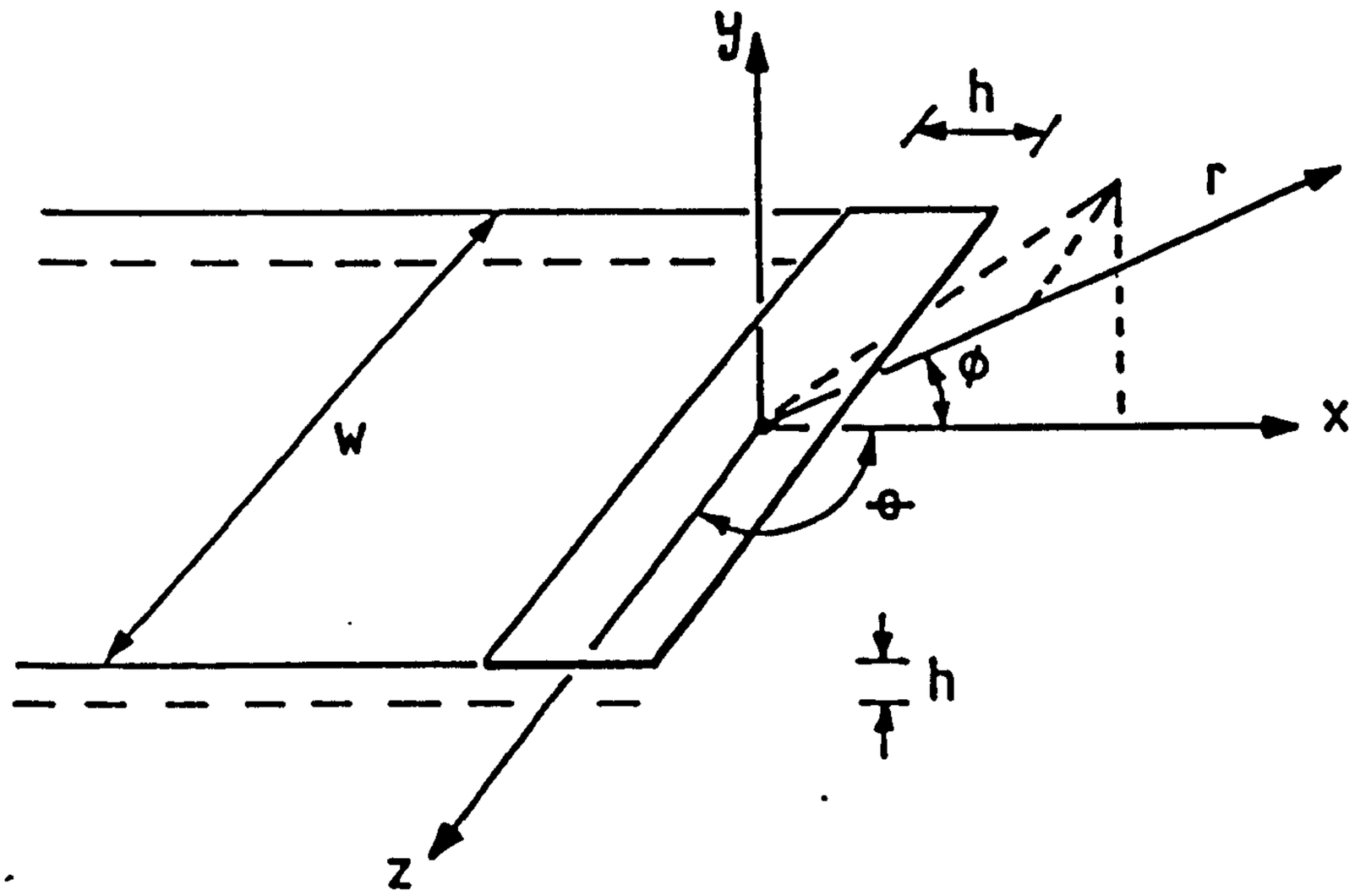

Figure 2.8. Geometry of radiating slot.

The input admittance of the radiating elements is found by transforming the slots through the low impedance to give :

$$Y_{in} = G_a + JB_a + Y_c \frac{G_a + J(B_a + Y_c \tan(\beta L))}{Y_c - B \tan(\beta L) + JG_a} \quad (\Omega^{-1}) \quad (2.34)$$

where

β is the propagation constant,

L is the length of the transmission line,

Y_c is the characteristic admittance.

G_a is the radiation conductance of the slot aperture. Ω^{-1}

B_a is the radiation susceptance of the slot aperture. Ω^{-1}

At resonance the imaginary part of the input admittance is zero. This occurs when :

$$\tan \beta L = \frac{2 Y_c B_a}{G_a^2 + B_a^2 - Y_c} \quad (2.35)$$

Practical values of the parameters give a resonant length slightly shorter than a half-wavelength,and the input admittance at resonance is given by :

$$Y_{in} = 2 G_a \quad (\Omega^{-1}) \quad (2.36)$$

2.5 Conclusions.

The analysis of the microstrip open circuited half-wavelength resonator enables the design limitations of microstrip antenna arrays to be assessed. This study gives qualified approval to the current method outlined by Lewin for microstrip radiation calculations. Fringe field effects to the extent that they affect directly the radiation process have not been evaluated, but are most likely to be unimportant for very narrow microstrip lines.

For much broader microstrip lines the distortion at certain discontinuities may be of considerable importance. These reservations apart, the "current method" can be applied to a number of microstrip discontinuities and can be used to calculate feeder radiation. It will be shown in chapter 3 that the feeder current is comparable in magnitude to the resonator current. If the strip is wide it is tempting to consider the microstrip line as a conventional aperture since the relative effects of fringing fields along the line can be ignored.

[10] Easter B. , Roberts R.J.,
Radiation from half-wavelength open-circuit Microstrip Resonators,
Electronics letters, No 18, Vol. 6, 1970 .

36

REFERENCES FOR CHAPTER 2.

[1] Ramo S., Whinnery, Duzer T.V.,
Fields and Waves in Communication Electronics,
Wiley, Chapter 12, 1965 .

[2] Schelkunoff S.A.,
A general radiation formula, Proc IRE 27,
page 660-666, October 1939 .

[3] Lewin L.,
Radiation from discontinuities in strip-line.
IEEE Monograph No 358 E, Feb. 1960

[4] Roberts J.R.,
An investigation into the application of microwave integrated circuits,
Ph.D thesis, U.C.N.W., Bangor, 1971 -Microstrip Resonators.

[5] Agrawl P.K. & Bailey M.C.
An analysis technique for microstrip antenna,
IEEE trans. AP - 25, page 756 - 759, 1977

[6] Kompa G.,
Approximate calculation of radiation from open-ended wide microstrip
lines, electronic lett. 12, page 222 - 224, 1976.

[7] Munson R.E.,
Conformal Microstrip Antenna,
IEEE trans. Vol AP-22, page 74-78, 1974

[8] Harrington R.F.,
Time Harmonic Electromagnetic fields, New York,
McGraw Hill, page 276, 1961 .

[9] Derneryd A.G.,
Linearly Polarised Microstrip Antenna's,
IEEE trans AP-24, page 846 - 851, 1976.

[11] Denlinger E. J.
"Radiation from Microstrip Resonators",
I.E.E.E trans. , MTT-17, page 235-236, 1969 .

Chapter 3.

3. Feed lines for Microstrip Antennas.

A linearly polarised microstrip antenna consist of surface mounted patches connected by a coplanar feed network to fully realise the advantages of planar fabrication. The radiation from the feed lines of this type of structure can make a significant unwanted contribution to the side lobe and cross polarisation radiation of the antenna, since the feed line currents are comparable in magnitude to the currents in the radiating elements. An example of the feed radiation affecting the radiation pattern can be observed by examining the cross-fed printed antenna as described by Williams [1]. This design uses an ingenious arrangement of feed lines at 45^0 to the radiating elements to give good gain and radiation efficiency.

From the symmetry of the dipole arrangement the two radiation patterns obtained at $\pm 45^0$ to the normal orientation of the antenna should be similar. But the measured radiation patterns at $\pm 45^0$ orientation to the normal are dissimilar, fig 3.1 . The differences in the two radiation patterns must therefore be due to feeder radiation.

3.1 Theoretical evaluation of feed line radiation.

The simplest form of feed system for a linear array is series feeding in which the radiating elements are directly attached to the feed line. In order to produce co-phase radiation the radiating elements are spaced at λ intervals along the feed line.

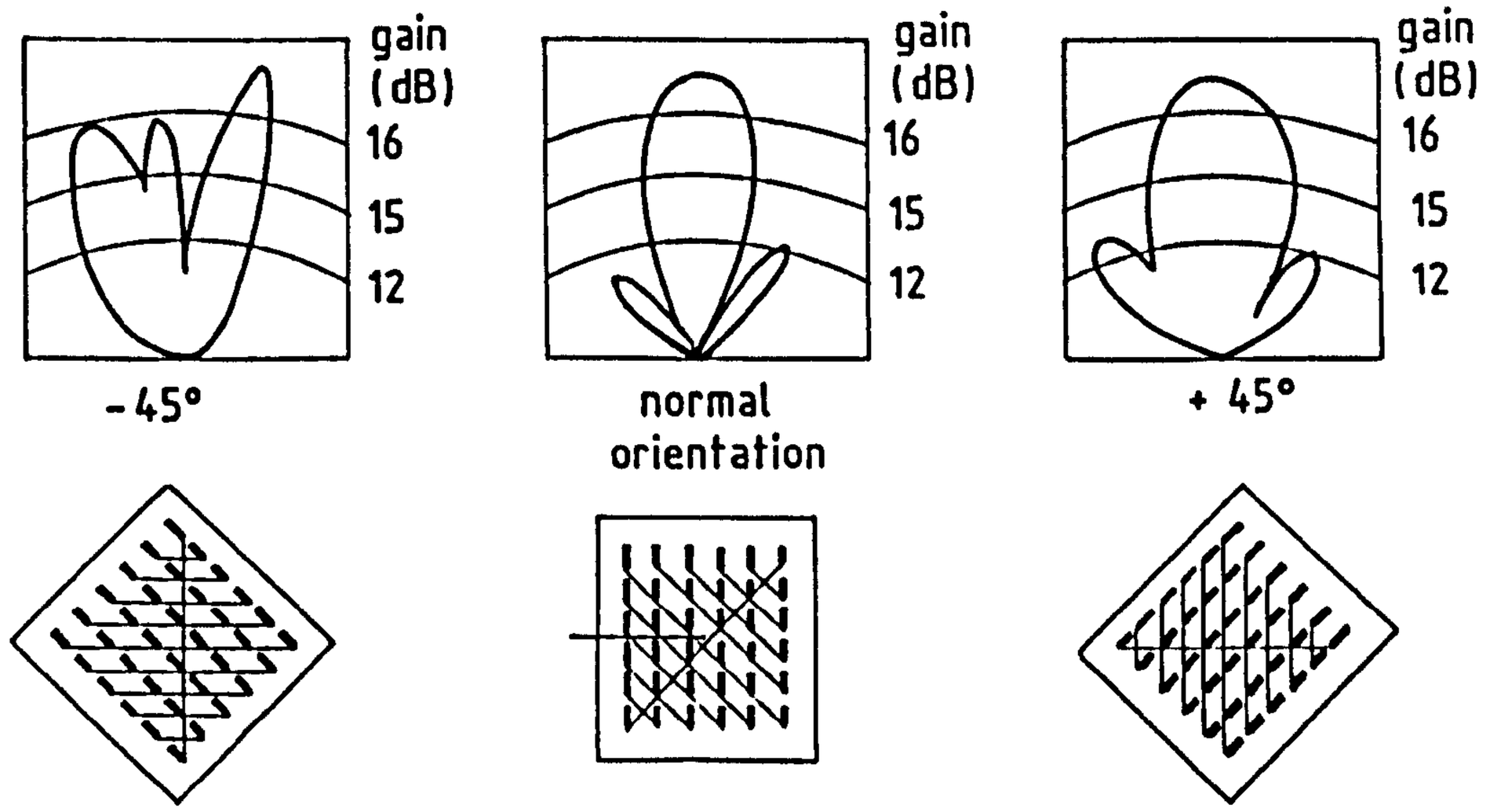

Polar diagram measured for vertical polarisation , show for normal orientation and ± 45°. Aerial consists of 84 λ/2 resonators.

Figure 3.1. Cross fed array due to Williams and its characteristics.

For a broadside array the travelling wave component of the current decreases as the feed current progresses down the array and the impedance mismatch between the radiating elements and the feed line increases. Thus a standing wave current distribution is set up along the feed line, fig 3.2 .

It can be shown that the peak current in each section of the feed line remains constant. In the absence of loss, the voltage at each load point is V_1. The current at the load points is given by :-

$$I_x = \frac{x \cdot V_1}{N \cdot Z_r} \quad (A) \qquad (3.1)$$

where,

I_x is the current at load point x.

N is the total number of radiating elements.

Z_r is the resistive load.

The standing wave in each section is given by :-

$$S_x = \frac{N Z_r}{x Z_{of}} \qquad (3.2)$$

where,

Z_{of} is the characteristic impedance of the feed line.

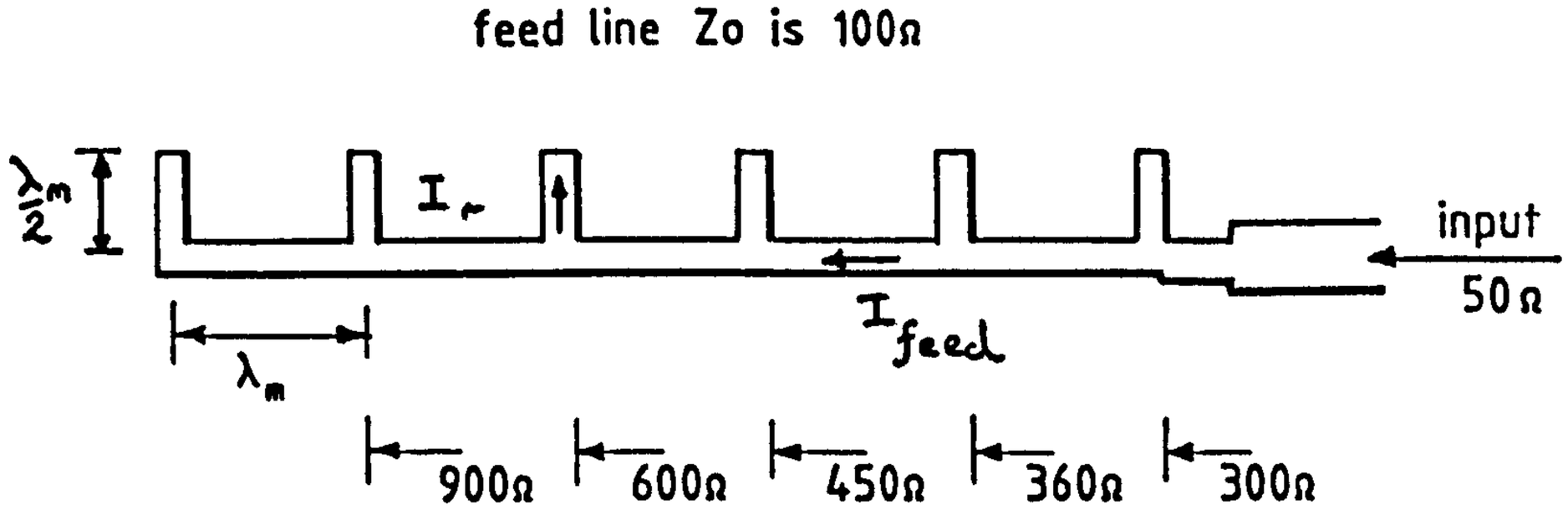

Figure 3.2. Resonant radiators coupled to microstrip line.

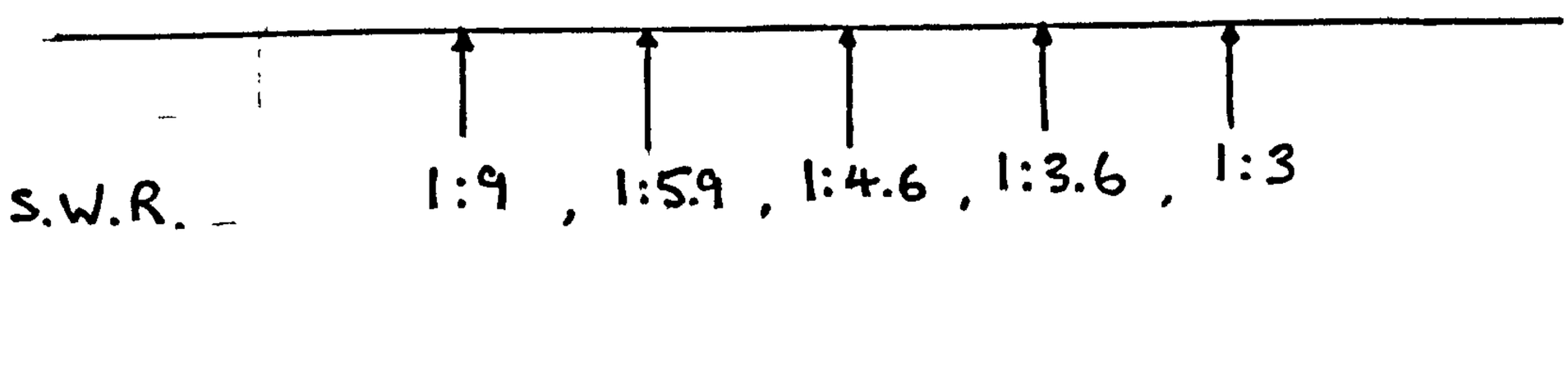

The load points and current minima are resistive. Current maxima Imax occur at a distance $\lambda/4$ and $3\lambda/4$ from the load.

$$I_{max} = I_x S_x \quad (A) \qquad (3.3)$$

substituting into equations (3.1) and (3.2) gives

$$I_{max} = \frac{x V_1}{N Z_r} \cdot \frac{N Z_r}{x Z_{of}} = \frac{V_1}{Z_{of}} \quad (A) \qquad (3.4)$$

Thus, the maximum current in each λ feeder section remains constant.

The maximum current Ir in the resonator is given by :-

$$I_r = \frac{V_1}{Z_{or}} \quad (A) \qquad (3.5)$$

where,

Z_{or} is the characteristic impedance of the resonator.

Thus, it can be seen from equations 3.4 and 3.5 that the feed line current is comparable in magnitude to the current in the radiating element.

The simplifying assumptions outlined by Lewin [2] and Roberts [3] in chapter 2. for a half-wavelength resonator can be used to calculate the far field radiation from a λ resonator or feed line. The strip radiation vector for a λ resonator is given by :-

$$\bar{N}_s = \frac{-4\sqrt{\varepsilon_e}\, I_m \sin(kh \sin(\theta) \sin\phi)}{k\,(\varepsilon_e - \cos\theta)^2} \sin\left\{\pi \cos\left[\frac{\theta}{\sqrt{\varepsilon_e}}\right]\right\} \bar{a}_z \qquad (3.6)$$

(A.m)

$\bar{a}_z$ is a unit vector in the z direction.

Since the current in the radiating system flows only along one axis :-

$$\bar{N}_\theta = - N_s \sin\theta \, \bar{a}_\theta \qquad (3.7)$$

The simplifying assumptions which were used to calculate the polarisation radiation for a $\lambda/2$ resonator in Chapter 2 can be used to calculate the polarisation radiation $\bar{N}_p$ for a λ feed line section.

$$\bar{N}_p = - 4 h I_m \sqrt{\varepsilon_e} \frac{(\varepsilon_r - 1)}{\varepsilon_r} \sin\left[\pi \frac{\cos\theta}{2\sqrt{\varepsilon_e}} \right] \bar{a}_y \qquad (3.8)$$

(A.m)

$\bar{a}_y$ is a unit vector in the z direction.

The components of $\bar{N}p$ in the Θ and φ directions are given by :-

$$\bar{N}_\theta = Np \cos\theta \sin\phi \, \bar{a}_\theta \quad ; \quad \bar{N}_\phi = N_p \cos\phi \, \bar{a}_\phi \qquad (3.9)$$

It is possible to calculate the power radiated by the strip and polarisation currents by substituting the value of N_θ, N_ϕ into equation 2.26 to calculate the power radiated. This integral was then evaluated using a numerical integration program based on Simpsons rule for double integrals.

3.2 Radiation from a linear feed.

Since the maximum current in each section of the feed line are equal the contribution to the radiation from each feed line section will add in phase. Since the feed line is long compared to the wavelength the phase contribution from various elements will change rapidly with angular displacement from the normal, given by the space factor of the array. Since the radiation pattern of a λ resonator consists of two lobes either side of the normal, the radiation pattern of set of λ resonators can be calculated.

From equations 3.4 the maximum current in each $\lambda/2$ open circuit resonator is given by $I_r = V_l/Z_{or}$, while the maximum current in the λ feed line is given by $I_{max} = V_l/Z_{of}$. Where, I_r is the maximum current in the resonator, I_{max} is the maximum current in each λ feed line section, Z_{or} is the characteristic impedance of the resonator, Z_{of} is the characteristic impedance of the feeder.

For a microstrip antenna comprising of 6 radiating elements fig 3.2, each having a radiation impedance of 1800Ω fed by a microstrip feeder of characteristic impedance 100Ω fabricated on a substrate of thickness 16mm and permittivity 2.55, the maximum current in the radiating elements and the feed line sections are equal.

By applying the equations detailed in Section 2.1 the radiation from the $\lambda/2$ radiating elements is calculated. Similarly, by applying the equations detailed in Section 3.1 the cross polar radiation from the λ feed sections is calculated.
The power radiated by the feed line sections is only 8 dB below the power radiated by the radiating elements of the system.

3.3 Feed line radiation from corporate antennas.

Combining patch antennas to form a two dimensional composite array is a natural progression from a single feed. A two-dimensional array of patch resonators has been described by Derneryd [4], fig 3.3. A 4 x 4 element planar array was formed by feeding four linear arrays in parallel. This construction allows two orthogonal feeding networks to be used to obtain horizontal or vertical polarisation.

A high gain modular antenna was designed by Murphy [5] for the SEASAT satellite. This antenna consisted of groups of radiating elements arranged into sub-groups. A 2 X 2 patch array is a sub group of a 4 X 4 array which in turn forms part of a larger group. This modular design approach may be used to design large antenna arrays.
By selecting a four element group from the composite array, the directive gain and radiation impedance of the patches can be calculated. A reasonable approximation to the magnitude of the feeder radiation can be achieved by separating the feed network into orthogonal segments and calculating the radiated power from each segment.

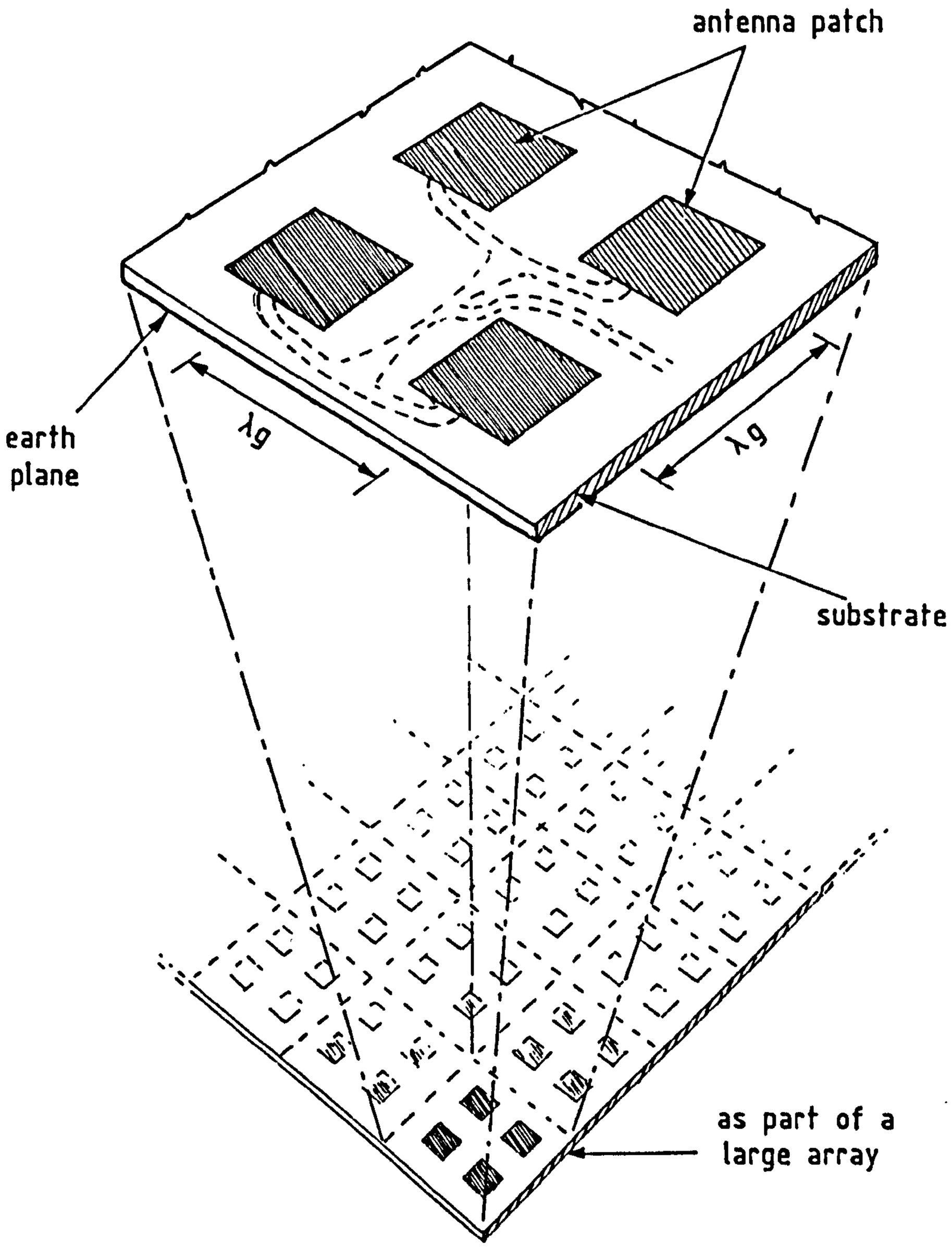

Figure 3.3. Corporate feed radiation from microstrip patch arrays.

Each segment feeder segment is then analysed as a loss free centre-fed transmission line, matched at both ends, which supports a travelling wave current from the centre of the feed line to the left and right patches. The current distribution along the feed line is assumed to be concentrated along the centre of the strip. The power radiated from the segment is then calculated from this approximate current distribution by a systematic application of the Poynting vector. For a modular patch antenna fed by 100Ω microstrip feed lines the cross polar radiation is only 8db down on the main lobe radiation. While, for the same patch antenna fed by 200Ω feed lines the cross polar radiation is 11db less than the main lobe. However, 200Ω feed lines are difficult to fabricate and greatly increase the ohmic losses within the array.

3.4 Methods of reducing feeder radiation.

It was shown in chapter 2 that the radiated power from a microstrip line is directly proportional to the substrate height and inversely proportional to the substrate permittivity and characteristic impedance.

Thus, the radiating elements should be fabricated on a thick, low permittivity substrate to maximise radiation, while conversely an above-ground feeder needs to be fabricated on a thin, high permittivity substrate to minimise feeder radiation. However, the use of thin, high impedance feed lines leads to greatly increased feeder losses.

One method of reducing the feeder radiation is to embed the feed line in a multilayer substrate and to capacitively couple the feed line to the radiating element, fig 3.4 . By using a multilayer structure the height of the microstrip feeder is substantially less than that of a conventional coplanar feed and results in greatly reduced feeder radiation, at the cost of greatly increased complexity during fabrication. A major problem with this type of array is the difficulty in calculating the antenna characteristics of the array.

3.5 Balanced line feeders

In order to fabricate the radiating elements and a coplanar feed network on a single substrate of uniform thickness an alternative feed arrangement leading to a cancellation of feeder radiation is required. For a microstrip feed line, it can be seen that the current in the strip, and its image are in anti-phase, and this leads to some cancellation of the radiation from the microstrip line. However, better cancellation will occur if two strip lines are configured as a balanced line with an earth plane, and operated in the odd mode, fig 3.5 .

The "coupled line" configuration consists of two transmission lines placed parallel to each other, in close proximity. In such cases there is a continuous coupling between the electromagnetic fields of the two lines. Because of the coupling of electromagnetic fields, a pair of coupled lines can support independent modes of propagation. These modes generally have different characteristic impedances and phase velocities. A good balun is required to selectively excite odd mode propagation along the line. The current distribution across the balanced line is assumed to be concentrated at the inner edges of the two coupled strips.

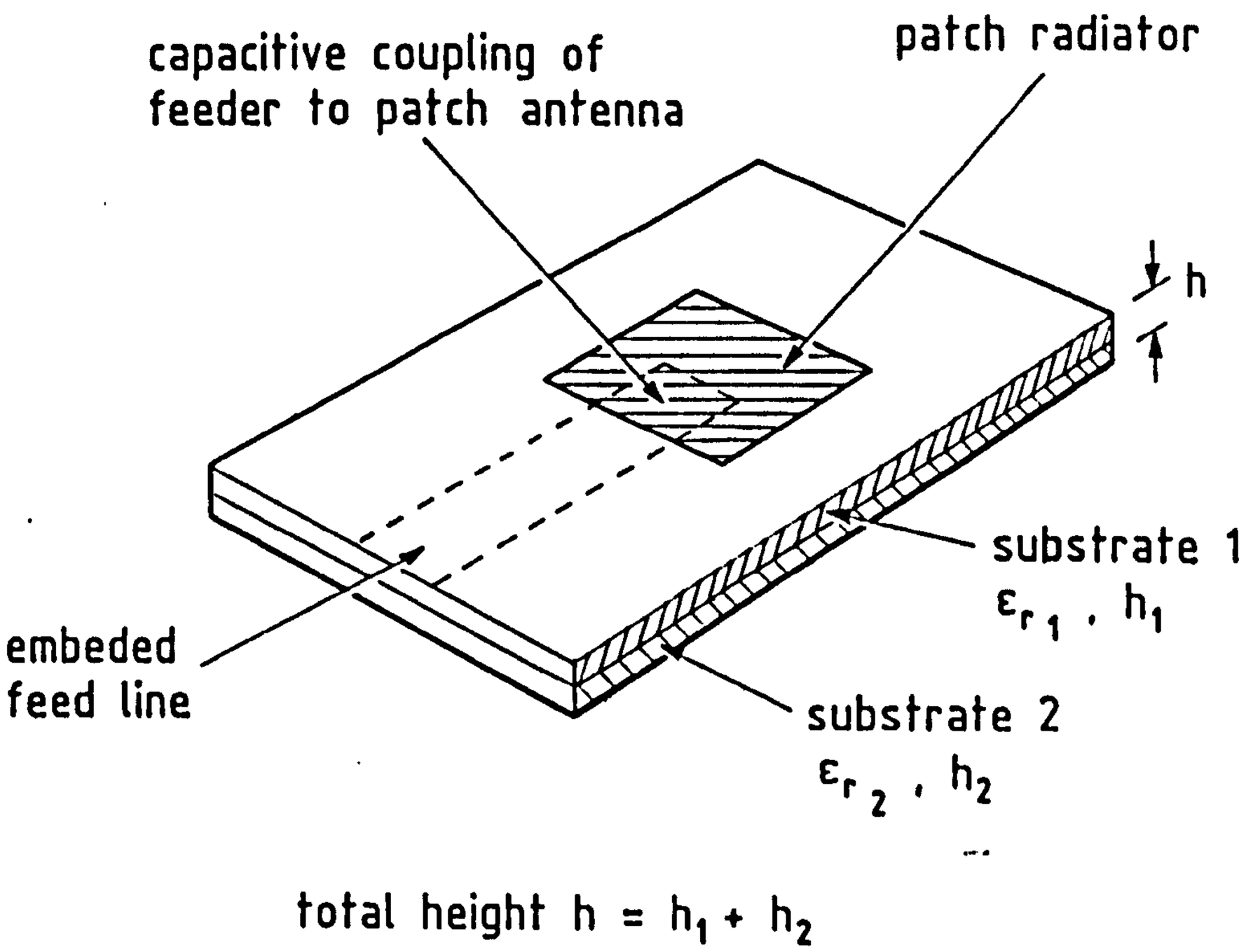

total height $h = h_1 + h_2$

Figure 3.4. Microstrip patch antenna with embeded microstrip feeder.

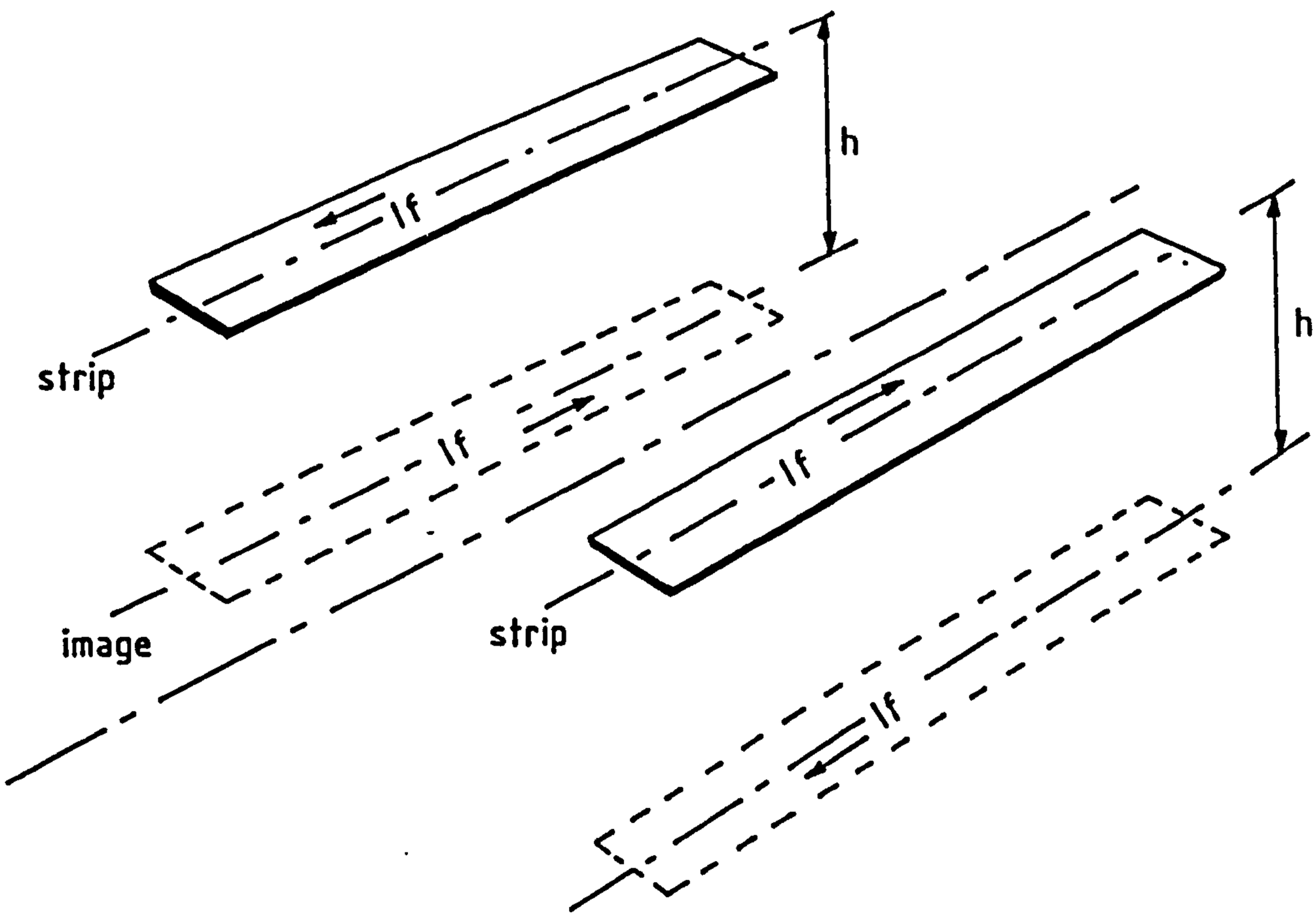

Figure 3.5. Currents in balanced line and image.

3.5.1 Dipole radiating elements.

In order to obtain a balanced load for push-pull line, two half-wavelength resonators are placed on opposite sides of the balanced line fig 3.6 . The simplifying assumptions outlined in section 2.2 for half-wavelength resonator can be used to calculate the far field radiation from a λ dipole, assuming that the separation between the two $\lambda/2$ elements is negligible.

The strip radiation vector $\bar{N}_s$ for the λ dipole is given by :-

$$\bar{N}_s = -8\ j\sqrt{\epsilon_e}\, I_m \frac{\sin(kh\sin(\Theta)\sin(\phi))}{k(\epsilon_e - \cos^2\Theta)} \cos\left\{\frac{\pi\cos(\Theta)}{\epsilon_e}\right\} \bar{a}_z \qquad (3.10(a))$$

(A.m)

Since current only flows along one axis :-

$$N_\Theta = -N_s \sin(\Theta)\,\bar{a}_\Theta \quad ; \quad N_\phi = 0$$

The simplifying assumptions which were used to calculate the polarisation radiation for the $\lambda/2$ resonator in section 2.2 can also be used to calculate the polarisation radiation vector $\bar{N}_p$ for a λ feed line section.

$$\bar{N}p = -8\ j\ h\ Im\sqrt{\epsilon_e}\ \frac{(\epsilon_e - 1)}{\epsilon_e}\cos(\Theta)\ \cos\left\{\pi\frac{\cos(\Theta)}{\epsilon_e}\right\}\bar{a}_y \qquad (3.10(b))$$

$$(\epsilon_e - \cos^2\Theta)$$

(A.m)

The components of $\bar{N}_p$ in the Θ and φ directions are given by :-

$$\bar{N}_\Theta = N_p\cos\Theta\sin\phi\,\bar{a}_\Theta \quad ; \quad \bar{N}_\phi = N_p\cos\Theta\,\bar{a}_\phi$$

The total power radiated can be obtained by integrating the power density over the half-hemisphere above the dipole (Appendix 1).

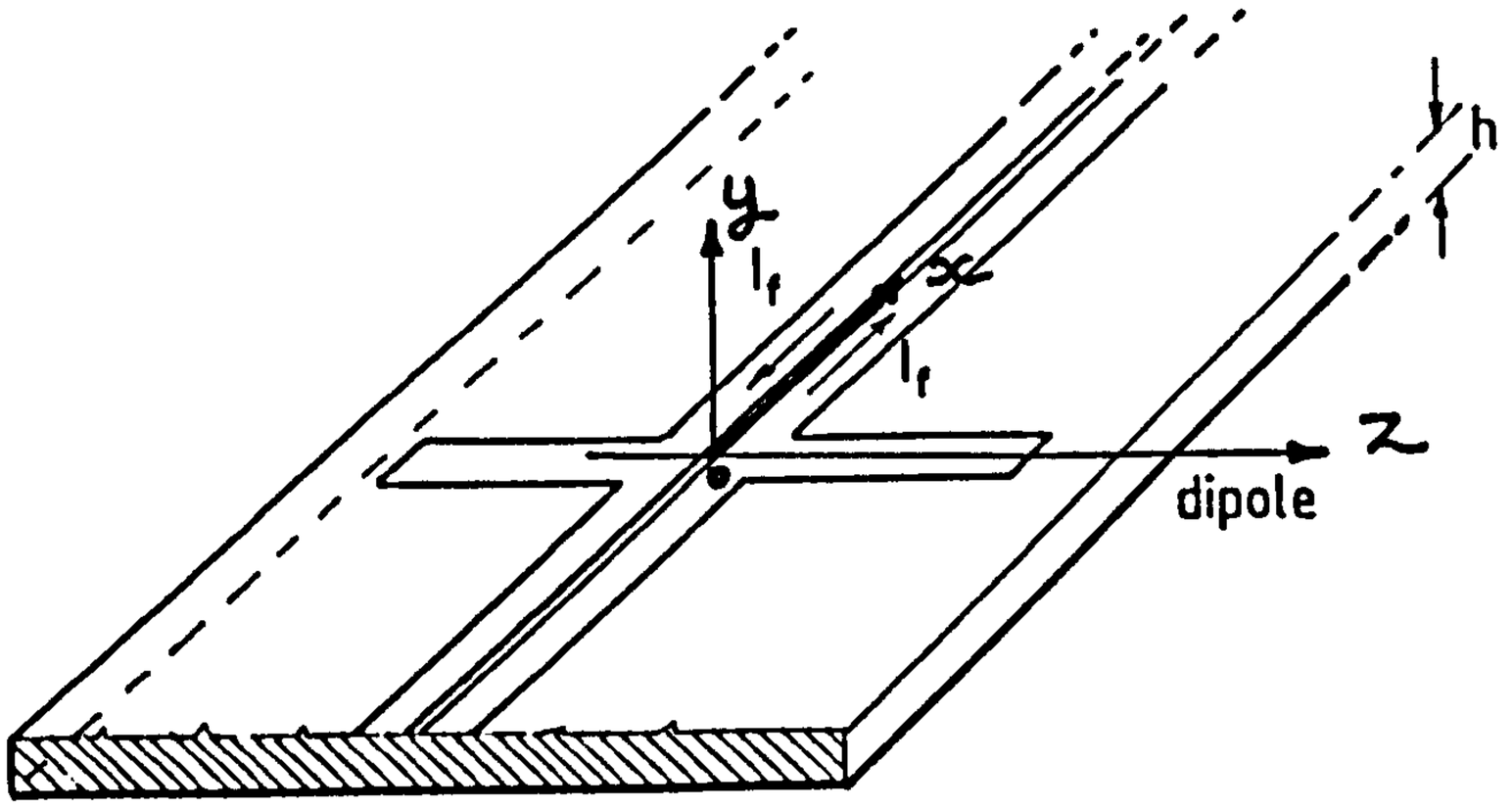

Figure 3.6. λ dipole fed by balanced line feeder.

3.6 Evaluation of balanced line feeder radiation.

The reduction in feeder radiation for a balanced line when compared with a single strip unbalanced feeder can be verified theoretically for a half-wavelength balanced line section, by taking a simple rectangular model of the structure, fig 3.7 and calculating the power radiated using the method described in section 2.2 [6].

The following assumptions are made for the balanced line :-

1) Strip and image currents are assumed to be concentrated along a line somewhere between the centre and inner edge of the strip.

2) The dielectric polarisation currents are considered to be concentrated in planes normal to the ground plane and containing the current axis of the strip. Components of polarisation current normal to the plane are considered to be small.

3) Sinusoidal distribution of current along the strip is assumed. End effects are thereby neglected, but may be reasonably be taken into account by taking the effective length ($\lambda_g/2$) rather than the physical length of the resonator.

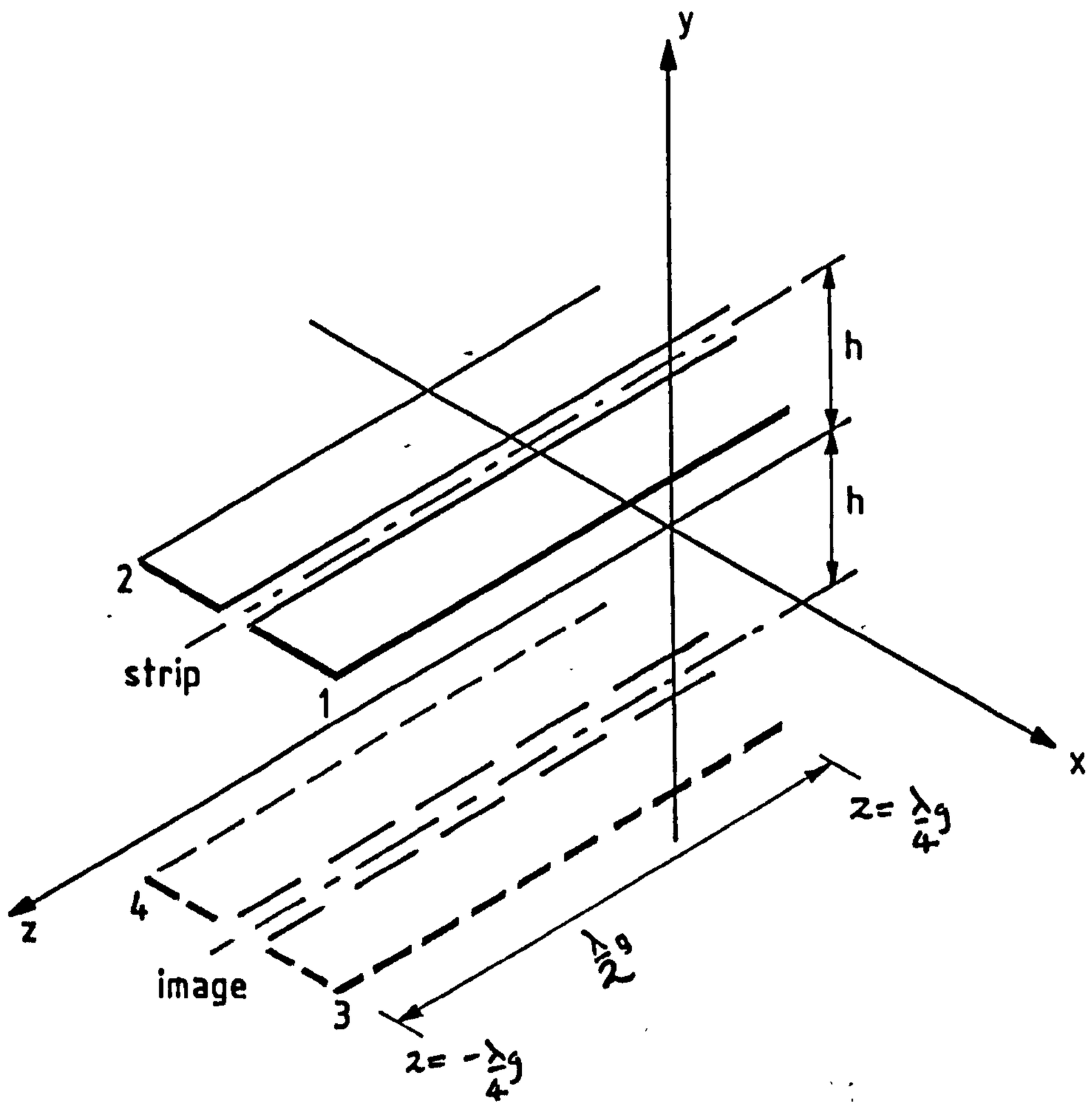

Figure 3.7. Coordinates of resonator.

✳

$$r' \cos\psi = z\cos\theta + \sqrt{h^2+w^2}\,\sin(\theta)\cos(\varphi - \varphi')$$

$$= z\cos\theta + \sqrt{h^2+w^2}\,\sin(\theta)\left\{ \frac{w\cos\varphi}{\sqrt{h^2+w^2}} + \frac{h\sin\varphi}{\sqrt{h^2+w^2}} \right\}$$

$$= z\cos\theta + w\sin(\theta)\cos(\varphi) + h\sin(\theta)\sin(\varphi) \qquad (3.16)$$

✳ (3.16 (a))

$$\bar{N}_s = \int_{-\frac{\lambda_g}{2}}^{\frac{\lambda_g}{2}} I_m \cos(k'z)\, e^{(jkz\cos\theta + jkw\sin(\theta)\cos(\varphi) + jkh\sin(\theta)\sin(\varphi))}\bar{a}_z\, dz$$

$$+ \int_{-\lambda_g/2}^{\lambda_g/2} I_m \cos(k'z)\, e^{(jkz\cos\theta - jkw\sin(\theta)\cos(\varphi) + jkh\sin(\theta)\sin(\varphi))}\bar{a}_z\, dz$$

$$+ \int_{-\lambda_g/2}^{\lambda_g/2} I_m \cos(k'z)\, e^{(jkz\cos\theta + jkw\sin(\theta)\cos(\varphi) - jkh\sin(\theta)\sin(\varphi))}\bar{a}_z\, dz$$

$$+ \int_{-\lambda_g/2}^{\lambda_g/2} I_m \cos(k'z)\, e^{(jkz\cos\theta - jkw\sin(\theta)\cos(\varphi) - jkh\sin(\theta)\sin(\varphi))}\bar{a}_z\, dz$$

$$\bar{N}_s = \int_{-\frac{\lambda_g}{2}}^{\lambda_g/2} I_m \cos(k'z)\, e^{(jkz\cos\theta)}\left\{ \left[e^{(jkw\sin(\theta)\cos(\varphi))} - e^{(-jkw\sin(\theta)\cos(\varphi))} \right] \left[e^{(jkh\sin(\theta)\sin(\varphi))} - e^{(-jkh\sin(\theta)\sin(\varphi))} \right] \right\}\bar{a}_z\, dz$$

$$\bar{N}_s = -4\sin(kw\sin(\theta)\cos(\varphi))\sin(kh\sin(\theta)\sin(\varphi)) \int_{-\frac{\lambda_g}{2}}^{\frac{\lambda_g}{2}} I_m \cos(k'z)\, e^{(jkz\cos\theta)}\bar{a}_z\, dz$$

53

The strip current (1), (2) will give rise to the following

$$i_z\,dz = I_m \cos(k'z)\,dz \qquad (3.11)$$

$$x = w \;,\quad y = h$$

and

$$i_z\,dz = -I_m \cos(k'z)dz \qquad (3.12)$$

for $x = -w \;,\quad y = h$

$$-\frac{\lambda_g}{4} < z < \frac{\lambda_g}{4}$$

$$k' = \frac{2\pi}{\lambda_g}$$

and the images in the ground plane (3), (4):

$$i_z\,dz = -Im \cos(k'z)dz \qquad (3.13)$$

$$x = w \;,\quad y = -h$$

and

$$i_z\,dz = Im \cos(k'z)dz \qquad (3.14)$$

$$x = -w \;,\quad y = -h$$

Consider an element on strip (1), the radiation vector N is given by :-

$$\bar{N} = \int_v \bar{i} \exp(Jkr'\cos\psi)\;\partial\, V \qquad (3.15)$$

For strip(1), $r'\cos\psi$ is given from equation 3.15 by :

$$r'\cos\psi = z\cos\theta + w\sin(\theta)\cos\phi + h\sin(\theta)\sin\phi \qquad (3.16)$$

This expression is also valid for current elements on (2), (3) and (4) using the correct signs for w and h given above.

* (3.16 (a))

Substituting the respective values of $\bar{i}$ and $r'\cos\psi$ in equation 3.15 and summing for both strips and image gives :-

$$\bar{N}_s = A \int_{-\frac{\lambda}{4}g}^{\frac{\lambda}{4}g} I_m \cos(k'z) \exp(Jkz\cos\theta)\,\bar{a}_z\,dz \qquad (3.17)$$

$$x = 0 \;,\; y = 0$$

$\bar{a}_z$ is a unit vector in the z direction.

54

where

$$A = -4 \sin(kw \sin(\theta) \cos\phi) \sin(kh \sin(\theta) \cos\phi) \qquad (3.18)$$

therefore

$$\bar{N}_s = \frac{2 A I_m \sqrt{\varepsilon_e}}{k(\varepsilon - \cos^2\theta)} \cos\left\{ \cos\theta \cdot \left[\frac{\theta}{2\sqrt{\varepsilon}} \right] \right\} \bar{a}_z \qquad (3.19)$$

(A.m)

there is no component of $\bar{N}_s$ in the ϕ direction

$$\bar{N}_\theta = - N_s \sin\theta \, \bar{a}_\theta \qquad (3.20)$$

The dielectric polarisation current gives rise to the following elements, fig 3.8 :

$$i_y \, dz = - 2h \left\{ \frac{\varepsilon_r - 1}{\varepsilon_r} \right\} I_m \, k' \sin(k'z) \, dz \qquad (3.21)$$

and

$$i_y \, dz = 2h \left\{ \frac{\varepsilon_r - 1}{\varepsilon_r} \right\} I_m \, k' \sin k'z \, dz \qquad (3.22)$$

with

$$r' \cos\psi = z \cos\theta + w \sin(\theta)\cos\phi \qquad (3.23)$$

Substituting in equation 3.15 :

$$\bar{N}_p = JB \int_{-\frac{\lambda}{4}g}^{\frac{\lambda}{4}g} \sin(k'z) \exp(jkz\cos\theta)\bar{a}_y dz \qquad (3.24)$$

$x = 0 \, , \; y = 0$

where

$$B = - 4h \left\{ \frac{\varepsilon_r - 1}{\varepsilon_r} \right\} I_m \, k' \sin(kw \sin\theta \sin\phi) \qquad (3.25)$$

Which integrates to give :-

$$\bar{N}_p = 2 B \sqrt{\varepsilon} \, \frac{\left\{ \frac{(\varepsilon_r - 1)}{\varepsilon_r} \right\}}{k'(\varepsilon - \cos^2\theta)} \cos(\theta) \cos\left[\pi \frac{\cos\theta}{2\sqrt{\varepsilon}} \right] \bar{a}_y \qquad (3.26)$$

(A.m)

$\bar{a}_y$ is a unit vector in the z direction.

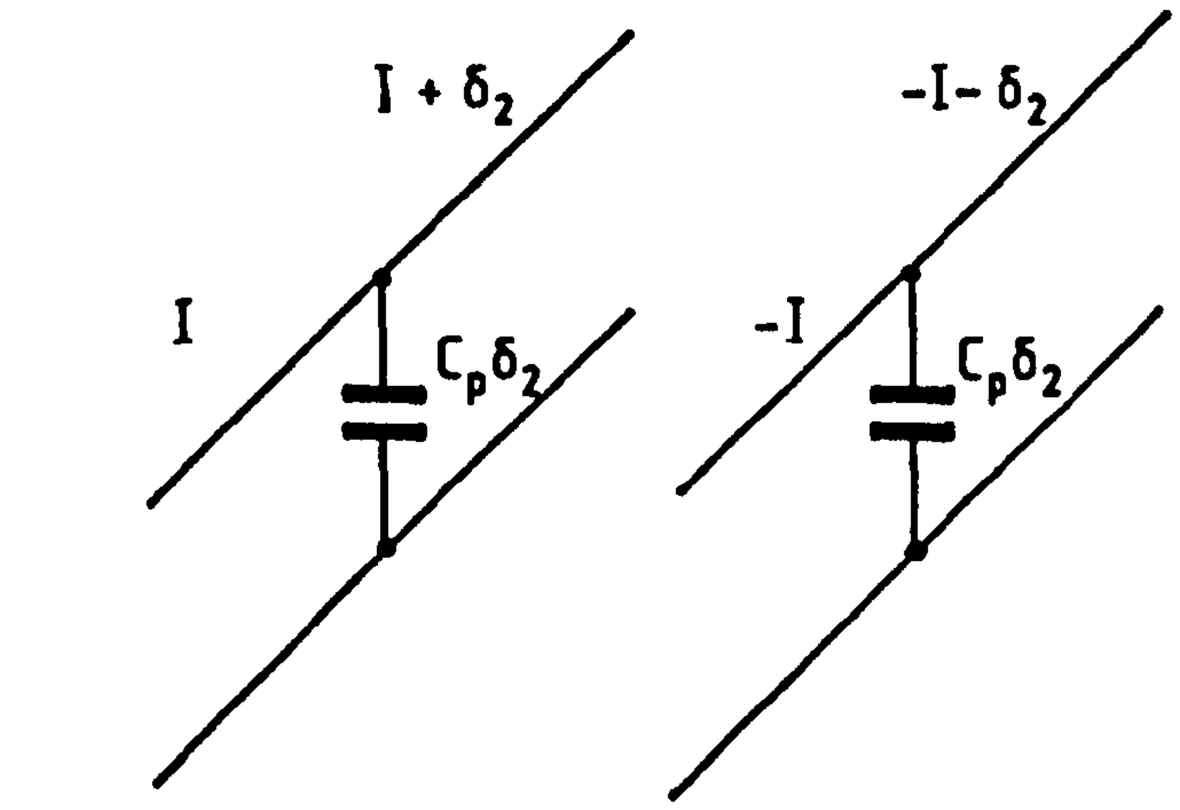

(a)

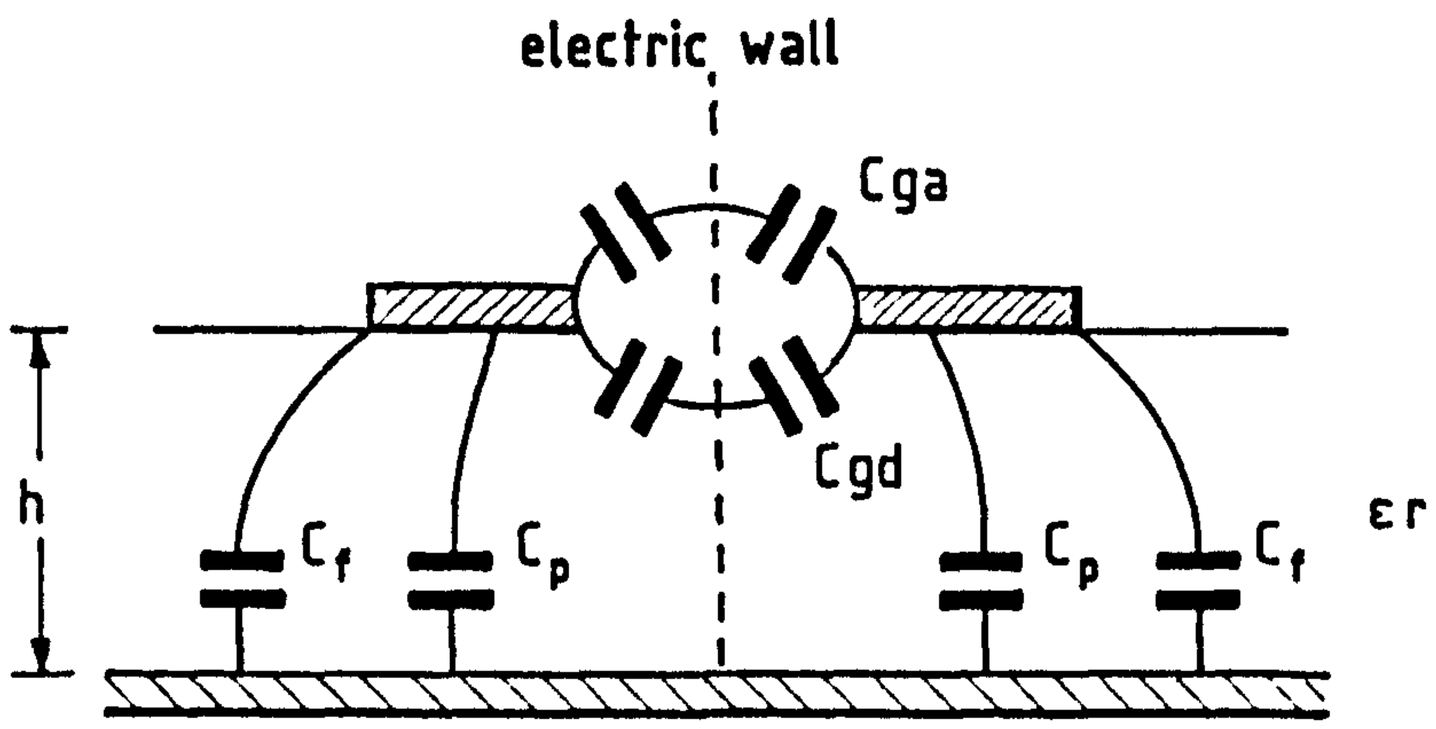

(b)

Figure 3.8. (a) Polarisation current.
(b) Decomposition of odd mode capacitance in coupled microstrip line.

The Θ and φ components of the polarisation vector $\bar{N}p$ are given by :-

$$\bar{N}_\theta = N_p \cos\theta \sin\phi \, \bar{a}_\theta \; ; \qquad \bar{N}_\phi = N_p \cos\phi \, \bar{a}_\phi \qquad (3.27)$$

The total power radiated is obtained by integrating the power density over the hemisphere above the ground plane :

$$P_r = \frac{\eta}{8 \lambda_0^2} \int_0^{\pi} \int_{-\frac{\pi}{2}}^{\frac{\pi}{2}} \left[|N\theta|^2 + |N\phi|^2 \right] \sin(\theta) \, \partial\theta \, \partial\phi \quad (W) \qquad (3.28)$$

$$-\frac{\pi}{2} < \varphi < \frac{\pi}{2}$$

This integral can be evaluated using the numerical integration program (appendix 1).

Experimental antennas were fabricated from CuClad 250 type Gt-0625-50-11, with a substrate height of 1.6mm and a permittivity of 2.55 . The measured and theoretical performance of representative unbalanced and balanced arrays is summarised in fig 3.9 . The unbalanced microstrip antenna comprised of 10 $\lambda/2$ resonant elements on alternate sides of a 100Ω microstrip feed line at $\lambda/2$ spacing. The balanced line array consisted of 10 pairs of $\lambda/2$ elements forming a λ dipole at λ spacing along a balanced line feed. It can be seen that the feed radiation for the balanced line antenna is much less than the feed radiation from a microstrip feed line.

Measurement conditions	No. of $\lambda/2$ elements	Theoretical gain	Measured cross polarisation	Measured gain
Microstrip fed antenna	10	14.5	7 dB	13.5
Balanced line	12	15	1 dB	14

Figure 3.9. Theoretical and measured radiation and cross polarisation.

3.7 Estimation of feeder loss.

The dissipative losses associated with microstrip lines is a major limitation of microstrip antenna. The overall loss in microstrip is generally assumed to be associated with conductor and dielectric loss. It is not unusual for half the input power in a large antenna array to be dissipated within the feeder. A major problem with microstrip antenna is to find methods of reducing this loss while retaining the geometrical simplicity of a coplanar feed. This loss has only a second order effect on the feeder radiation mechanism, and the existing loss equations are adequate for antenna design.

3.7.1 Conductor loss.

Conductor loss is the most significant loss effect over a wide frequency range, due to the high current density in the edge region of the conducting strip. The loss due to the finite conductivity in the strip and ground plane of the microstrip can be calculated if the current distributions in the conductor and the resistivity of the conductor are known. Some authors [6,7] have assumed a uniform current distribution over the strip to give :-

$$\alpha_c = \frac{8.68\ R_s}{w\ Z_m} \quad db/m \qquad (3.29)$$

and

$$Rs = \sqrt{\frac{\pi f \mu}{\sigma_c}} \qquad (3.30)$$

where

R_s is the surface resistivity ($X\ /\square$)

w is the strip width.

Z_m is the strip impedance.

σ_c is the conductivity of the copper.

This formula overestimates the theoretical loss by 80% and more accurate estimate was determined by Pucel et al [7] using Wheeler's [8] 'incremental inductance rule'.

3.7.2 Dielectric loss.

The calculation of dielectric loss involves the extensive use of numerical techniques. A crude approximation by Welch [9] following an approach by Wheeler [8] has been developed. However an adequate formula for low loss dielectrics is given by Schneider [10] :-

$$\alpha_d = \frac{27.3\ \varepsilon_r(\varepsilon_e - 1)\ \tan\delta}{\lambda_m \varepsilon_e\ (\varepsilon_r - 1)} \quad {}^{db}/_{cm} \qquad (3.31)$$

where,

λ_m is the wavelength in microstrip.

δ is dielectric lóss tangent.

Assuming a reasonable quality thin substrate, the dielectric attenuation constant is small when compared with the conductor attenuation constant, and is usually ignored in the antenna design.

3.7.1 Losses in Coupled line.

A great deal of work has been published on losses in coupled lines. However very little practical data exists to verify this literature. The losses are evaluated in term of odd and even mode attenuation constants. These can be calculated using Wheeler's incremental inductance rule [8]. As with single microstrip lines, the most significant course of loss is conduction loss. Some work has been published on methods of calculating the losses due to the conduction of the odd and even mode microstrip. Davies [11] computer programs 'ZERO1' and 'ZERO2' (Appendix 2) have been used to calculate these losses. 'ZERO1' computes the effective dielectric and propagation constant, while 'ZERO2' determines the characteristic impedance, conduction loss and dielectric loss for low loss substrates using a perturbation formula.

In practice the losses derived by these programs tend to be 80% higher than the measured loss, but can be accepted as an approximation until more reliable data is obtained.

3.8 Conclusions.

The balanced line feeder can significantly reduce cross polar radiation when compared with a single strip unbalanced feeder. This reduction in feeder radiation is due to the relatively close proximity of the oppositely directed currents in the coupled strips. Reducing the strip separation decreases the feeder radiation, but increases the attenuation of the balanced line. Additional losses are introduced by the use of a balun, and these losses are investigated in latter chapters.

REFERENCES FOR CHAPTER 3.

[1] Williams J.C.,
Cross-fed printed aerials,
Proc 7th European Microwave Conf, Copenhagen,
page 292 - 296, 1977 .

[2] Lewin L.,
Radiation from discontinuities in strip-line.
IEEE Monograph No 358 E, Feb. 1960

[3] Roberts J.R.,
An investigation into the application of microwave integrated circuits,
Ph.D thesis, U.C.N.W., Bangor, 1971 -Microstrip Resonators.

[4] Derneryd A.G.,
Linearly Polarised Microstrip Antenna's,
IEEE trans AP-24, page 846 - 851, 1976.

[5] Murphy L.R.,
SEASAT and SIR - A microstrip antenna's,
Proc. workshop on printed antenna technology,
New Mexico State University, U.S.A, page 18 - 21, 1981.

[6] Watkins J.,
Radiation loss from open circuit dielectric Resonators,
IEEE trans MTT - 21, page 636 - 639, 1973.

[7] Pucel R.A., Massey P., Hartwig C.P.,
Losses in Microstrip, IEEE trans. MTT - 16,
page 342 - 350, 1980

[8] Wheeler H.A.,
Transmission line properties of parallel strips separated by a dielectric sheet, IEEE trans. MTT - 12, page 280 - 288, 1964 .

[9] Welch J.D. & Pratt H.J.,
Losses in microstrip transmission systems for integrated microwave circuits, NEREM Rec. 8, page 100, 1966 .

[10] Schneider M.V.
Microwave and Millimetre wave hybrid integrated circuits for radio circuits, BSTJ, Vol 48, 1969, page 1703 - 1729.

[11] Davies J.B. & Mirshekar-Syahkal D.,
Spectral domain solution of arbitrary coplanar line with multilayer substrate, IEEE trans. MTT-25, page 143, 1977 .

CHAPTER 4.

4. MEASUREMENT OF RESONATOR LOSS.

The efficiency and bandwidth of an antenna can be described in terms of the circuit concept of Q factor where,

$$Q = 2\pi \frac{\text{Energy Stored}}{\text{Energy loss per cycle}} \qquad (4.1)$$

The power absorbed by the resonant antenna includes power dissipated in the loss mechanism as well as the power radiated in the far field. These mechanisms included conductor loss Pc in the stripline conductor and dielectric loss Pd in the substrate.

$$P_t = P_r + P_c + P_{sw} \qquad (4.2)$$

The power loss due to surface waves Psw is assumed to be negligible for thin, low permittvity substrates [1].

The total Q factor for the resonator is given by :-

$$\frac{1}{Q_t} = \frac{1}{Q_r} + \frac{1}{Q_c} + \frac{1}{Q_d} \qquad (4.3)$$

where,

Q_t is the total Q factor

Q_r is the radiation Q factor

Q_c is the Q factor due to copper loss

Q_d is the Q factor due the dielectric

If the resonator is placed inside a shielded box to suppress radiation, the Q factor inside the box is given by :-

$$\frac{1}{Q_o} = \frac{1}{Q_c} + \frac{1}{Q_d} \qquad (4.4)$$

The dielectric and strip line Q factor's can be approximated by [2] :-

$$Q_d = \frac{(\varepsilon_r - 1)\ \varepsilon_e}{(\varepsilon_e - 1)\ \varepsilon_r} \quad \frac{1}{\tan \delta} \qquad (4.5)$$

and

$$Q_c = 1.26 \quad W_{(mm)}\ Zo\ \varepsilon_e\ f_{(GHz)} \qquad (4.6)$$

where

ε_r is the permittivity of the substrate

ε_e is the effective permittivity of the substrate.

w(mm) is the effective width in mm.

Z_o is the characteristic impedance of the line.

$f_{(Ghz)}$ is the frequency in GIIz.

4.1 Q factor.

If the power radiated, Pr for a half-wavelength resonator can be estimated (Appendix 1), it is possible to relate the radiation loss to a reduction in the unloaded Q factor of the resonator.

$$\frac{1}{Q_r} = \frac{1}{Q_t} - \frac{1}{Q_o}$$

where,

Q_t is the Q factor of an unshielded resonator.

Q_o is the Q factor of the same resonator in a loss free enclosure.

Qr is the radiation Q factor.

The energy stored in a half-wavelength resonator is given by $P_{i/f}$, where Pi is the power incident at each end of the resonator and f is the frequency. The power incident at each end of the resonator P_i is given by :-

$$I_m = \frac{1}{8} |I_m|^2 Z_o \qquad (4.7)$$

Thus

$$Q_t = 2\pi \frac{P_i}{P_r}$$

65

Q_t and Q_o can be measured to determine the power radiated P_r by the half-wavelength open circuit resonator :-

$$\frac{P_r}{P_i} = 2\pi \left[\frac{1}{Q_r} - \frac{1}{Q_t}\right] \qquad (4.8)$$

The radiation efficiency η of the antenna is given by :-

$$\eta = \frac{\text{power radiated}}{\text{total power loss}} = \frac{\frac{1}{2\pi f}\ \text{total power loss - (conductor and diclectric loss)}}{\frac{1}{2\pi f}\ \text{total energy stored}} = \frac{\text{total energy stored}}{\text{total power loss}}$$

$$\eta = \frac{\frac{1}{Q_r}}{\frac{1}{Q_t}} = \frac{\frac{1}{Q_t} - \frac{1}{Q_o}}{\frac{1}{Q_t}} \qquad (4.9)$$

where,

Q_t is the Q factor of an unshielded resonator.

Q_o is the Q factor of the same resonator in a loss free enclosure.

Qr is the radiation Q factor.

4.2 Q factor Measurements.

The radiating and non-radiating Q measurements were undertaken by measuring the complex reflection coefficient of the resonator coupled to the measuring equipment by a small capacitive gap [2], fig 4.1 .

The unloaded Q-factor of the resonator is given by :-

$$Q_o = \frac{f_o}{\Delta f} \qquad (4.10)$$

where,

f is the resonant frequency.

and,

Δf is the frequency band over which the resonator reactance is equal to the resonator resistance.

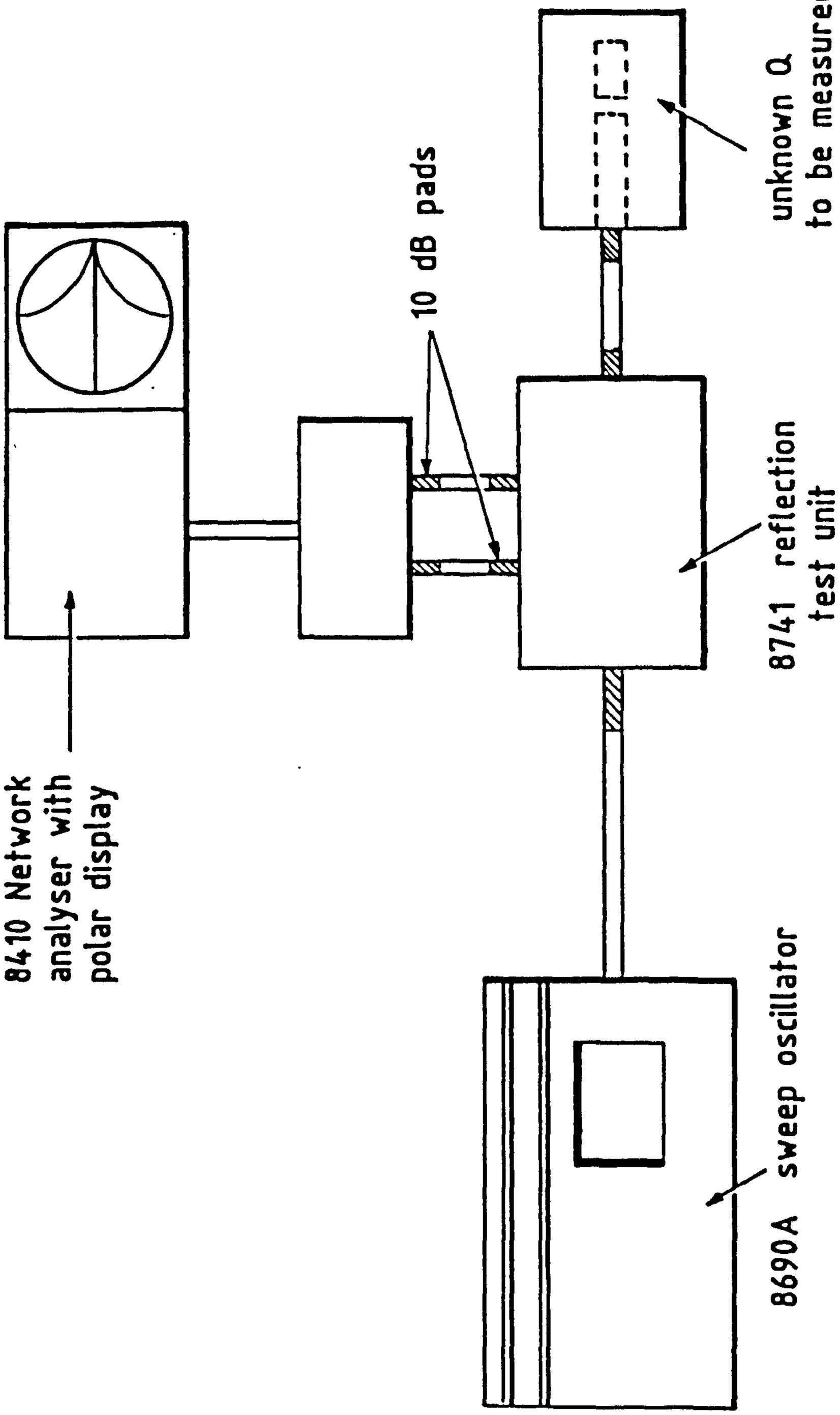

Figure 4.1. Equipment for measuring Q-factors.

The complex reflection coefficient of the gap coupled resonator is plotted against frequency on a smith chart using a network analyser, fig 4.2 . The resonant frequency and the points at which the resonator reactance is equal to the resonator resistance can be obtained from the smith chart using the following procedure :-

1) Set up the network analyser and chart recorder at the unknown port, over the frequency range in question.

2) Connect the resonator to the unknown port, and move the reference plane on the reflection test unit to the plane of the coupling gap. Since off resonance the coupling gap will look like an open circuit independent of frequency. The reference plane setting is then adjusted so that the circle obtained lies symmetrically on the smith chart.

3) The gain control on the network analyser is then adjusted, so that off resonance, the circuit appears to be an open circuit, i.e. the gain control is thereby adjusted to allow for losses in the line to the coupling gap.

4) The sweep generator is then set to manual and the resonant and half-power frequencies are measured with a frequency counter.

The greatest measurement accuracy occurs when the resonator is nearly critically coupled.

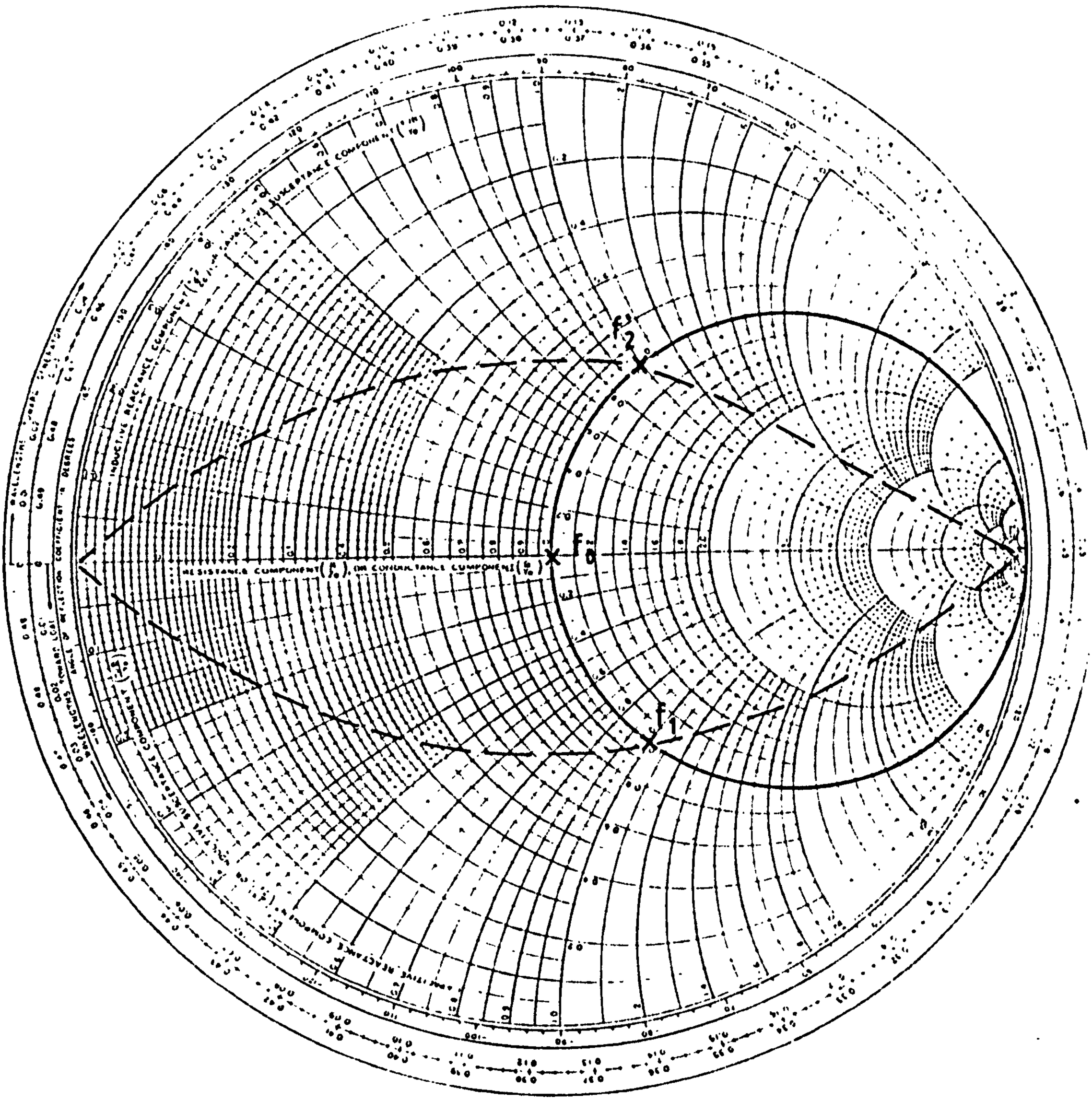

Figure 4.2. Idealised responce of resonator.

For a cavity with sides c > b > a of small depth d, fig 4.3, the resonant frequency of the dominant mode is given by [2] :-

$$f_r = f_o \left[1 - \frac{1}{2} \left\{ 1 - \frac{\varepsilon_2}{\varepsilon_1} \right\} \frac{d}{a} \right] \qquad (4.11)$$

where

$$f_o = \frac{1}{\sqrt{\mu_o \varepsilon_o}} \sqrt{\left[\frac{\pi}{b} \right]^2 + \left[\frac{\pi}{c} \right]^2} \qquad (4.12)$$

This box must be made small enough to avoid cavity resonances, giving increased Q factors but at the expense of unpredictable coupling to the radiating elements. The dimensions found to be most suitable for the cavity are :-

a = 24mm b = 10mm d = 30mm

giving a fundamental, and second resonant frequencies of :-

E101 = 8 Ghz

E102 = 11.8 Ghz

This cavity was milled from brass and fitted into an aluminium housing, which had been used for Q-measurements on 1.6mm thick substrates. Connection to the feed was made via an O.S.M connector fitted to the aluminium housing.

4.2.1 Resonator Radiation Measurements.

A 100Ω open circuit halfwave resonator designed to resonate at 10 GHz was coupled to a 100Ω microstrip line by a capacitive gap of 0.1mm. This resonator was fabricated on a 1.6mm substrate which has a permittivity of 2.55. The physical properties of the strip line from its dimensions was calculated by two programs 'Zero 1' and 'Zero 2' developed by Davies [3].

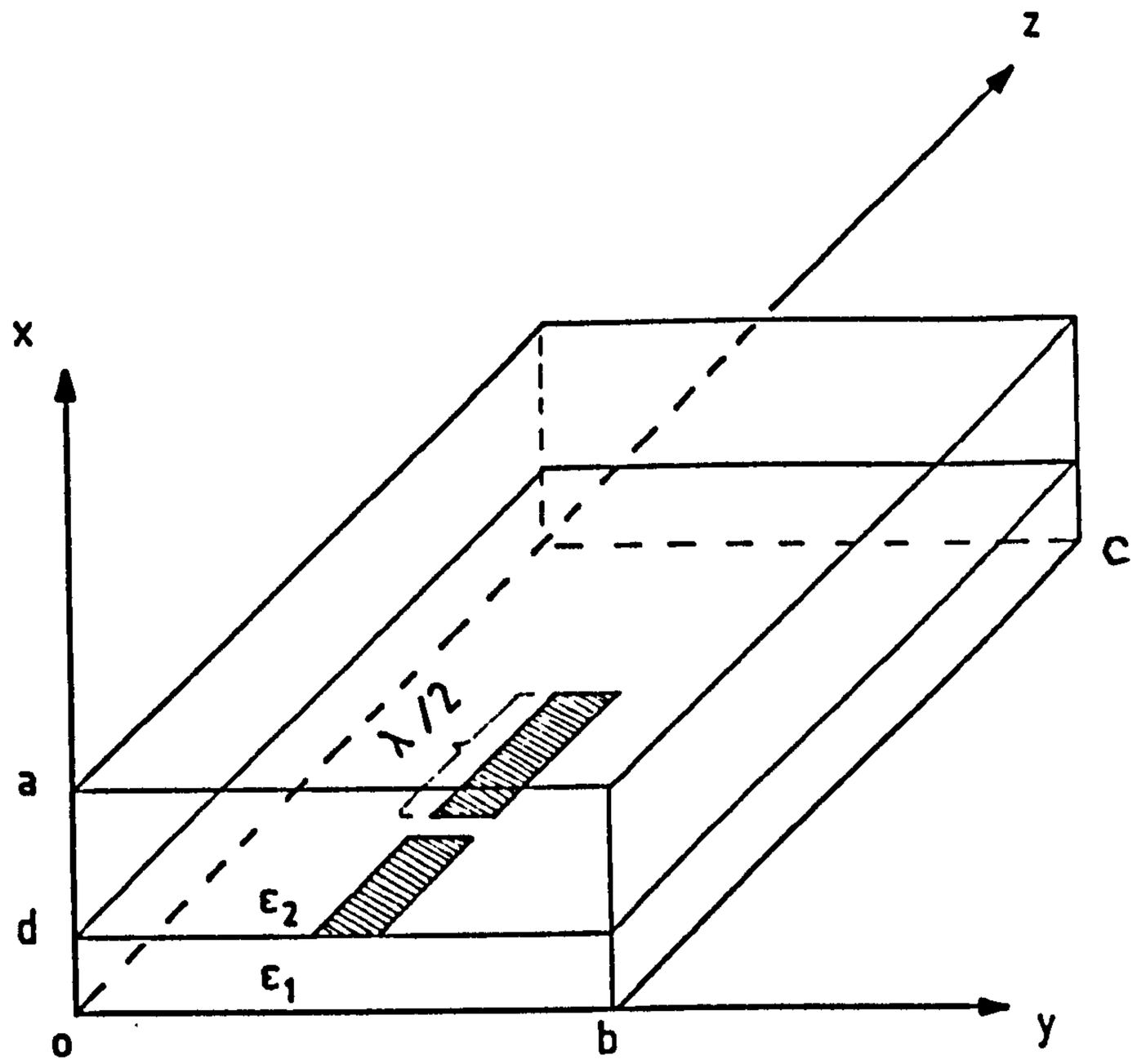

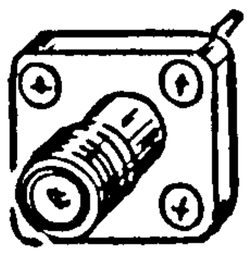

O.S.M.
to microstrip

Figure 4.3. Cavity dimensions.

From Network Analyser measurements it was deduced that the feed line was modifying the radiation from the resonator. In order to investigate this effect a resonator was fed by a capacitive feed from underneath the earth plane to minimise feed radiation. From measurement and theory the radiation impedance of a 100Ω halfwave resonant stub fabricated on a 1.6mm substrate of permittivity 2.55 was 1800Ω .

*

It was difficult to obtain accurate measurements of Qt and Qo when making measurements at X band. So a scaled up easily fabricated model designed to resonate at 1 GHz was constructed. The strip line and ground plane of the scaled up model were made from copper foil fixed to the substrate by an adhesive. The substrate consisted of several layers of Perspex sandwiched together and bolted to a brass plate to minimise the air gap between the sheets. Initial measurements with microstrip resonators fed by microstrip feeds did not agree with the radiation theory. The value of Qo obtained where about half the predicted value,

At first it was thought that the low values of Qt obtained were due to the adhesive between the copper conductor and the substrate, but subsequent investigation showed that the microstrip feeder was radiating energy, reducing the measured radiation Q factors by about 50%. The low values of copper loss and dielectric loss obtained for the shield measurements was due to radiation leakage from the shielded box. After the box had been sealed a more accurate set of readings was obtained. In order to eliminate feed line radiation the halfwave resonator were fed from underneath the substrate by an o.s.m connector. It was then found that the measured radiation from the resonator was in good agreement with the values predicted by Lewin. The results of these measurements are given in fig 4.4, were it can be seen that the general variation of the radiated power is well predicted by theory.

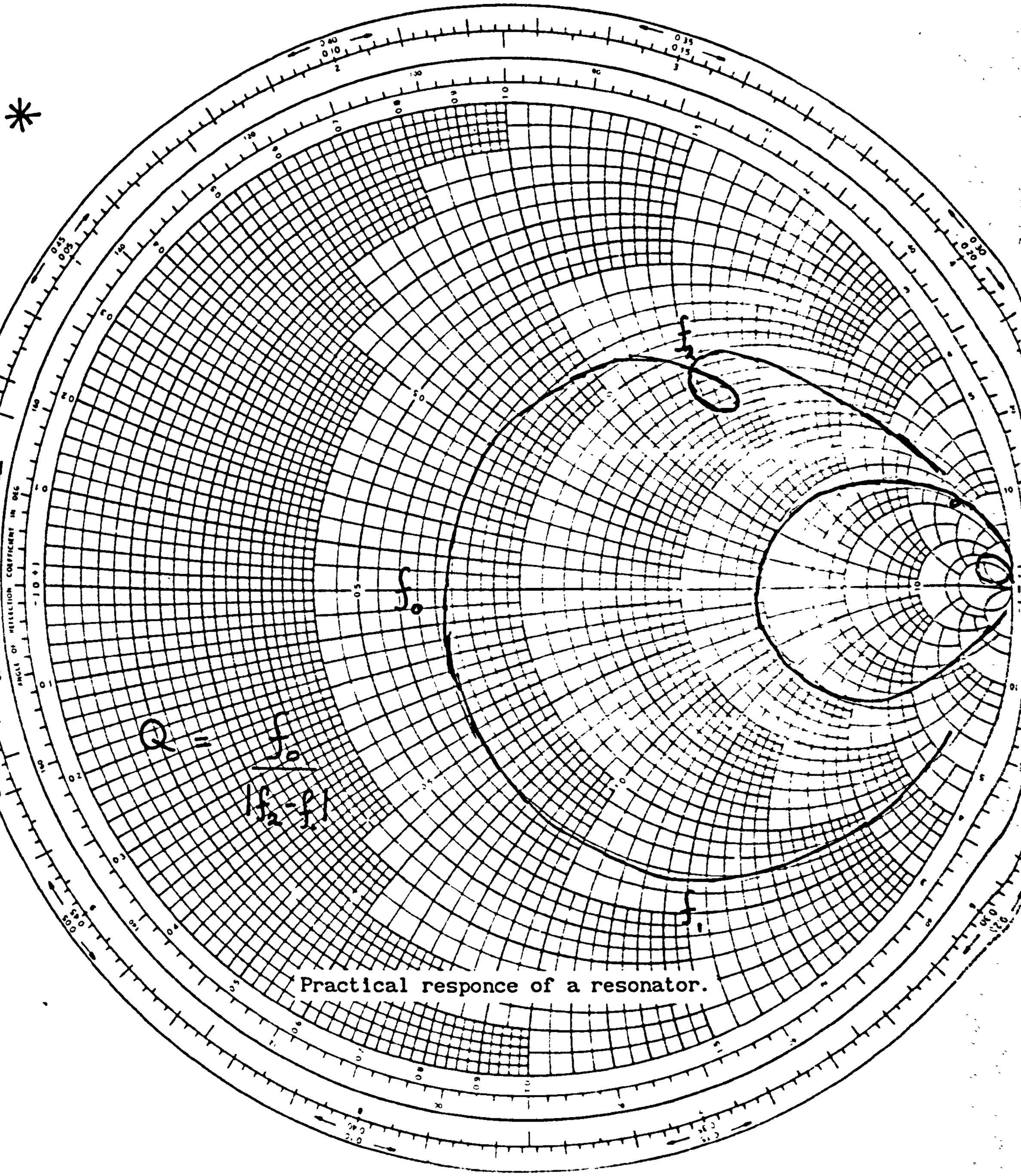

Practical responce of a resonator.

From Network Analyser measurements it was deduced that the feed line was modifying the radiation from the resonator. In order to investigate this effect a resonator was fed by a capacitive feed from underneath the earth plane to minimise feed radiation. From measurement and theory the radiation impedance of a 100Ω halfwave resonant stub fabricated on a 1.6mm substrate of permittivity 2.55 was 1800Ω .

*

It was difficult to obtain accurate measurements of Qt and Qo when making measurements at X band. So a scaled up easily fabricated model designed to resonate at 1 GHz was constructed. The strip line and ground plane of the scaled up model were made from copper foil fixed to the substrate by an adhesive. The substrate consisted of several layers of Perspex sandwiched together and bolted to a brass plate to minimise the air gap between the sheets. Initial measurements with microstrip resonators fed by microstrip feeds did not agree with the radiation theory. The value of Qo obtained where about half the predicted value,

At first it was thought that the low values of Qt obtained were due to the adhesive between the copper conductor and the substrate, but subsequent investigation showed that the microstrip feeder was radiating energy, reducing the measured radiation Q factors by about 50%. The low values of copper loss and dielectric loss obtained for the shield measurements was due to radiation leakage from the shielded box. After the box had been sealed a more accurate set of readings was obtained. In order to eliminate feed line radiation the halfwave resonator were fed from underneath the substrate by an o.s.m connector. It was then found that the measured radiation from the resonator was in good agreement with the values predicted by Lewin. The results of these measurements are given in fig 4.4, were it can be seen that the general variation of the radiated power is well predicted by theory.

Q measurements on half-wavelength microstrip radiating elements.

Measurements conditions	Elements width (mm)	(Radiation loss only)	(Ohmic loss only)	Calculated Q	Measured Q (total loss)
fo = 1 Ghz h = 16 mm er = 2.55	50	8		8	15
	20	18	> 1000	18	17
	10	22		22	25
fo = 1 Ghz h = 16 mm er = 2.55	50	12		12	9
	5	31	> 1000	31	23
fo = 10 Ghz h = 16 mm er = 2.55	4	47	390	42	41
	3	60	360	51	48
	2	75	320	61	72

theoretical values

Figure 4.4. Measurements on half-wavelength microstriip radiating elements.

Radiation Measurements on a Single Dipole.

In order to obtain a balanced load for a 'push-pull' balanced line, two halfwavelength resonators should be placed on opposite sides of the balanced line. For network analyser measurements a single λ dipole was coupled to a microstrip feed line via a small capacitive gap of 0.1mm. The correct phasing of the two half lambda elements was achieved by connecting the two resonators by a 180^0 phase shift line. By bending this line into a hairpin shape the two resonant elements were placed in their correct positions, fig 4.5 .

The hairpin shape ensures that radiation from one side of the hairpin will tend to cancel with radiation from the other side of the hairpin thus minimising the radiation from the phase shift network. In order to feed a single λ dipole the source would have to be matched to a radiation impedance of 900Ω. This match is unrealisable using practical circuit fabrication techniques so multi-element arrays are fabricated.

4.3 Strip line Discontinuities.

Discontinuities in microstrip line are an integral part of microstrip antenna occurring in both the feeder lines and radiating elements. These discontinuities in the feed lines create unwanted radiation which may corrupt the radiation pattern of the antenna.

Numerous papers have been written proposing equivalent circuits and formulas for these discontinuities. However, with the possible exception of open ends and steps in line width there is a shortage of reliable data on which to base these equivalent circuits.

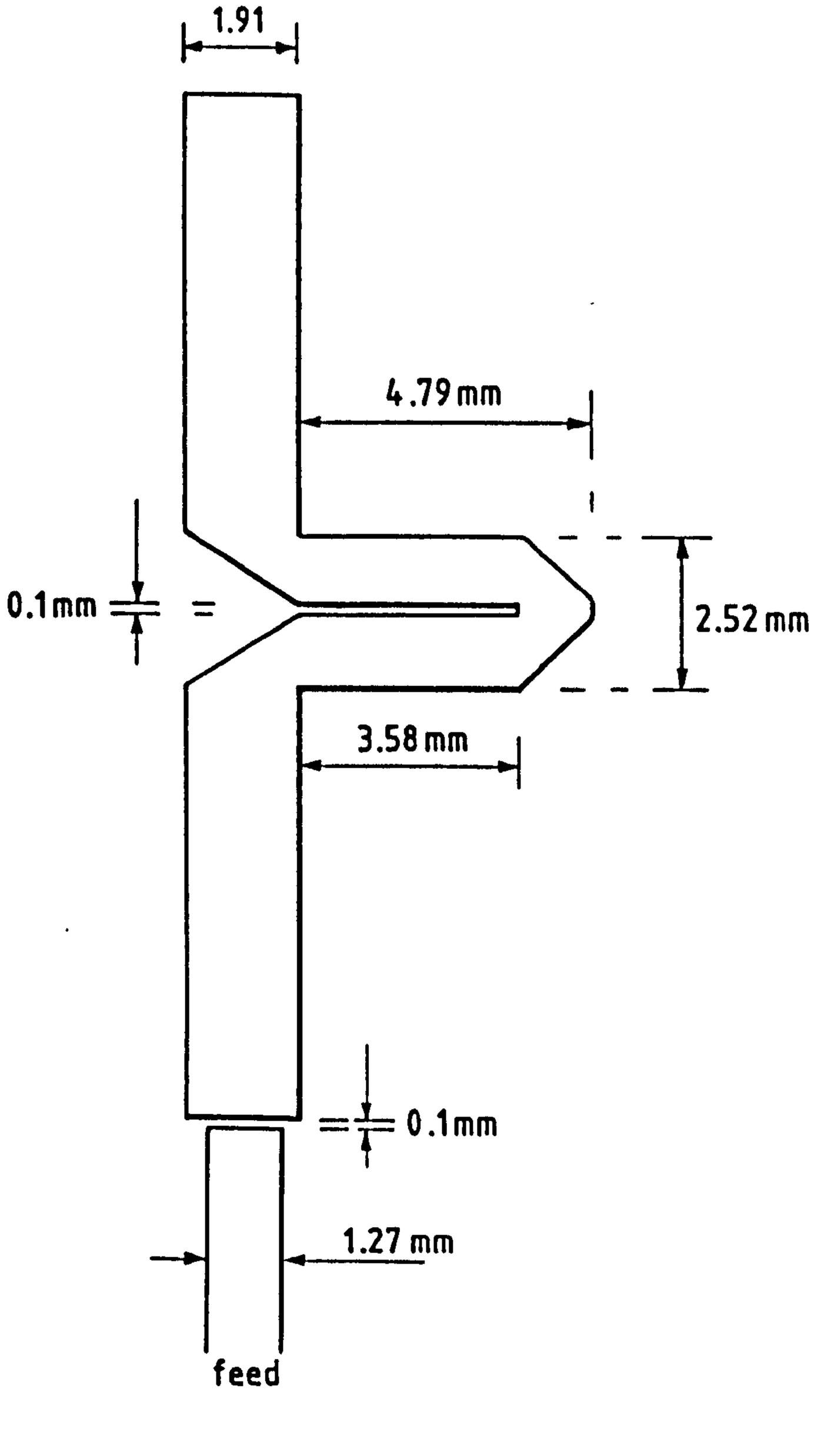

Figure 4.5. A λ dipole to test model.

The open circuit end of a resonator can be represented by a capacitor to ground, or as an excess line length, knowing the capacitance per unit length, both forms are interchangeable.

A closed form extension which can be used to obtain excess line length is given by Hammerstad [4]. While a microstrip gap can be represented by a π network of capacitance. Silvester [5] presented a method of deriving the capacitance values in terms of a symmetrically and asymmetrically gap, C_{even} and C_{odd}. Symmetrical step discontinuities such as a quarterwave transformer have been model by Garg and Bahl [6].

4.3.1 Coupled line discontinuities.

The analysis of a finite open circuit coupled line and the cross coupling to a dipole array is complex to analyse with very little published data on this type of discontinuity. However data for a symmetric step, such as a quarter wave transformer or a Tee-junction has been presented by Garg and Bahl [6]. Hammerstad [7] has since presented an improved model for the symmetric Tee-junction.

4.4 Antenna substrates.

Microstrip antennas are a relatively new application area for microstrip substrates, and only recently has it been possible to obtain high quality, low permittivity substrates. However, good quality substrates are still expensive to obtain. In order to fabricate these antenna arrays at a more economical cost other substrates must be used.

In order to calculate the strip and dielectric loss of the radiating element it is necessary to measure the bulk conductivity of the conductor and the complex permittivity of the copper clad substrate.

4.4.1 Measurement of conductivity.

The conductor loss in a strip line is due to high current densities in the edge region of the thin conducting strip and is related to the conductivity of the copper. Horton [1] has shown that the roughness and thickness of the conductor only has a small effect on conductor loss. The d.c conductivity on a selection of samples was measured using a four point probe and a sensitive voltmeter. A small current is passed through the outer probes and the floating potential is measured on the inner probes [2]. The d.c conductivity of a 30 micron copper coating agreed with the value obtained for bulk copper.

4.4.2 Measurement of dielectric loss.

Dielectric loss associated with tan δ is usually much less than the conductor loss at high frequency, except for poor quality substrates.

In order to measure the permittivity ε' and complex permittivity ε'', a dielectric sample was inserted into a microwave cavity. The loaded and unloaded Q factors of the cavity were then measured.

The relative permittivity ϵ' and the dielectric loss factor ϵ'' of the sample material can be derived by measuring the change in the resonant frequency and Q-factor of the cavity [2]. The cylindrical cavity used for the measurement of the complex permittivity resonates in TE111 mode at a frequency of 9.9 Ghz.

For a thin circular disk placed in the centre of the cavity the frequency shift and 1/Q change in terms of ϵ' and ϵ'' are given by :-

$$\frac{\Delta f}{f} = (\epsilon' - 1)\frac{t\ R}{L} \qquad (4.14)$$

and

$$\Delta\left[\frac{1}{Q}\right] = \frac{2\ t\ R\ \epsilon''}{L} \qquad (4.15)$$

where

t is the sample thickness

L is the length of the cavity

R is a geometrical factor to account for the fact that the electric field is not constant over the face of the disk (2). $R = 0.085$.

4.5 Conclusions.

It was difficult to obtain accurate results due to the feed line radiation. Unloaded Q measurements were difficult to measure accurately due to radiation loss. The Q factor of a microstrip resonator is a complex function of the conductor conductivity, dielectric constant and losses, characteristic impedance, frequency and dielectric thickness. For maximum radiation, low Q can be obtained on thick, low dielectric constant substrates, with low characteristic impedance lines. It should be noted that in thick, low permittivity substrates, the radiation losses dominates, giving values of Qt less influenced by the conductor loss as shown by the copper conductors. In using these results it should be remembered that the side walls can screen the resonator, so reducing radiation.

REFERENCES FOR CHAPTER 4.

[1] Horton R., Easter B., Gopinath A.,
Variation of microstrip losses with thickness of strip.
Electronic Lett., 7, page 490, 1971 .

[2] Ginzton E.L.,
Microwave Measurements, McGraw - Hill, 1975

[3] Davies J.B. & Mirshekar-Syahkal D.,
Spectral domain solution of arbitrary coplanar line with multilayer substrate, IEEE trans. MTT-25, page 143, 1977 .

[4] Hammerstad E.O., Methus, Jensen 0.,
Simulation of microwave components,
ELAB Report STF F80127, 1980 .

[5] Silvester P., Benedict P.,
'Equivalent capacitances of microstrip open circuits',
IEEE trans. MTT-22 , page 857 - 864, 1974 .

[6] Garg R., Bahl I.J.,
Microstrip Discontinuities, Int J. Electronics, 1978,
vol 45, page 81 - 87 .

[[7] Hammerstad E.O.,
Computer aided design of microstrip couplers with accurate discontinuity models, IEEE Int. Microwave Symposium, 1981 .

CHAPTER 5.

5. Microstrip Antennas Design and Testing.

The simplest form of feed system for a linear array is series feeding in which the elements are periodically attached to the feed line. For a standing wave antenna the microstrip feed line is terminated in an open-circuit. The standing wave array consists of half-lamda resonant elements placed at λ intervals along the feed line to produce an co-phase aperture radiating a broadside beam. A co-phase array can also produced by placing halfwave length resonators on alternative sides of the feed line at half-lamda intervals, fig 5.1 .

5.1 Antenna Arrays.

Assuming that the mutual coupling between radiating elements is negligible the far field radiation pattern of the antenna can be calculated from the vector sum of all the radiating elements. The effective phase difference between each radiating element is illustrated in fig 5.2.

$$E_\theta = E_o \left\{ 1 + \exp\left[\frac{J2\pi d}{\lambda_o} \sin\phi\right] .... \exp\left[\frac{Jn\pi d}{\lambda_o} \sin\phi\right] \right\} \quad (5.1)$$

Where,

Eo is the radiating pattern of a single resonator.

n is the nth radiating element.

d is the spacing between the elements.

Thus

$$E_\theta = \frac{E \sin\left[\frac{n\pi d}{\lambda_o} \sin\phi\right]}{n \sin\left[\frac{\pi d}{\lambda_o} \sin\phi\right]} \quad (5.2)$$

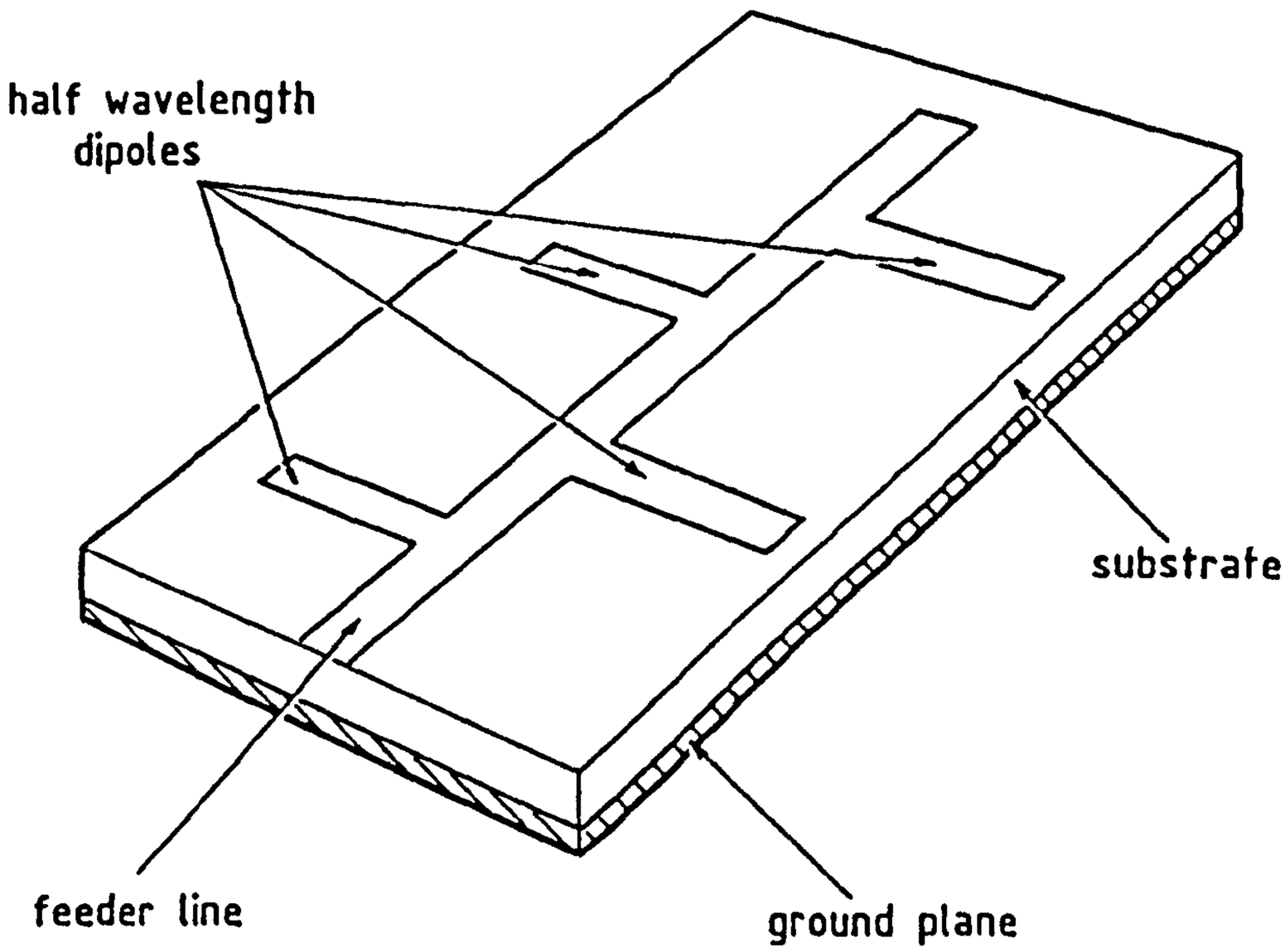

Figure 5.1. Diagram of a microstrip aerial.

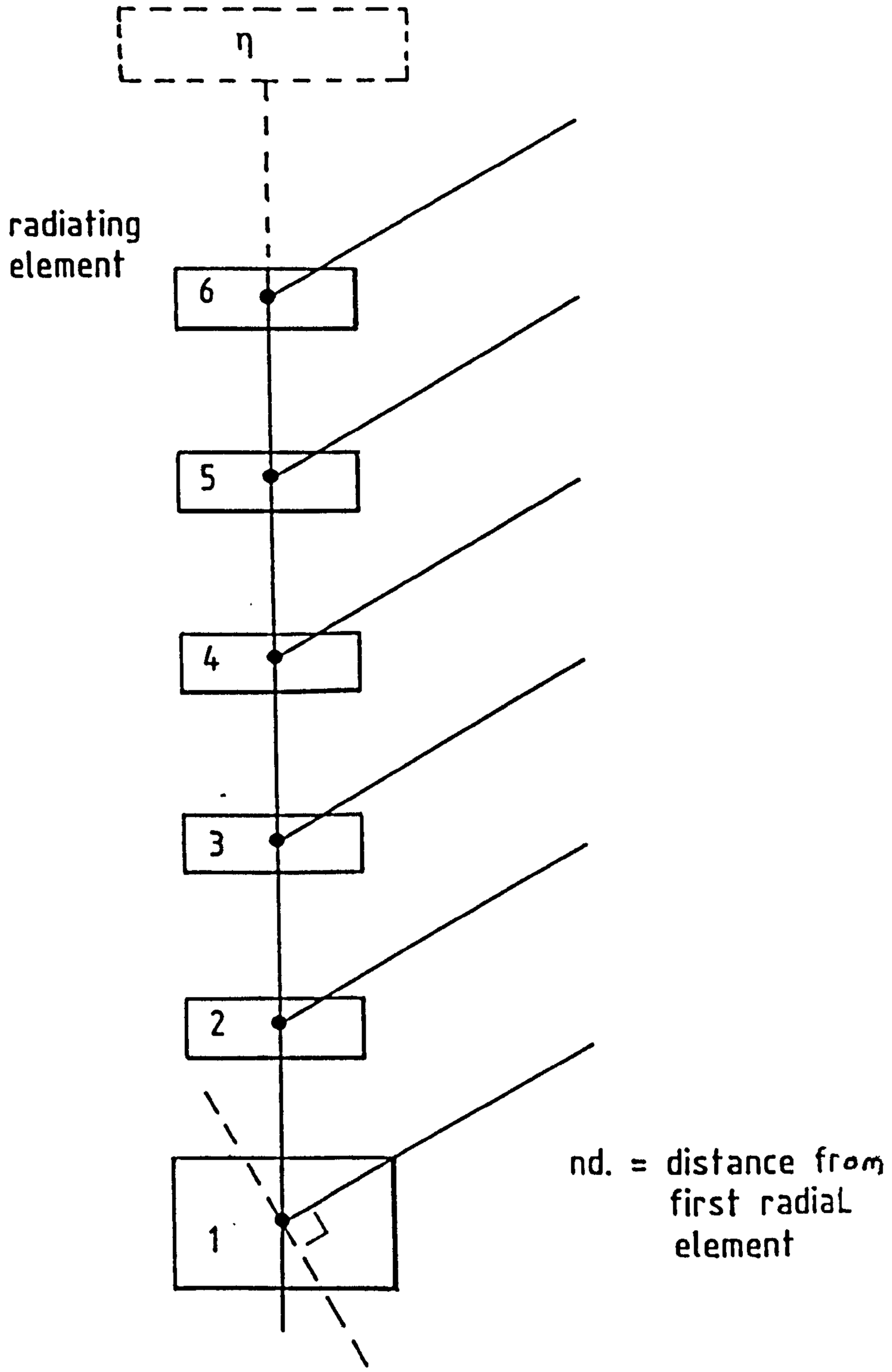

Figure 5.2. Calculation of phase difference for η radiating element.

An overall gain for the antenna array can be estimated by assuming that each halfwave resonator radiates in phase :-

$$\text{Gain} = \frac{\text{Power density in the direction of interest}}{\text{average power density}} \qquad (5.3)$$

5.2 Antenna Measurements.

The radiation pattern of the antenna is obtained by moving a detector at a fixed distance from the antenna under investigation. However, it is more practical for the receiving antenna to remain fixed in one position while rotating the antenna under test, fig 5.3 . This antenna is fed with power from a calibrated signal source and the incident power at the receiver is measured. Ideally the detector should be working in the far field zone of the transmitting aerial [1] given by F :-

$$F = \frac{G\,\lambda}{2\,\pi} \qquad (5.4)$$

where,

F is far field distance.

λ is wavelength.

G is gain in specific direction.

The receiving antenna is connected to a demodulator which produces an I.F. frequency of 50 Mhz which is fed to a log-amplifier, fig 5.4 . The output from the log-amp is fed to a pin diode detector which generates a d.c output voltage proportional to the input power to the receiver.

This information together with angular position of the antenna under test is sent to a chart recorder on which a polar plot of the radiation in db is produced. The antenna measurement system was calibrated using 3 antenna of gains G1, G2, G3 in terms of the path losses between antennas L12, L23, L13 respectively.

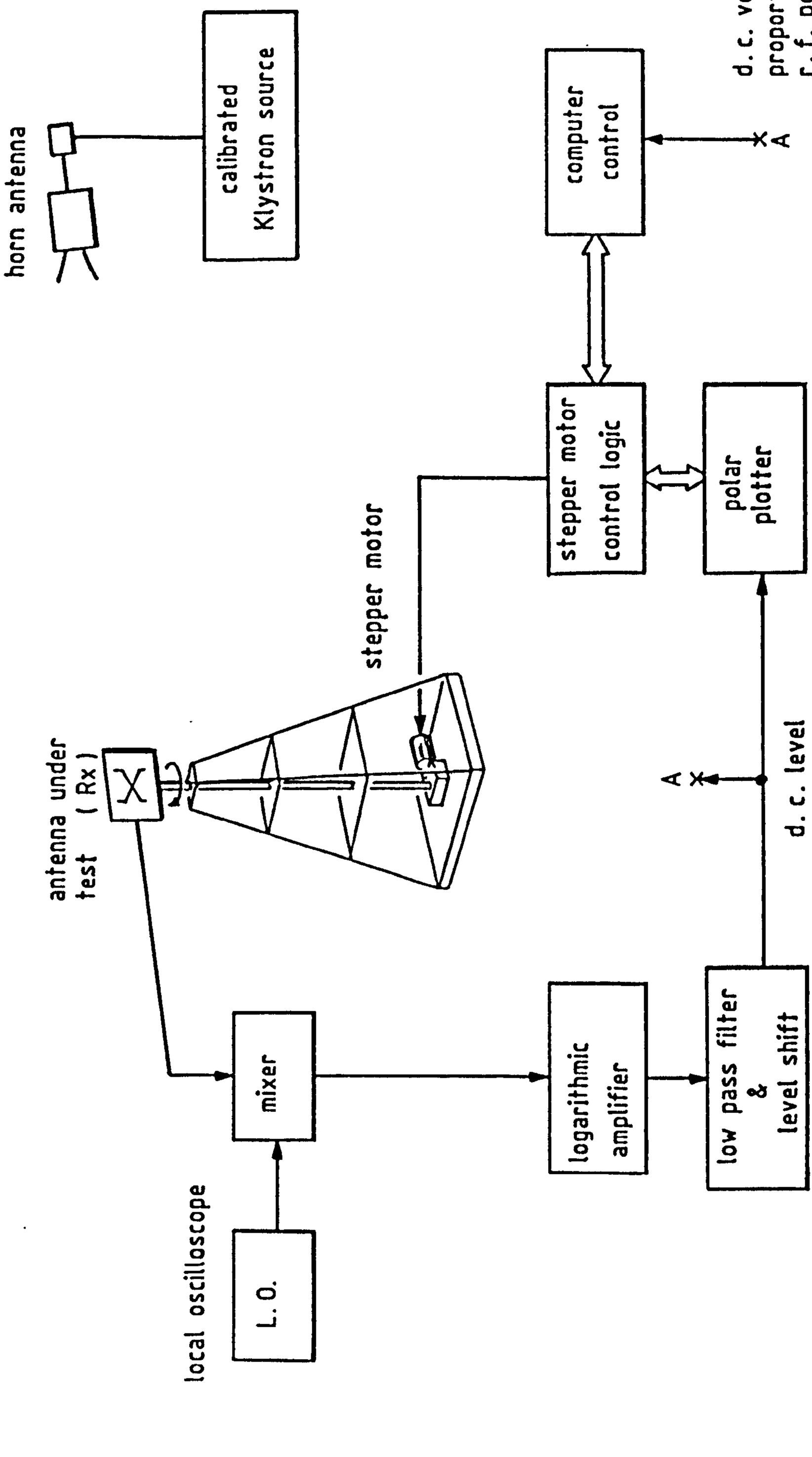

Figure 5.3. Antenna plotting system.

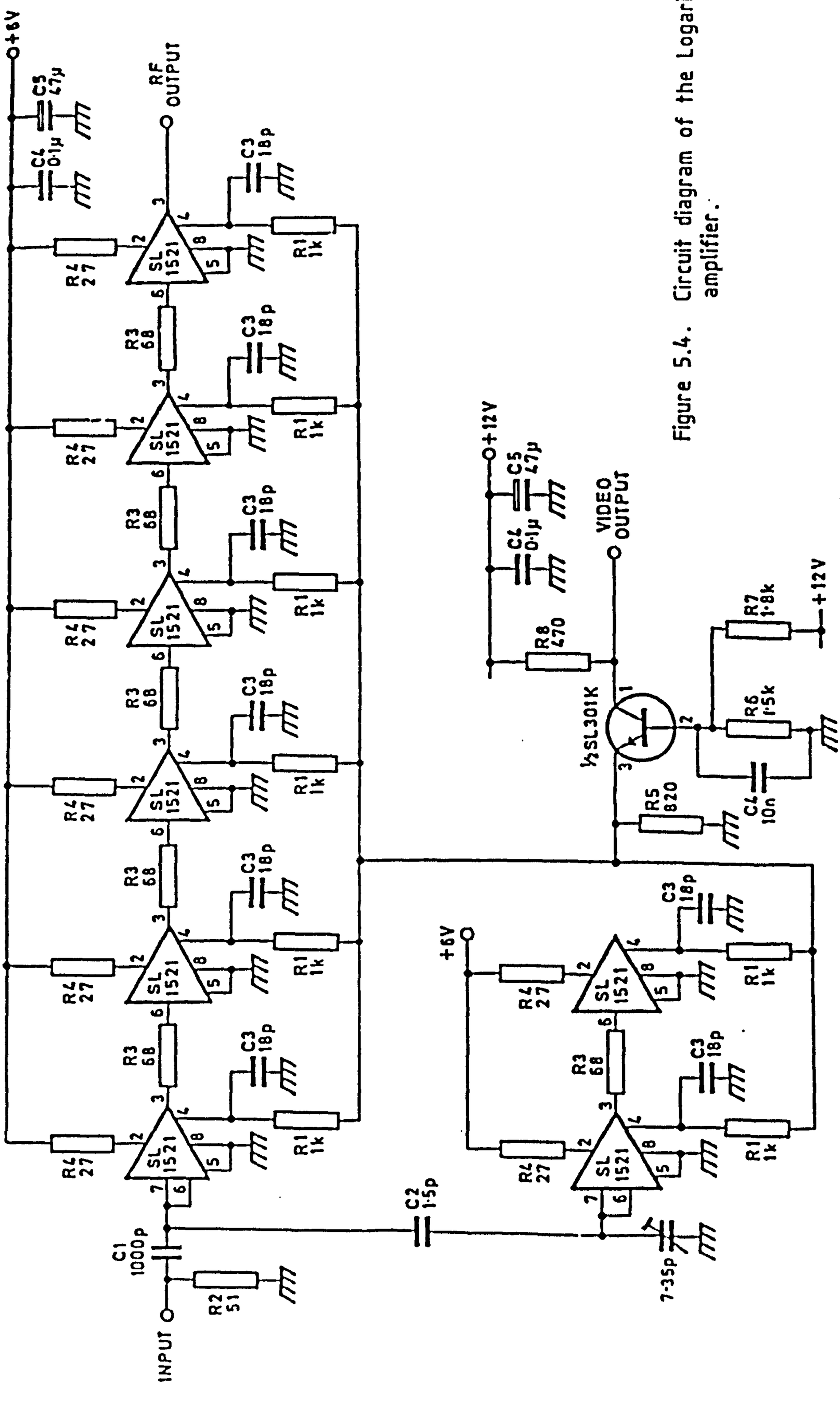

Figure 5.4. Circuit diagram of the Logarithmic amplifier.

5.3 Microstrip fed linear array.

A microstrip linear array consisting of five radiating elements spaced at λ intervals along a 100Ω microstrip feed line was fabricated, fig 5.5(a). Each radiating element had a radiation impedance of 1800Ω. The 180Ω input impedance was matched feed line by a 132Ω quarter wave transformer.

The physical dimensions of the strip line sections was derived from the two computer programs 'Zero1' and 'Zero2' [2]. The reflection coefficient of the array, fig 5.5(b), was measured on a Hewlett-Packard network analyser and a reasonable V.S.W.R of 1.5 to 1 was obtained from 9.5 to 10.5 Ghz.

This array radiated in a broadside direction with an isotropic gain of 10.5 db, fig 5.5(c) as compared with a theoretical gain of 12 db. The 3db beamwidth in the E and H planes is 20^0 and 30^0 respectively. The two main side lobes at $\pm 22^0$ had gains of 5dB and 3dB respectively. This array suffered from significant cross polarisation in both the E and H planes. Two cross polar radiation lobes of 4 dB were obtained in the E plane with similar lobes in the H plane, fig 5.5(d). The theoretical and measured value of the cross polarised radiation is 4 dB, indicating that the feeder radiation is comparable in magnitude to the side lobe radiation of the array. The loss within the feeder and radiating elements is an acceptable 1.5 dB.

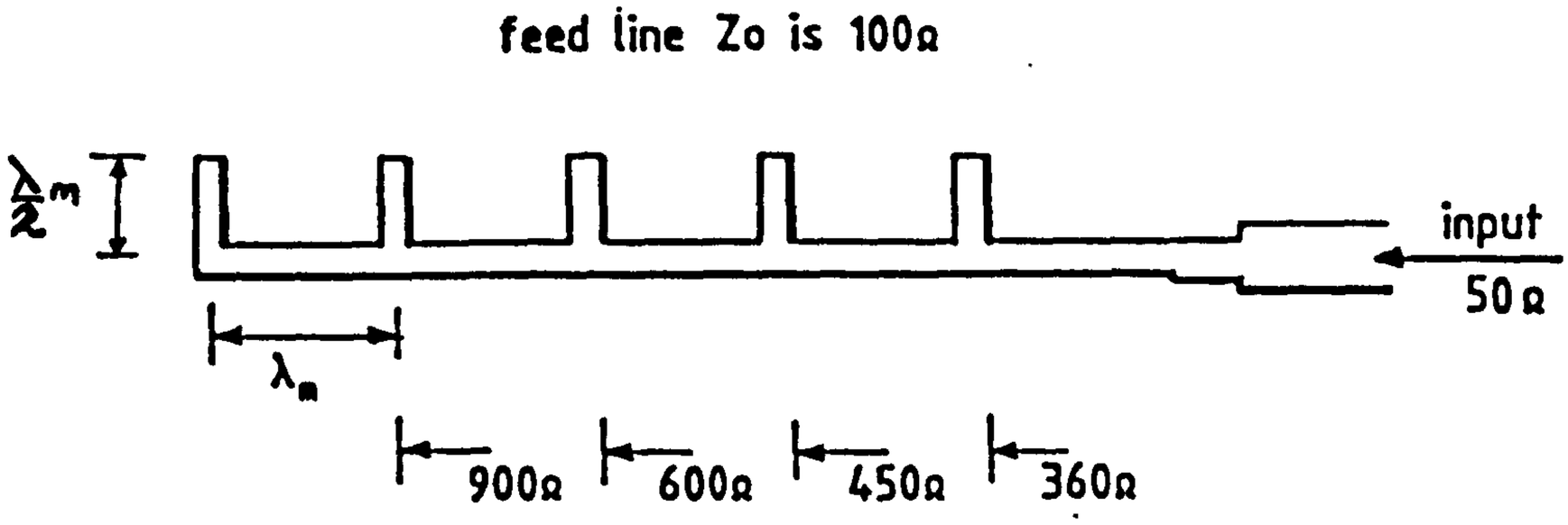

Figure 5.5 a, Five element microstrip antenna.

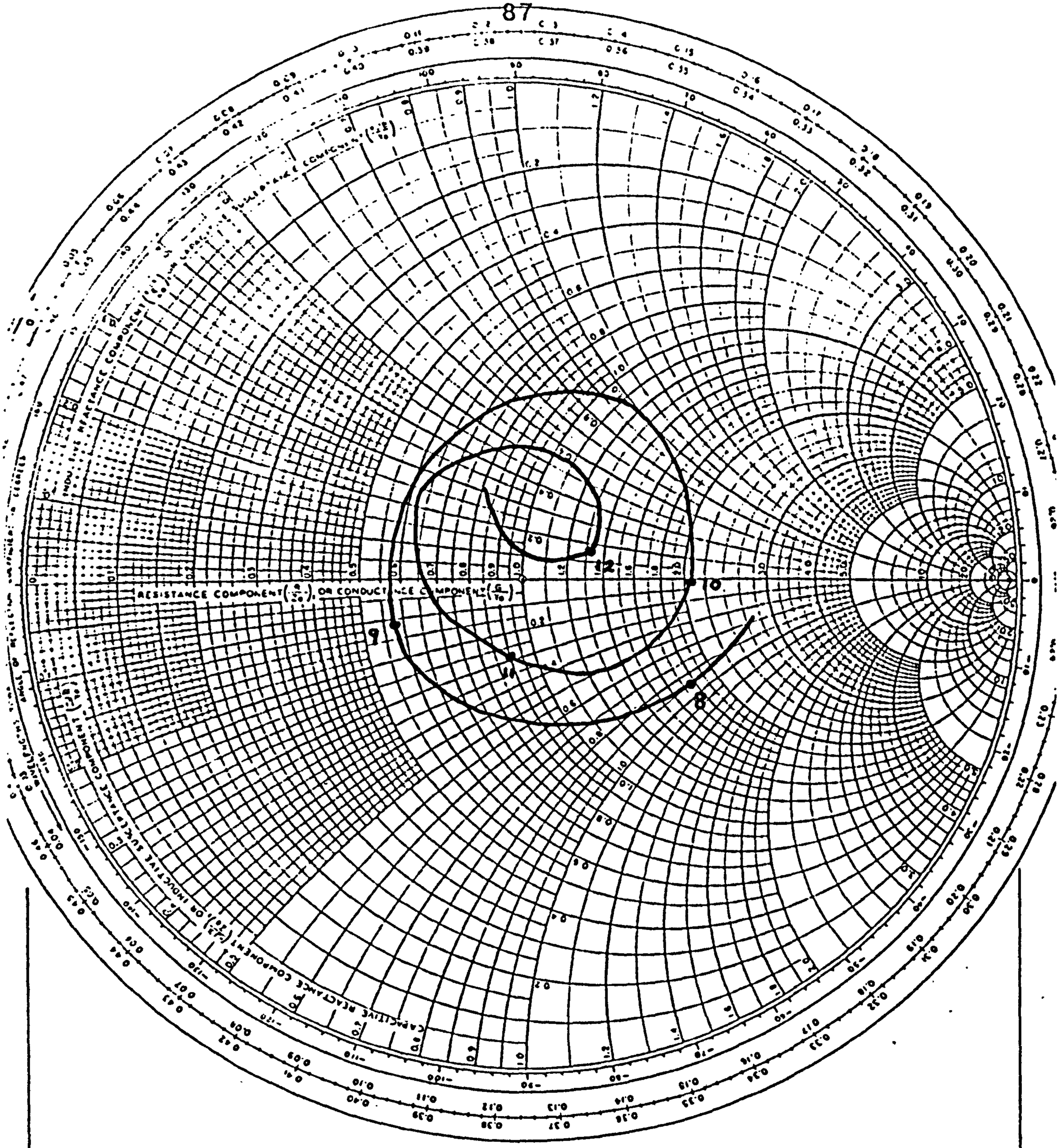

Figure 5.5(b). Five element microstrip antenna.

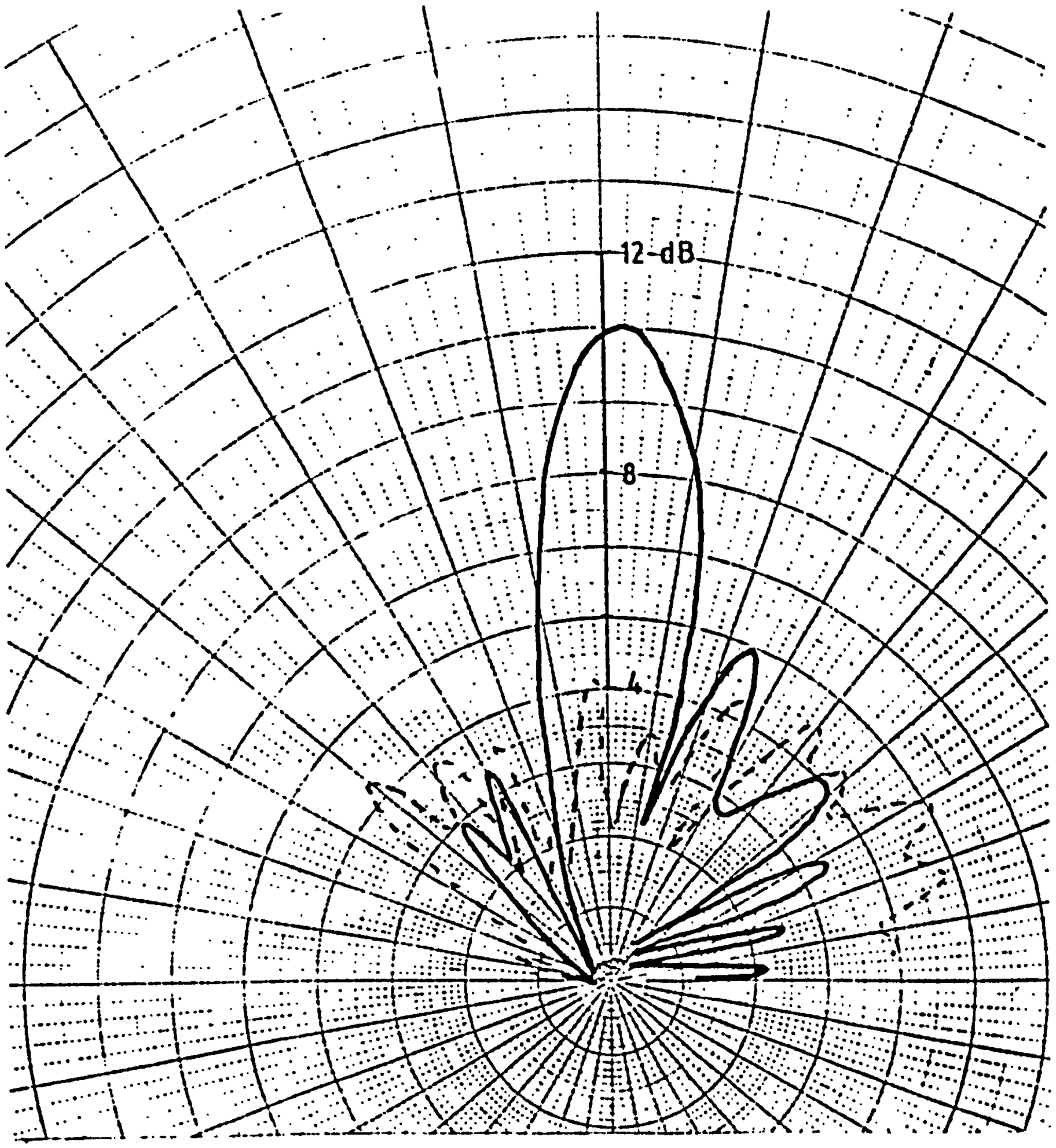

——— E plane radiation
———. Cross polar radiation

Figure 5.5(c). Five element microstrip antenna.

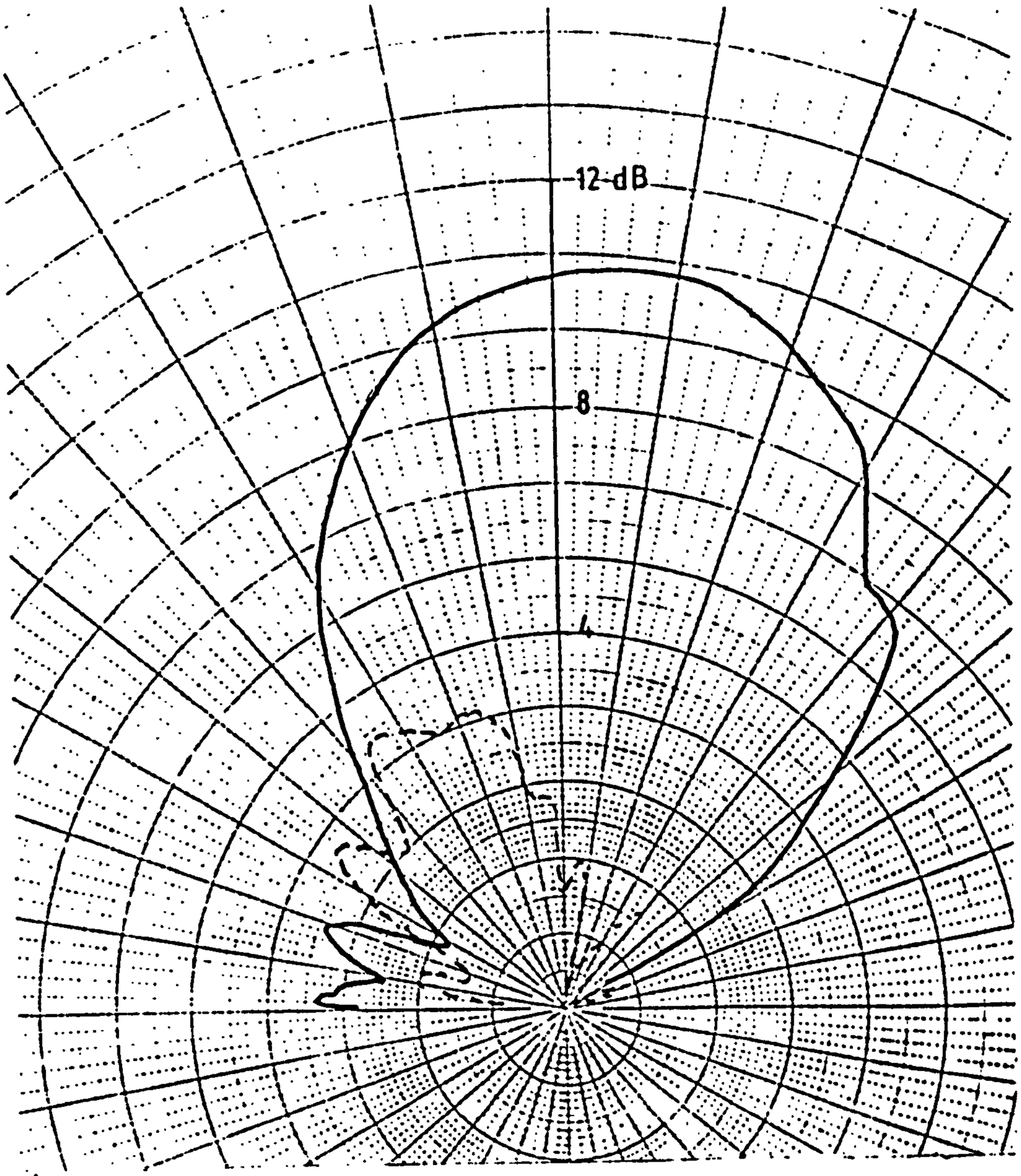

——— H plane radiation
_ _ _ _ Cross polar radiation

Figure 5.5(d). Five element microstrip antenna.

5.3.1 10 element microstrip array.

A broadside co-phase array consisting of 10 half-lamda open circuit stub elements on alternate sides of the feed line at half lambda intervals was fabricated, fig 5.6(a). Each radiating element had a radiation impedance of 1800Ω and were interconnected by a 100Ω microstrip feed lines. The input impedance to the array was matched to a 50Ω source by quarter wave transformer. The strip line dimensions and characteristic impedance was calculated by computer programs 'Zero 1' and 'Zero 2'.

This antenna is well matched to the source over a wide frequency range, with a Vswr of better than 1.2 to 1 . This array radiated in a broadside direction with an isotropic gain of 13.4 dB compared to a theoretical gain of 15.2 dB, fig 5.6(b,c). As the antenna frequency was shifted from 9.7 to 10.1 GHz the main lobe moved by about 5° due to the change in phase. A similar radiation pattern to that expected from theory was obtained for the on axis radiation. The 3dB beamwidth in the E and H planes was 15^0 and 35^0 degress respectively, with two main side lobes occurring either side of the main lobe at $\pm 24^0$ and -30^0 with gains of 5dB and 3dB respectively. The cross polarisation remained constant at 4 dB as expected due to the use of a similar feed line and current distribution as the 5 element array. For both the 5 element and 10 element arrays a bore sight error of 1^0 was obtained for the main lobe, due to errors within the antenna measurement system.

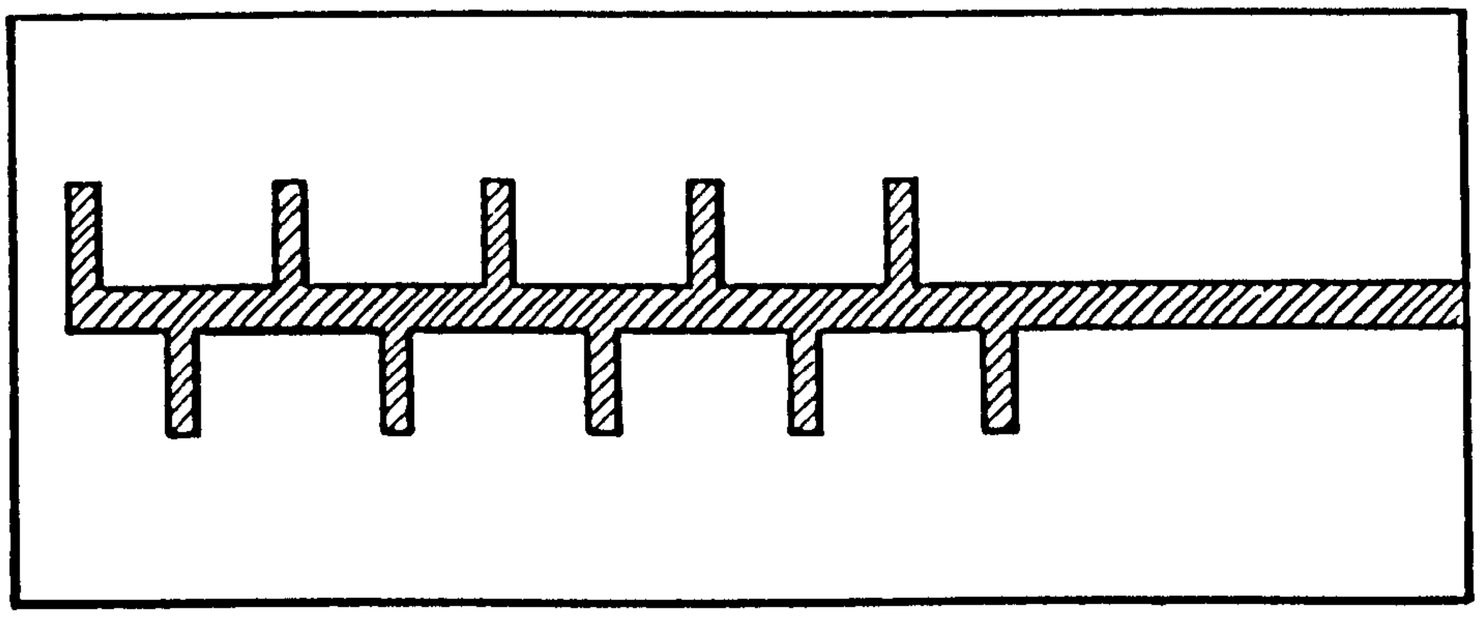

Figure 5.6 (a). 10 element microstrip antenna.

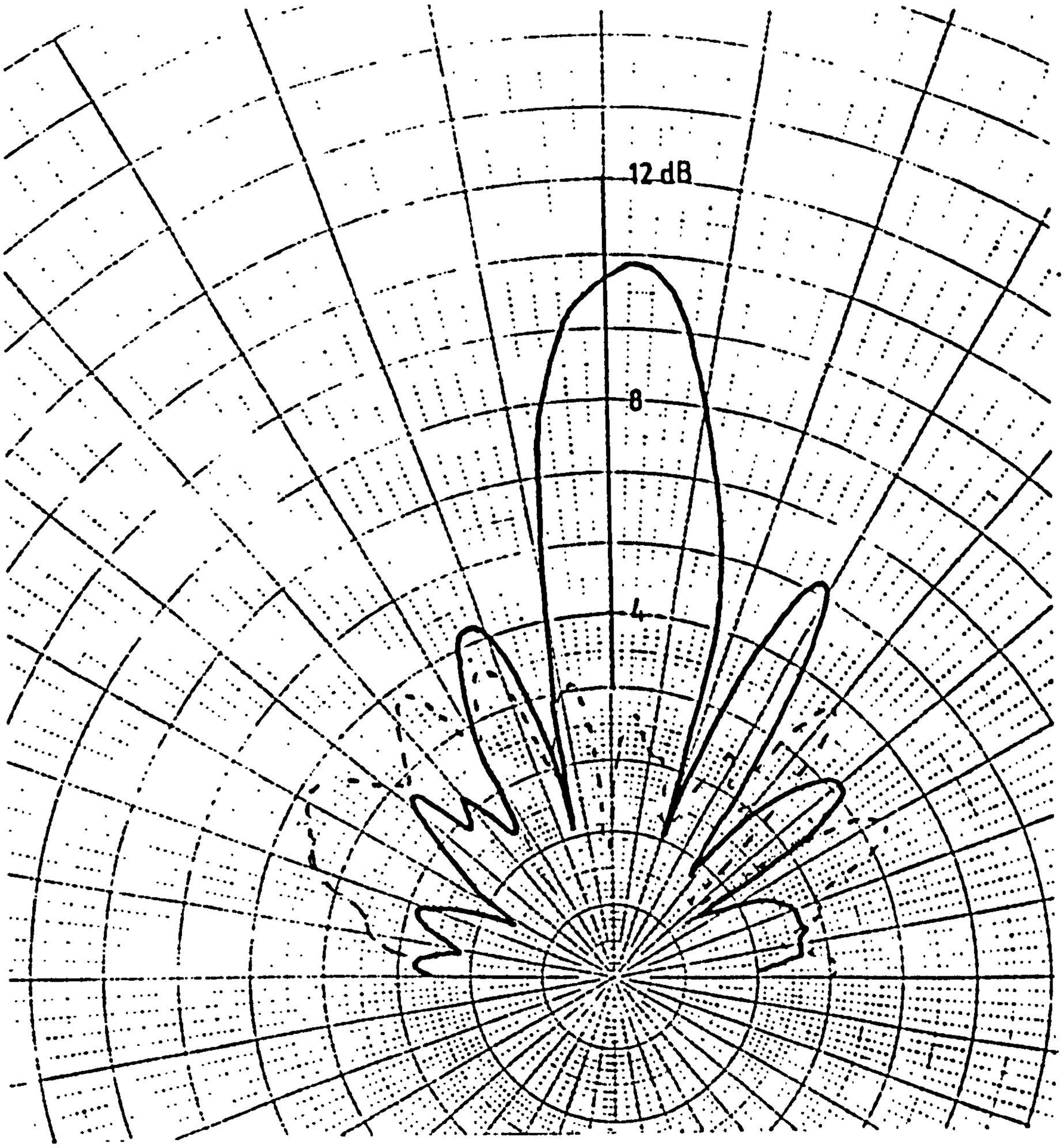

——— E field radiation
– – – – – Cross polar radiation

Figure 5.6 (b). 10 element microstrip antenna.

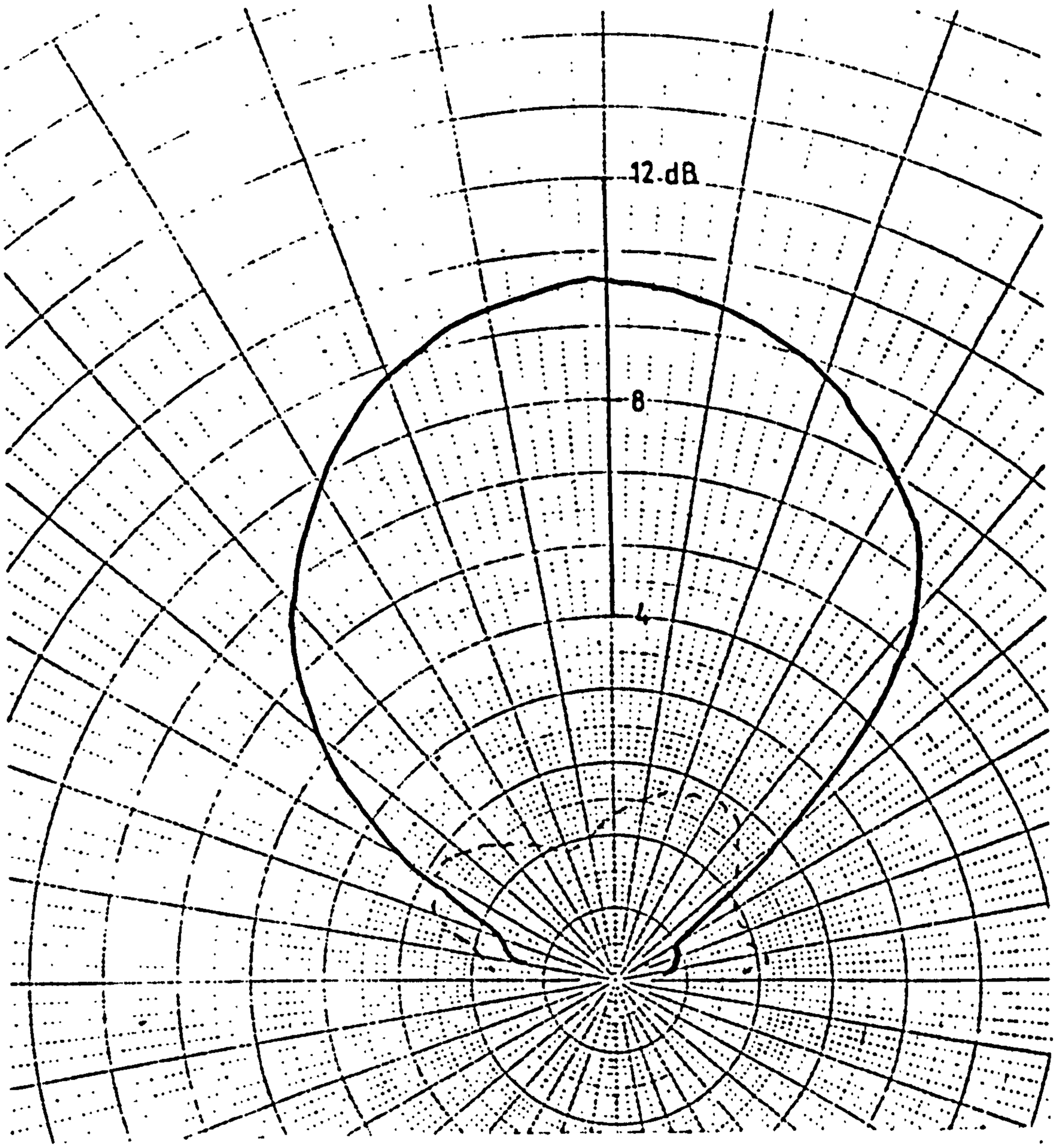

——— H field radiation
_ _ _ _ Cross polar radiation

Figure 5.6 (c). 10 element microstrip antenna.

5.3.2 Cross polar radiation.

A set of antennas were designed to suppress radiation from the resonators, fig 5.7(a) in order to study feeder radiation, fig 5.7(b). The maximum measured feed radiation was 4dB in both the E and H planes as predicted by theory. Cross-polar radiation occurred in two main lobes at $\pm 45^0$ as shown by other microstrip antenna. With secondary endfire lobes due to the travelling wave component of feeder current moving down the antenna.

5.4 Corporate Fed Microstrip Antenna.

Beam squint with frequency is a particular disadvantage of travelling wave arrays accentuated by increasing line lengths In principle this beam movement can be eliminated by equalising the path lengths between the input source and each radiating element. A series compensated antenna consisting of an array of 24 radiating elements was fabricated. The radiating elements were arranged in a tapered in order to reduce the cross lobe radiation, fig 5.8 . This antenna had a broadside gain of 17dB, with a 3dB bandwidth in the E and H planes of 20^0x25^0. Side lobe radiation was reduced to 6dB due to the feed line taper. However, the cross polarisation radiation in the H plane was extremely high due to the co-phase radiation from the feed line structure.

An interesting example of feed line radiation is observed by examining the cross-fed printed antenna described by Williams [3]. This antenna consisted of a two dimensional array of directly fed elongated elements connected by a diagonal high impedance microstrip lines, one wavelength apart.

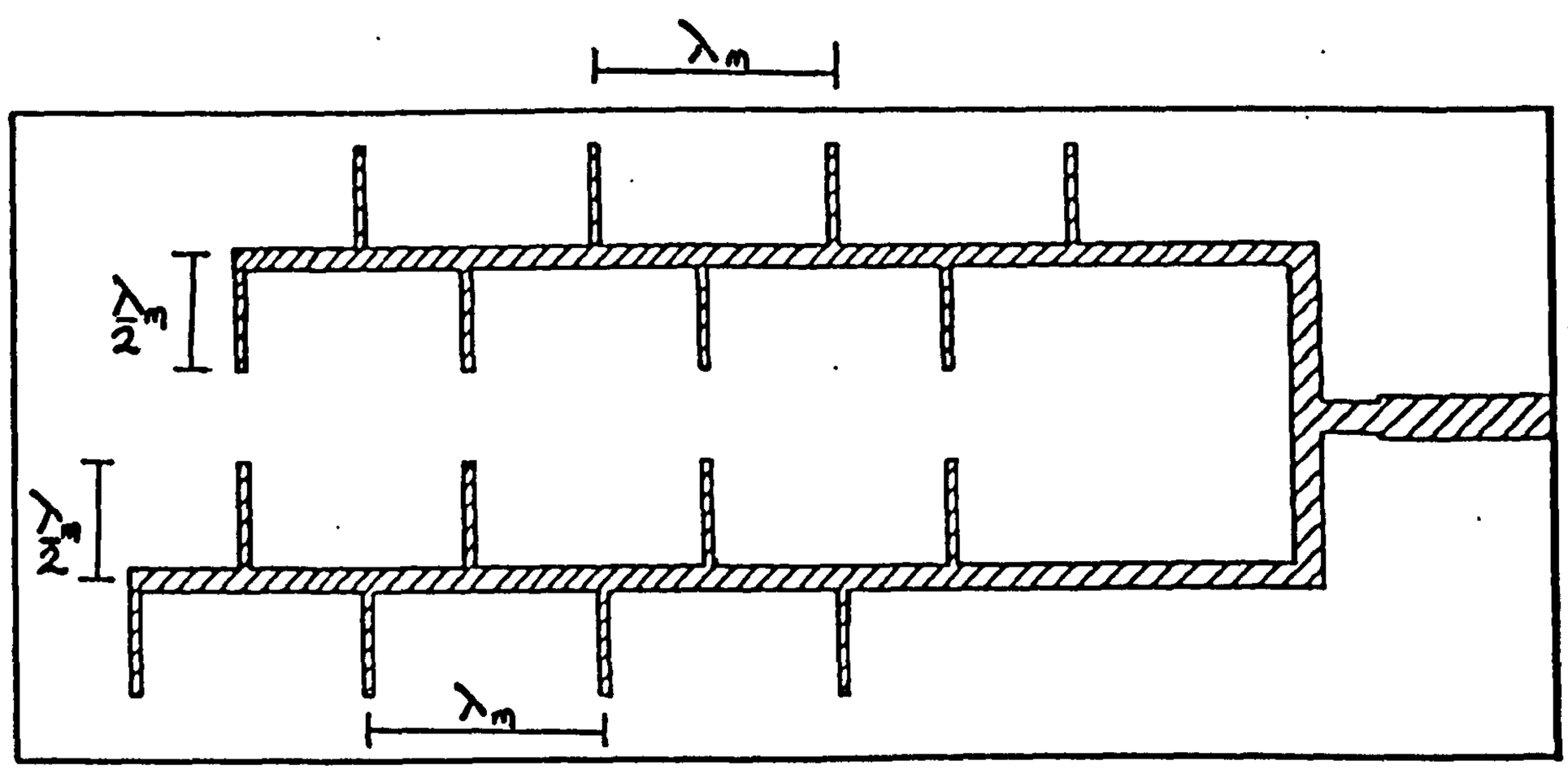

Figure 5.7 (a). Radiation supprassed antenna.

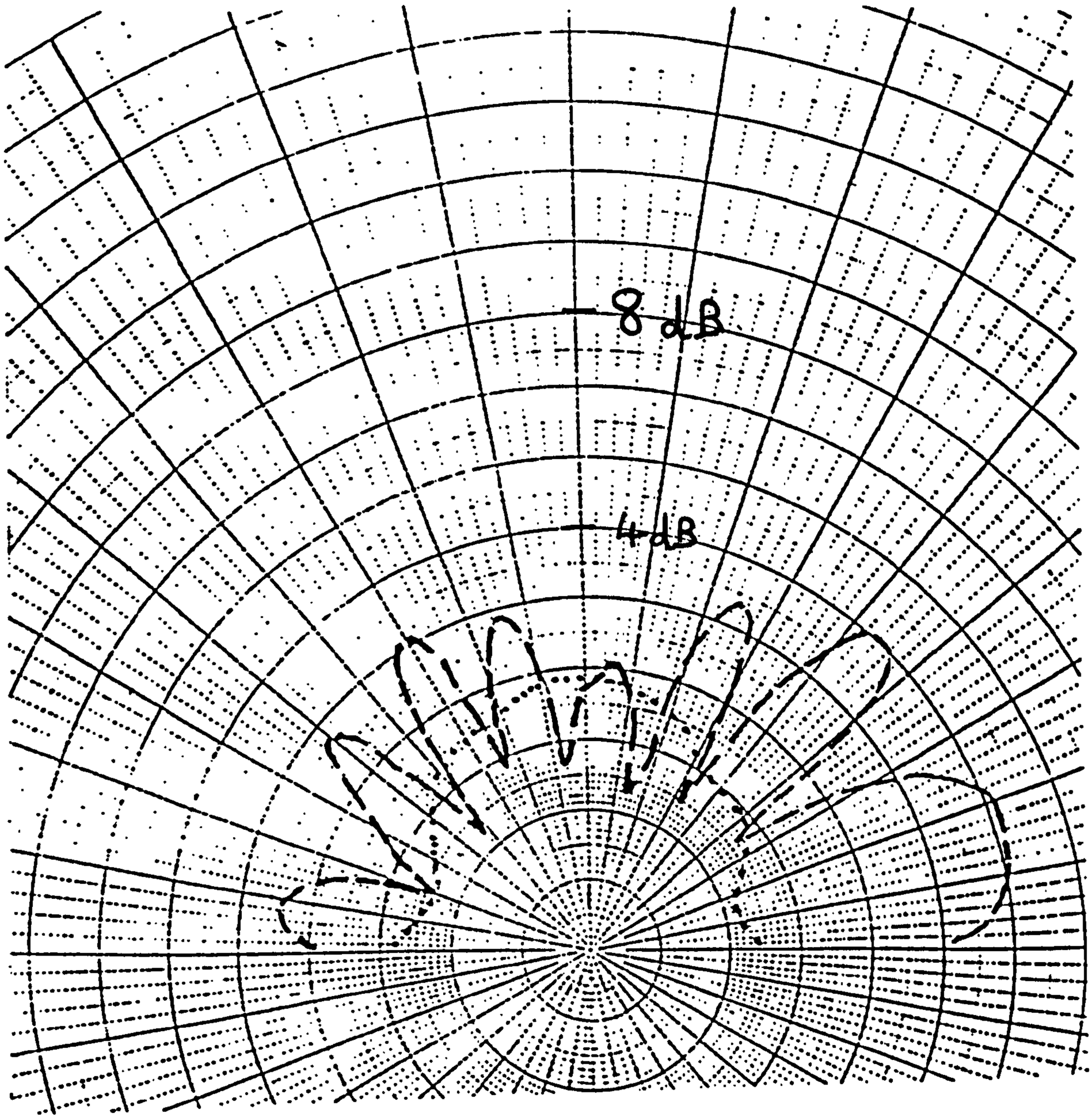

E plane cross polar radiation

H plane cross polar radiation

Figure 5.7 (b). On axis radiation suppressed antenna .

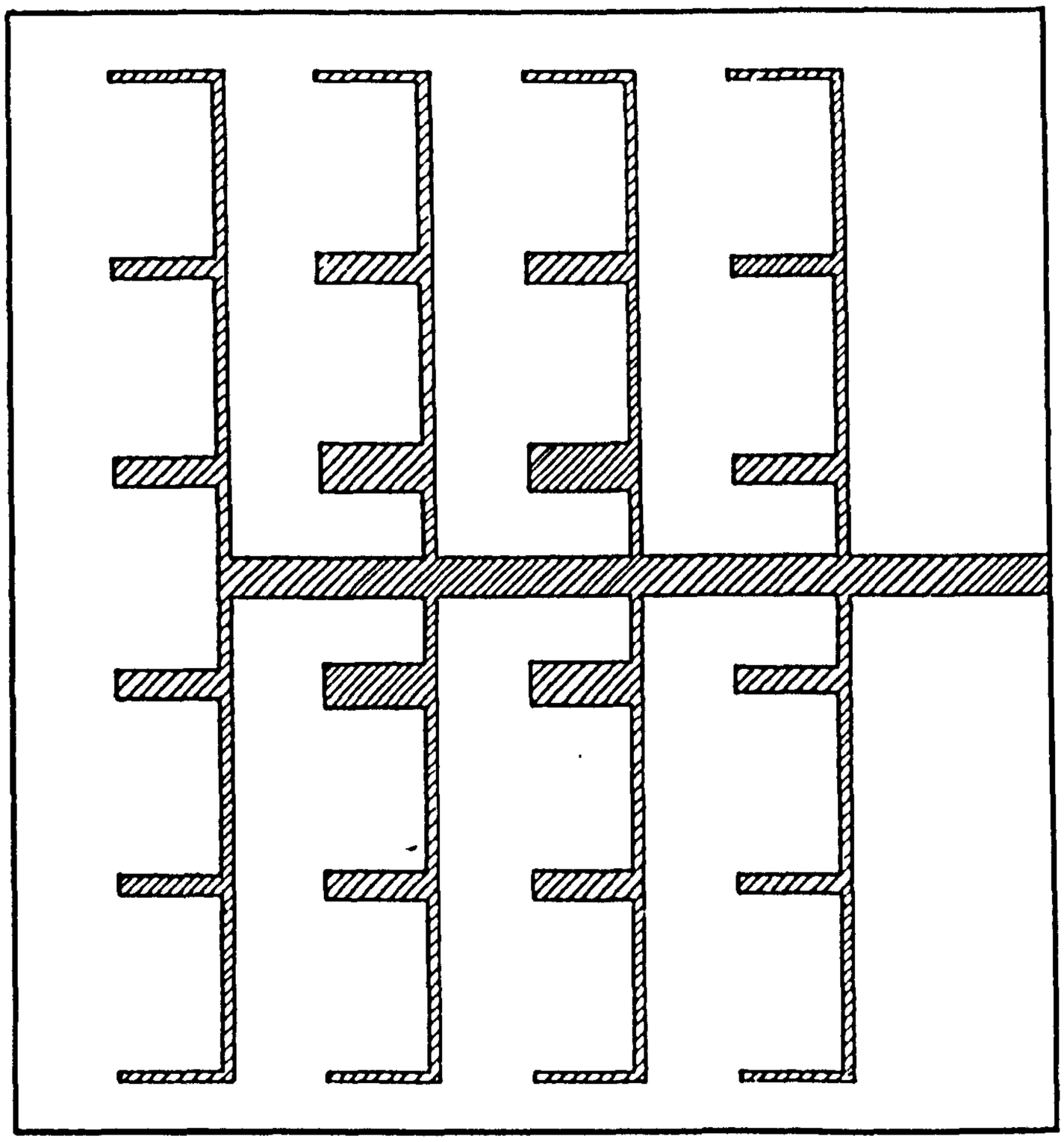

Figure 5.8. Corporate fed microstrip antenna.

This design utilises an ingenious arrangement of feed lines at 45^0 to the radiating elements and gives good gain and radiation symmetry, fig 5.9 . It is assumed that the feed line intersections are equal way splitters, in order to estimating the power radiated from each element in the array.

For an array of 36 elements arranged as a 6 X 6 matrix, the theoretical gain of the array was 21dB with a beam width of 8.1° . In practice a measured gain of 16dB with a beamwidth 8^0 and 8.5^0 was obtained fig 5.9(a). The measured gain is fairly close to this theoretical value and suggested that the array had a radiation efficiency of about 60%. Fig's 5.9(b) and 5.9(c) show the two patterns obtained at $\pm$ 45^0 to the normal orientation and indicate the effect of the feeder radiation.

5.5 Balanced Line fed Antenna.

A balanced line antenna consisting of 6 λ dipoles spaced at λ intervals along the balanced line was designed to resonate at 10 Ghz was fabricated, fig 5.10(a). The 150Ω input impedance to this array was matched to 70Ω slot line by a 110Ω quarter wave balanced line transformer. This slot line was then matched to a 50Ω signal source by a slot line to microstrip transition, fig 5.10(b).
The microstrip line was enclosed in a special housing in order to shield the array from strip line radiation.

From radiation measurements on the balanced line, figs 5.10(c,d), a broadside gain of 13.2dB was measured, with a 3dB beamwidth in the E and H plane of 14^0 and 35^0 respectively. This gain is 3dB less than the theoretical gain of 16.2dB calculated for the array. As the antenna frequency was shifted from 9.8 Ghz to 10.2 Ghz the main lobe moved by about 10^0. The main side lobe occurred at $+15^0$ with a gain of 6dB.

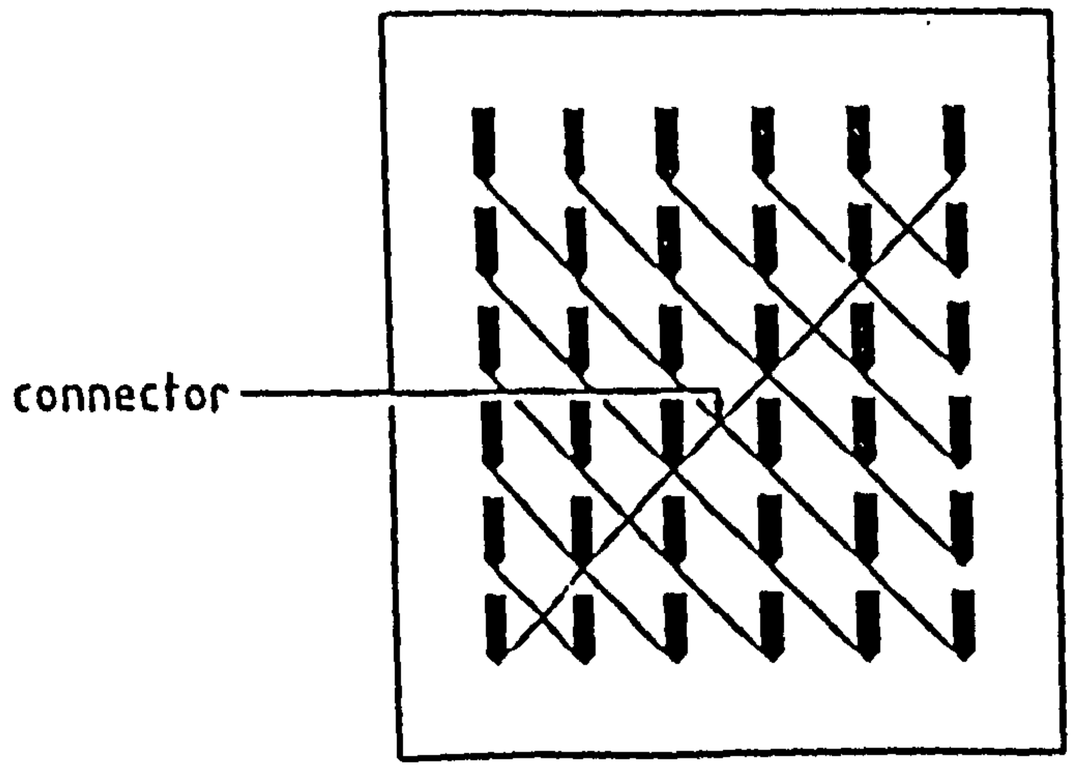

Figure 5.9 Cross-fed antenna by Williams.

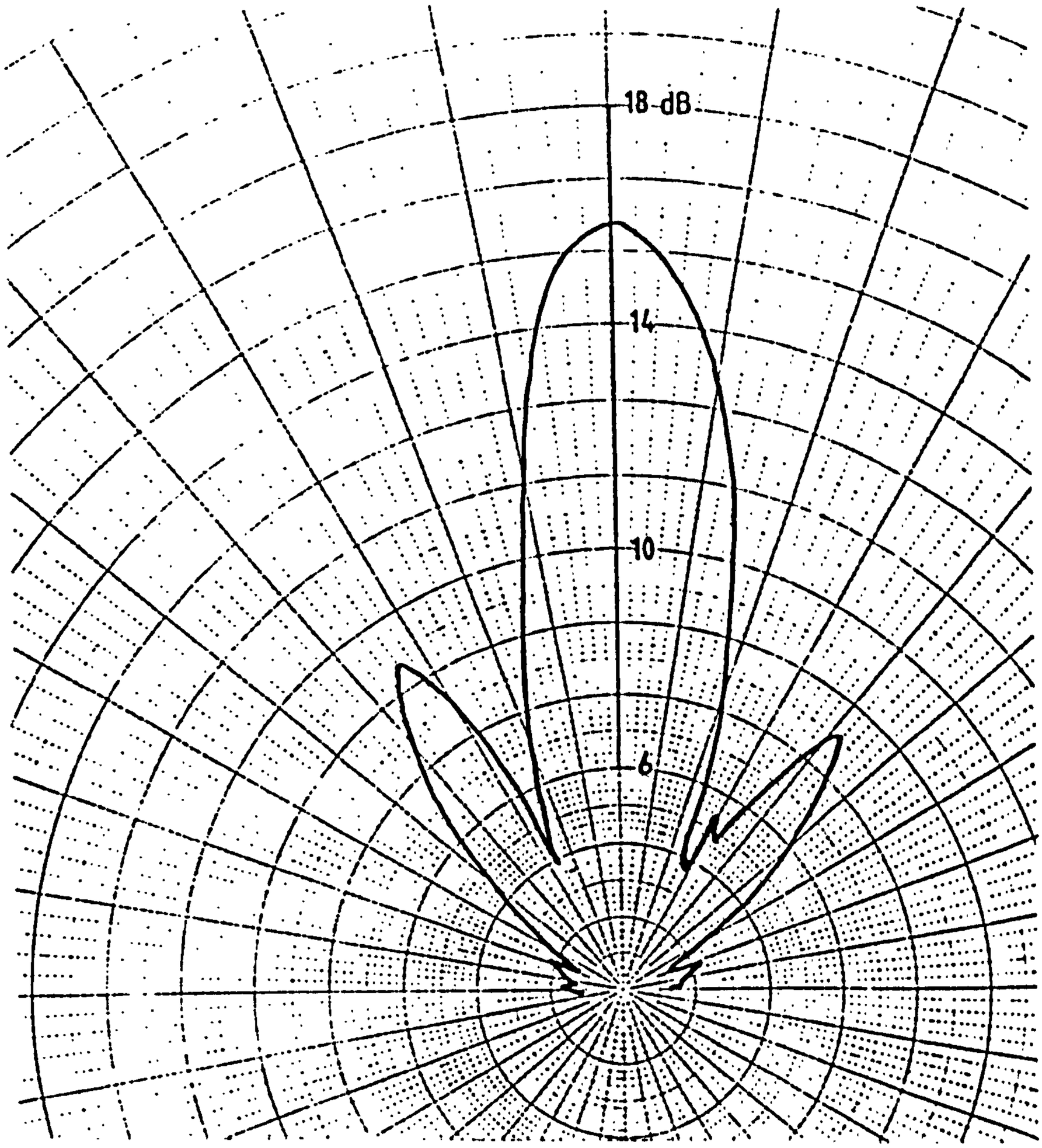

Figure 5.9 (a). On axis radiation of an across fed array.

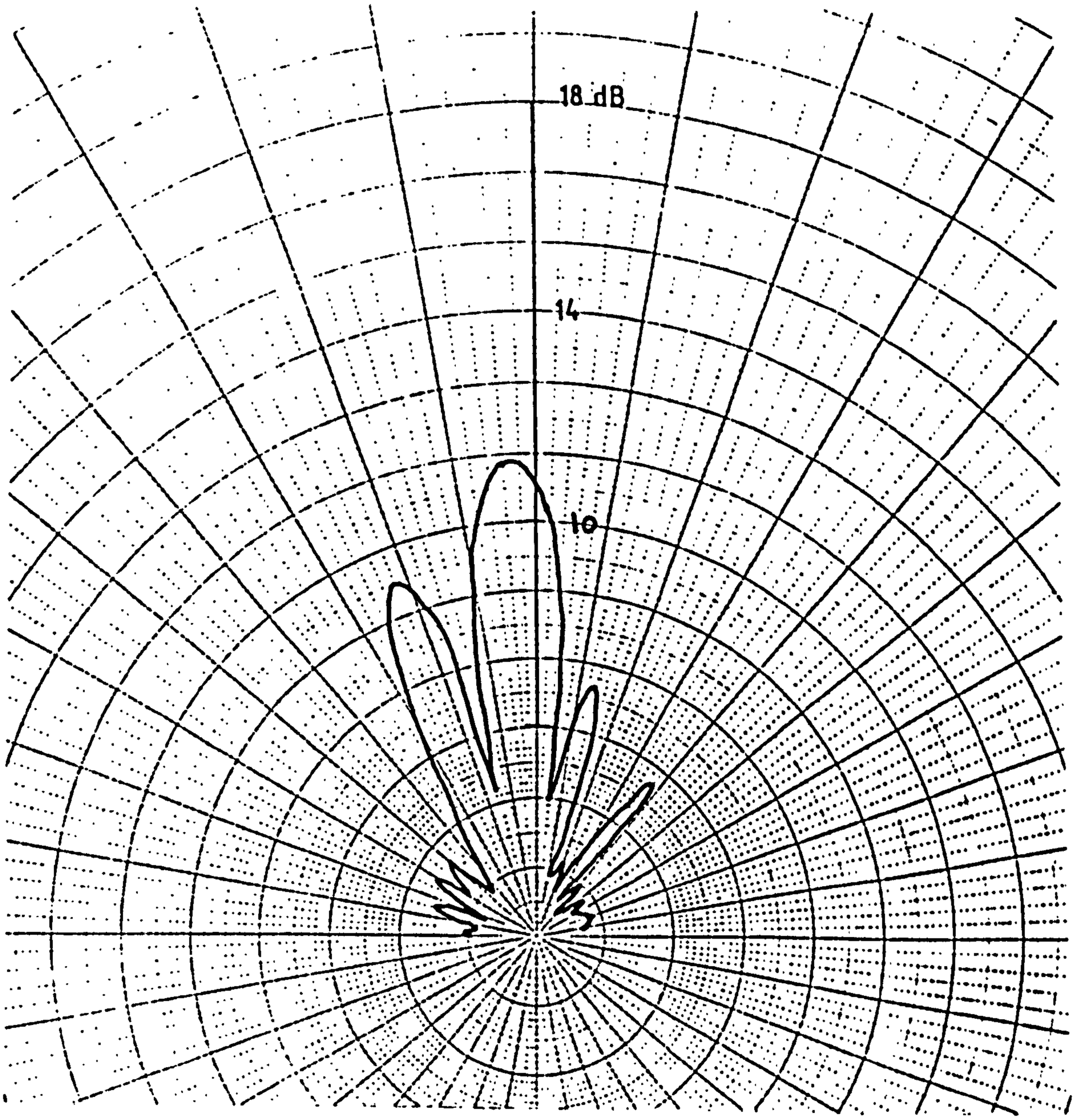

Figure 5.9 (b). +45° diagonal of the cross fed array.

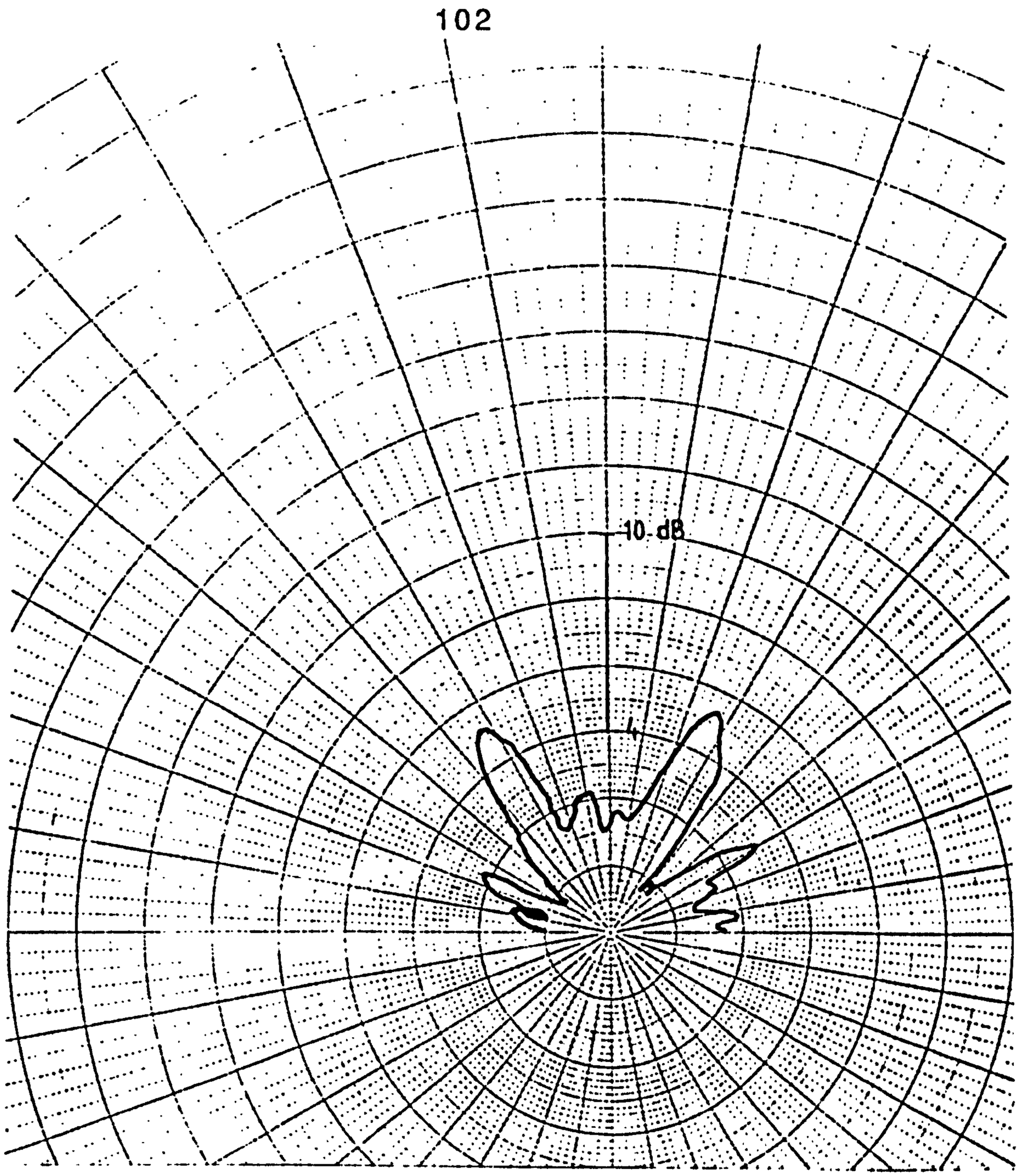

Figure 5.9 (c). -45° diagonal of the cross fed array.

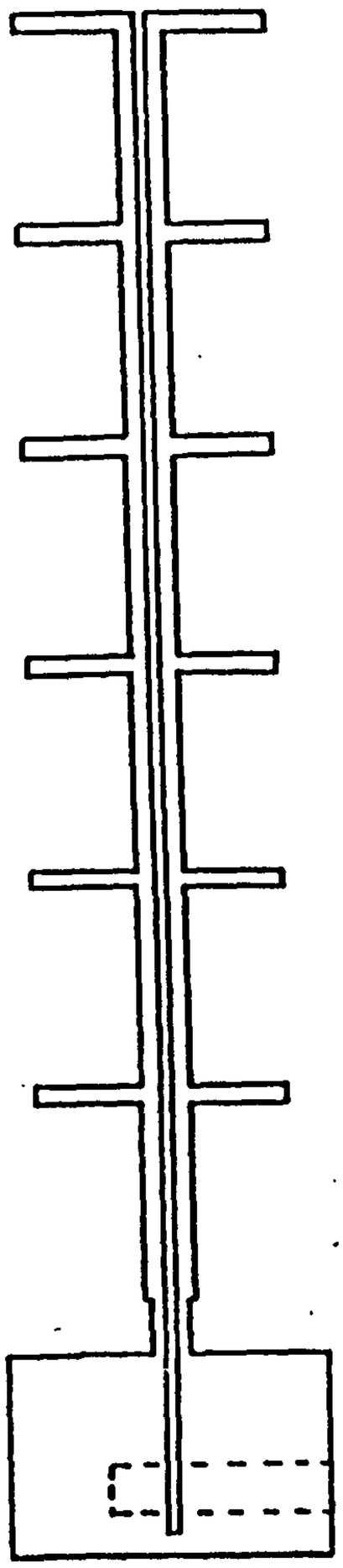

Figure 5.10(a) Balanced line fed antenna.

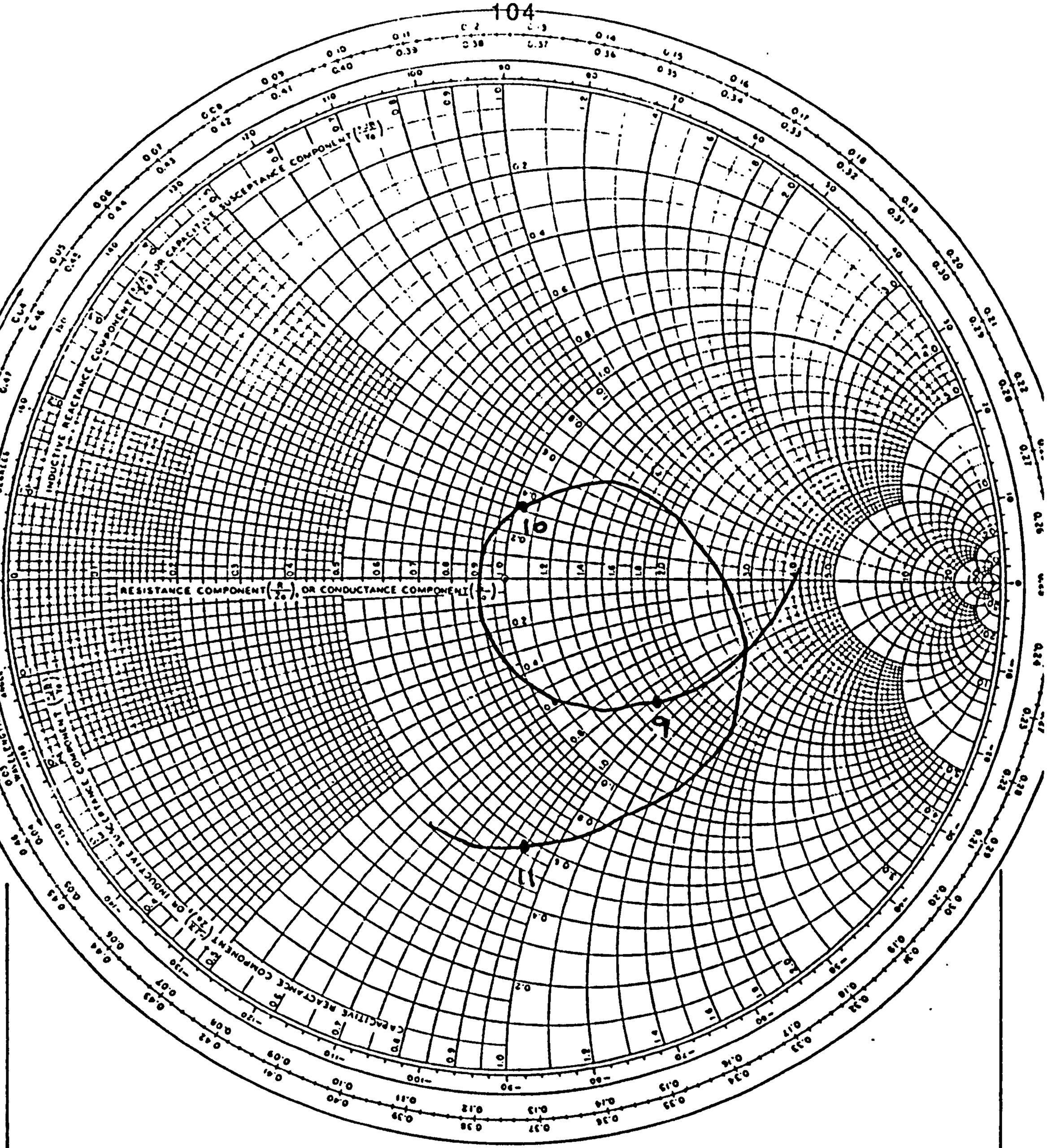

Figure 5.10 (b). Impedence plot of a 6 λ dipole balanced line fed antenna.

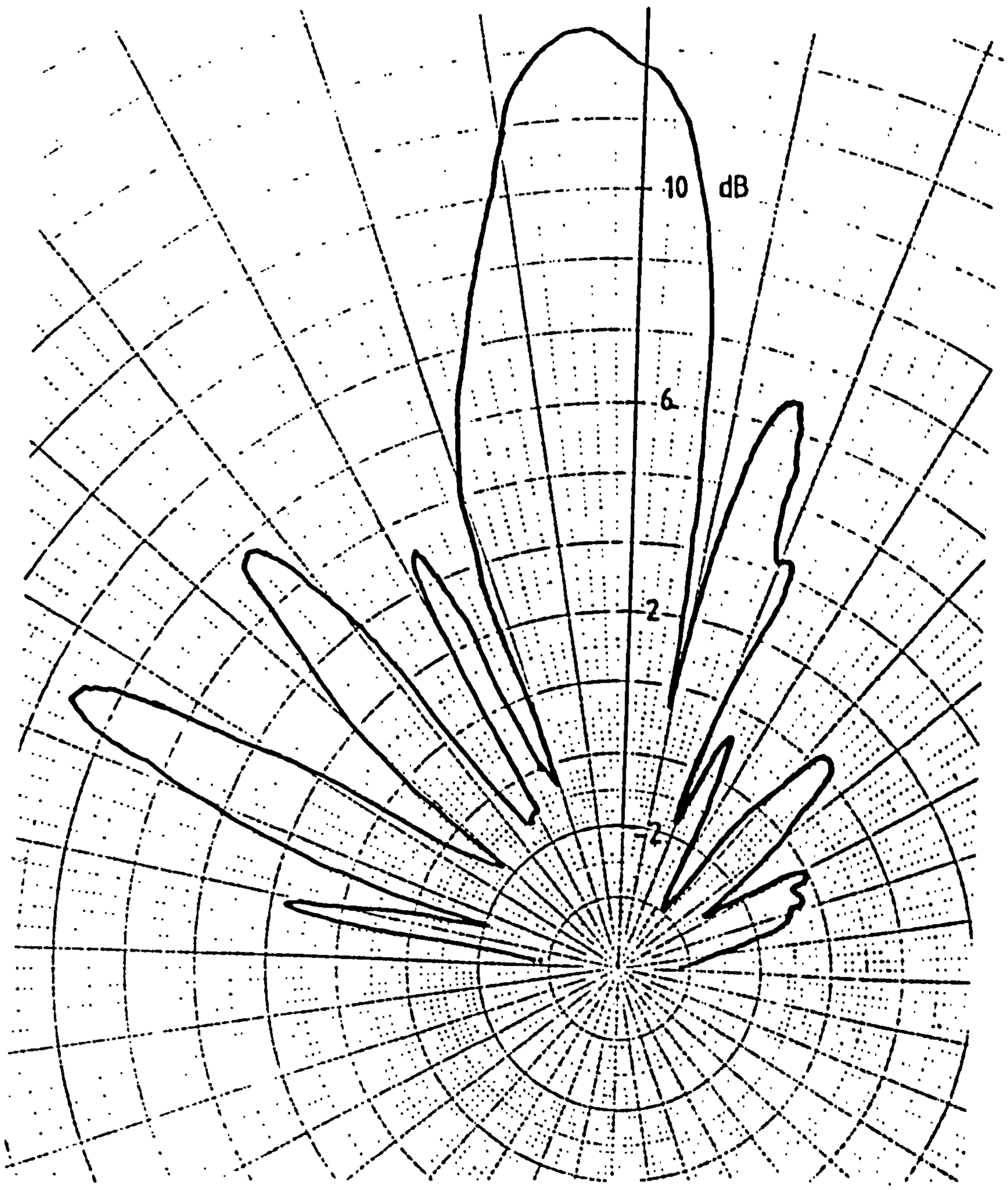

Figure 5.10 (c). E plane radiation of a 6 λ dipole, balanced line fed array.

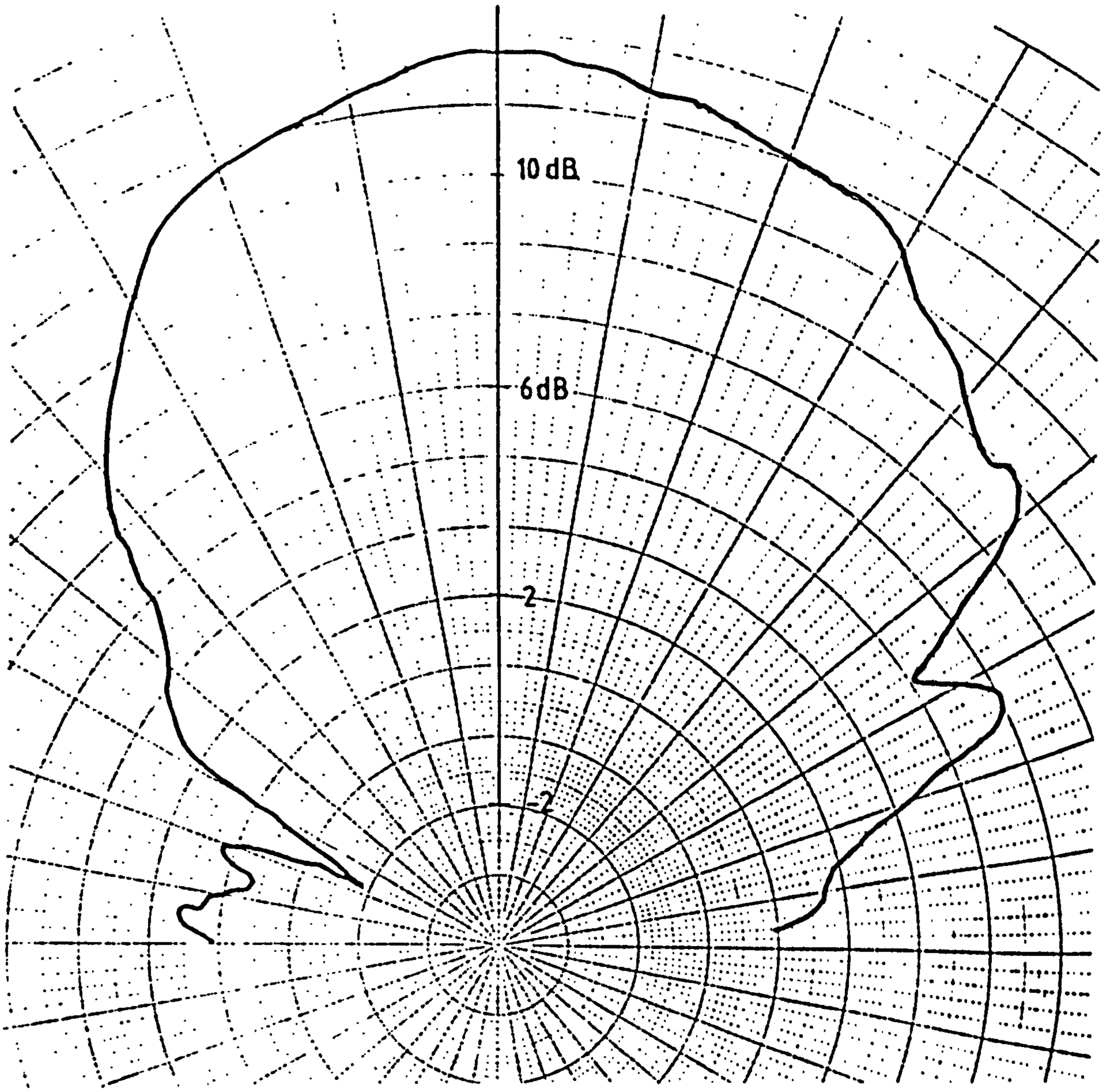

Figure 5.10 (d). H plane radiation of a 6 λ dipole, balanced line fed array.

The cross polarisation was significantly reduced to -6dB in both the E and H planes.

A significant reduction in cross polar radiation when compared with the 10 element microstrip fed array.

5.5.1 12 element antenna array.

In order to investigate the asymmetry in the on axis and cross polar radiation, an antenna array consisting of two rows of 6, λ dipoles spaced at λ intervals along two balanced line feeders was fabricated, fig 11(a). By feeding alternate pairs of resonators in anti-phase at half-lamda intervals, mismatches in the array which cause asymmetry in the radiation pattern was suppressed. The two balanced line feeders were driven by two push-pull microstrip to slot line transitions. The microstrip feed structure on the lower side of the slot line consists of two sections. The first section is a 50Ω match to standard connectors. While section two branches from section one into 100Ω lines which are matched to two 100Ω slot lines. The two sets of balanced line are matched to the 100Ω slot line by a pair of 120Ω quarter wave transformers.

The physical dimensions of the antenna were determined from computer programs 'Zero1' and 'Zero2'. This antenna resonated at a frequency of 10 Ghz, with a good impedance match, fig 5.11(b) . A reasonably symmetrical radiation pattern was obtained, fig 5.11(c,d) with a broadside main lobe gain of 13.5 dB and a 3dB beamwidth of 10^0x16^0. The main side lobes were symmetrical about the main lobe and occurred at $\pm 20^0$ with a gain of 4dB. The maximum cross polarisation was -6dB in both the E and H planes compared with a theoretical value of -14 dB.

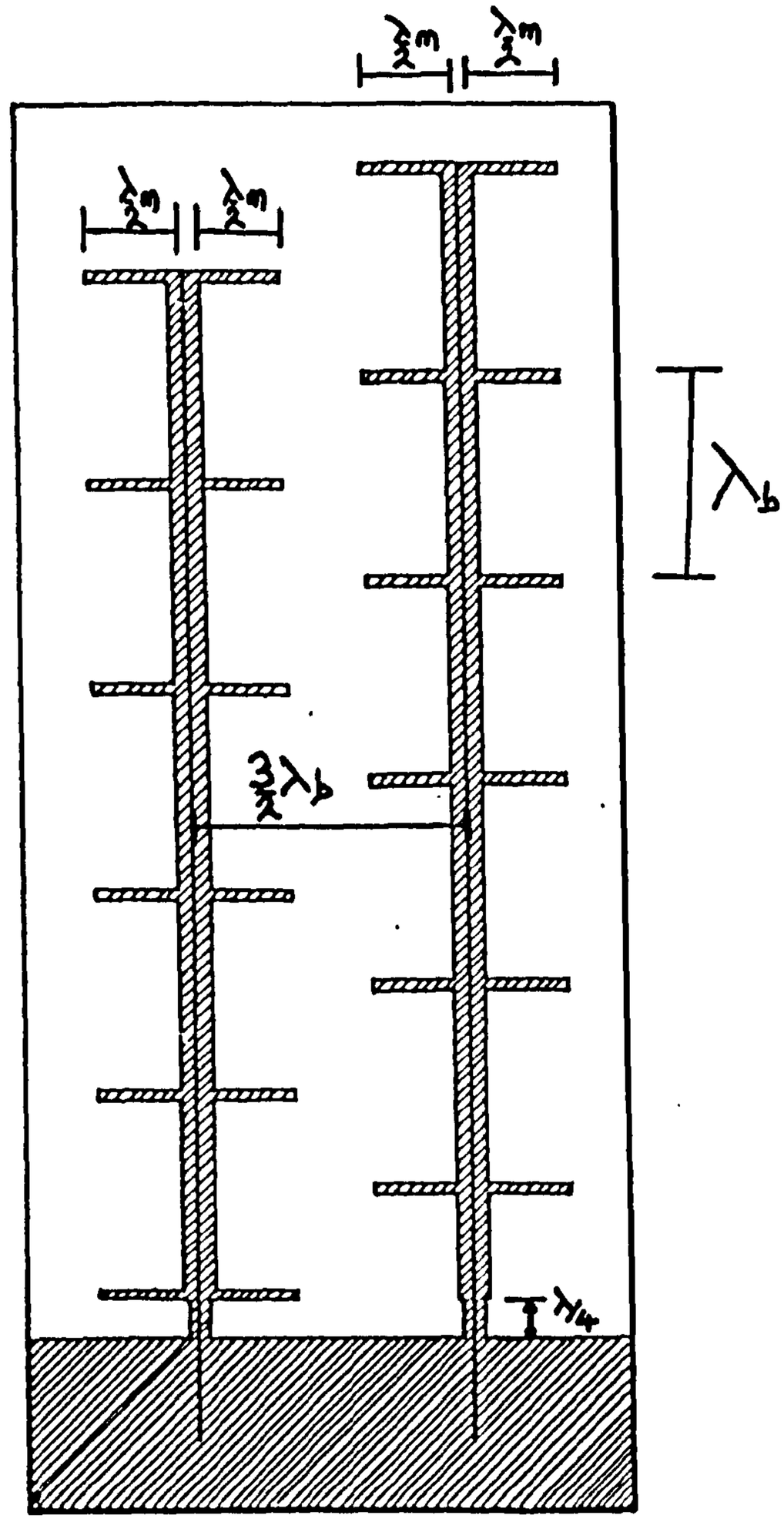

Figure 5.11 (a). 12 λ dipole, balanced line fed array.

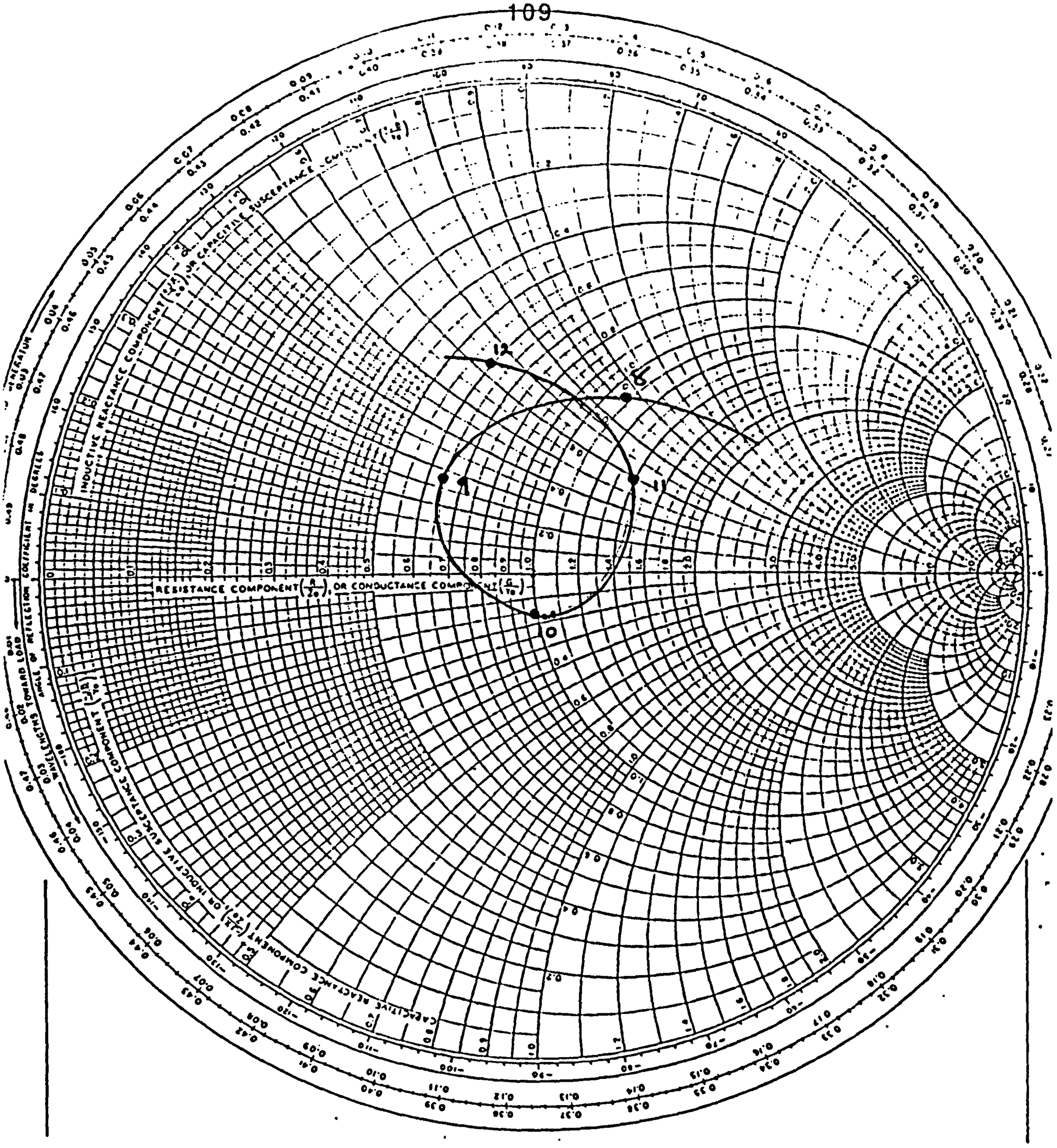

Figure 5.11 (b). Impedence plot of a 12 λ dipole, balanced line fed array.

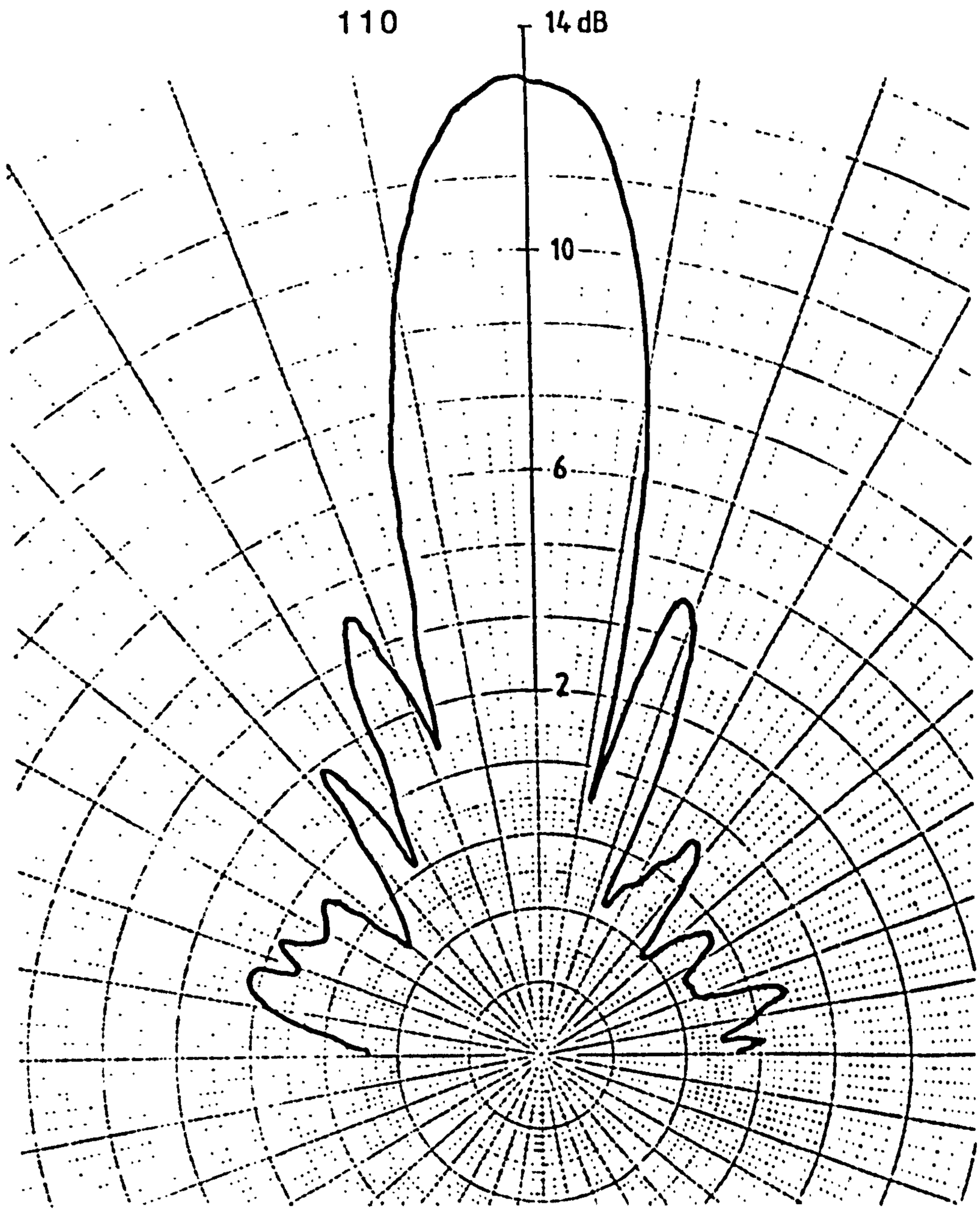

E field pattern

Figure 5.11(c). A 12 λ dipole, balanced line fed antenna.

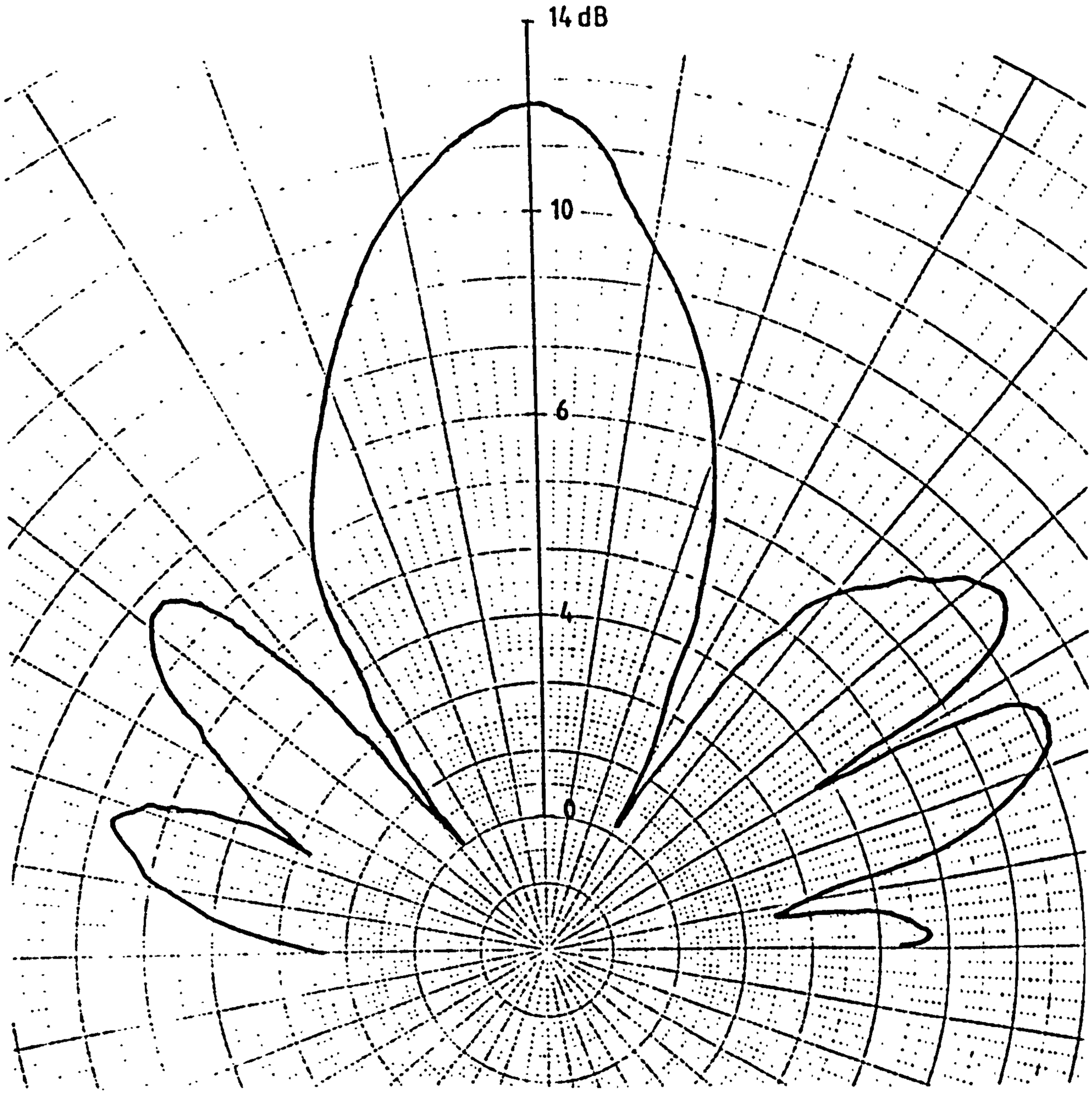

——— H field pattern

Figure 5.11 (d). A 12 λ dipole, balanced line fed antenna.

5.5.2 24 element array.

A 24 element array designed to operate at 10GHz was fabricated. In order to obtain a more symmetrical radiation pattern the radiating elements were arranged in 4 rows of 6 λ dipoles, fig 5.12 . The four balanced lines were driven from slot lines of 100Ω impedance. The technique used to feed these slot lines was to use T-splitter strip lines on the reverse side of the substrate. The two branch lines of each splitter (100Ω) are in parallel and join up to a 50Ω feed line. Quarterwave transformer are used to implement matching when required, fig 5.12(a). In order to avoid feeder radiation and external noise an aluminium shield was placed on top of the feed section. This shield was designed to prevent cavity resonances. A symmetrical radiation pattern was obtained with a slight boresight error of about 10^0. The broadside main lobe radiation was 17 dB with a beamwidth of 14^0x12^0 in the E and H plane, fig 5.12(b,c).

This array was very frequency sensitive with a pronounced frequency squint due to the complex feed structure. The main side lobes were symmetrical about the main lobe and occurred at $\pm 20^0$ with an isotropic gain of 6dB. A reduction of 10db when compared with the main lobe radiation. The cross polarisation in the E and H planes of - 6dB can be compared with a theoretical value of - 14 dB.

5.6 Centre Fed Balanced Line Antennas.

If the line losses in the balanced line feeders are significant cause of loss then some improvement in efficiency can result from centre feeding the array, fig 5.13(a,b). A centre fed six element balanced line array was designed to give a more directive gain system and to reduce feeder loss. Six λ dipoles are spaced at λ intervals to produce a broadside array.

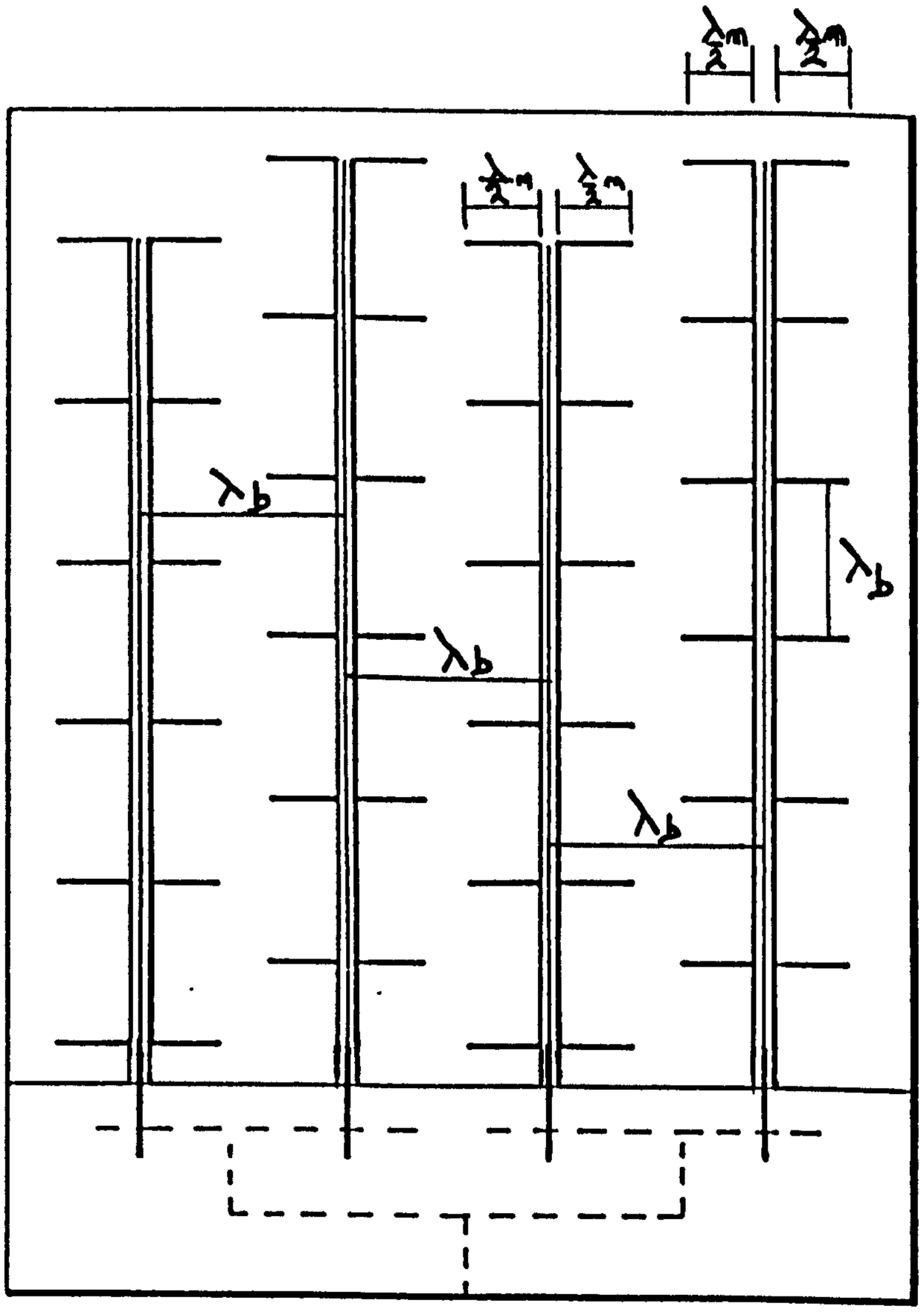

Figure 5.12. 24 λ dipoles fed by four balanced line feeders.

NAME	TITLE
	114

IMPEDANCE OR ADMITTANCE COORDINATES

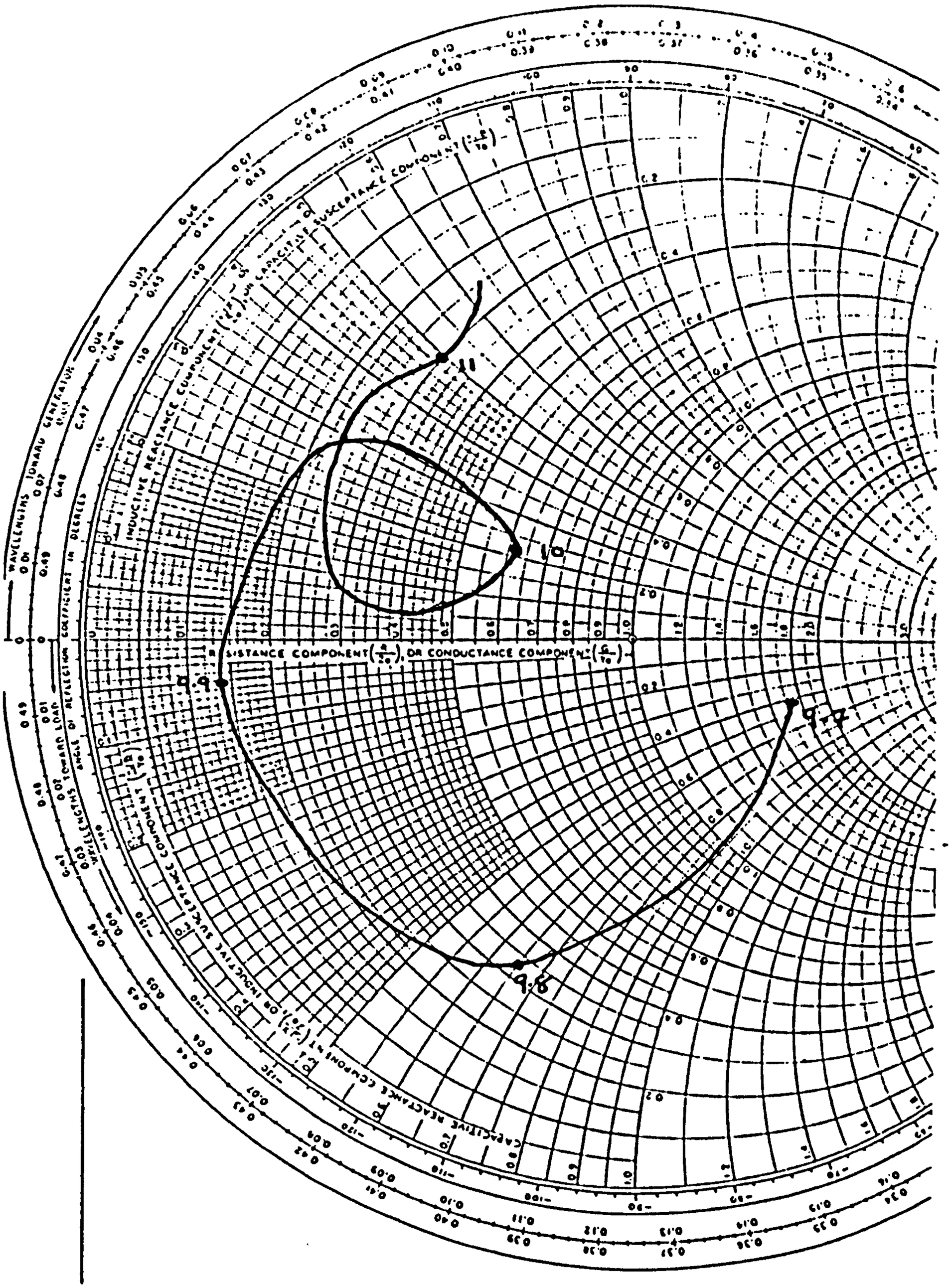

Figure 5.12(a). Impedence plot of 24 λ dipole fed by 4 balanced line feeders.

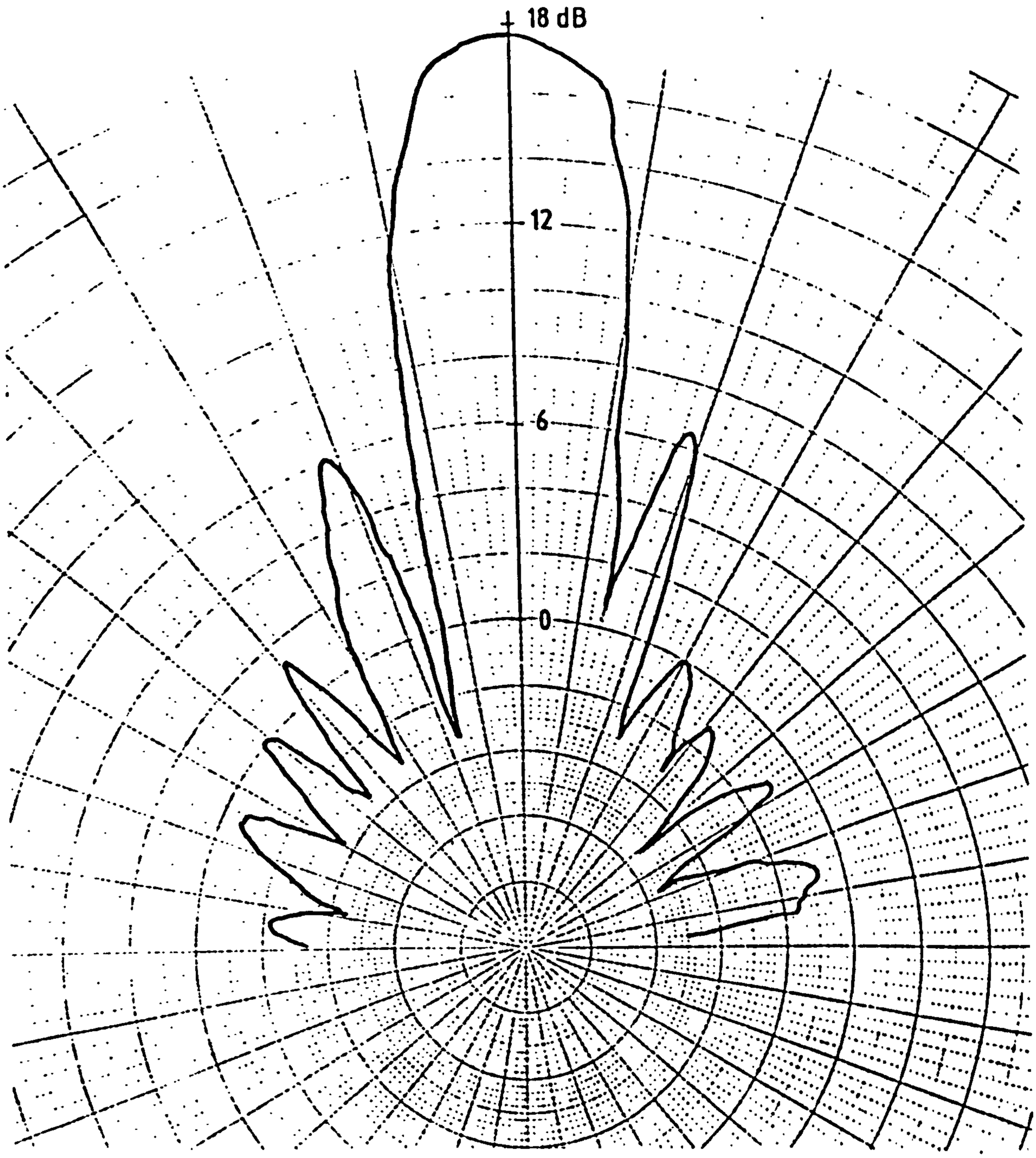

E plane radiation

Figure 5.12 (b). A 24 λ dipole array, fed by 4 balanced line feeders.

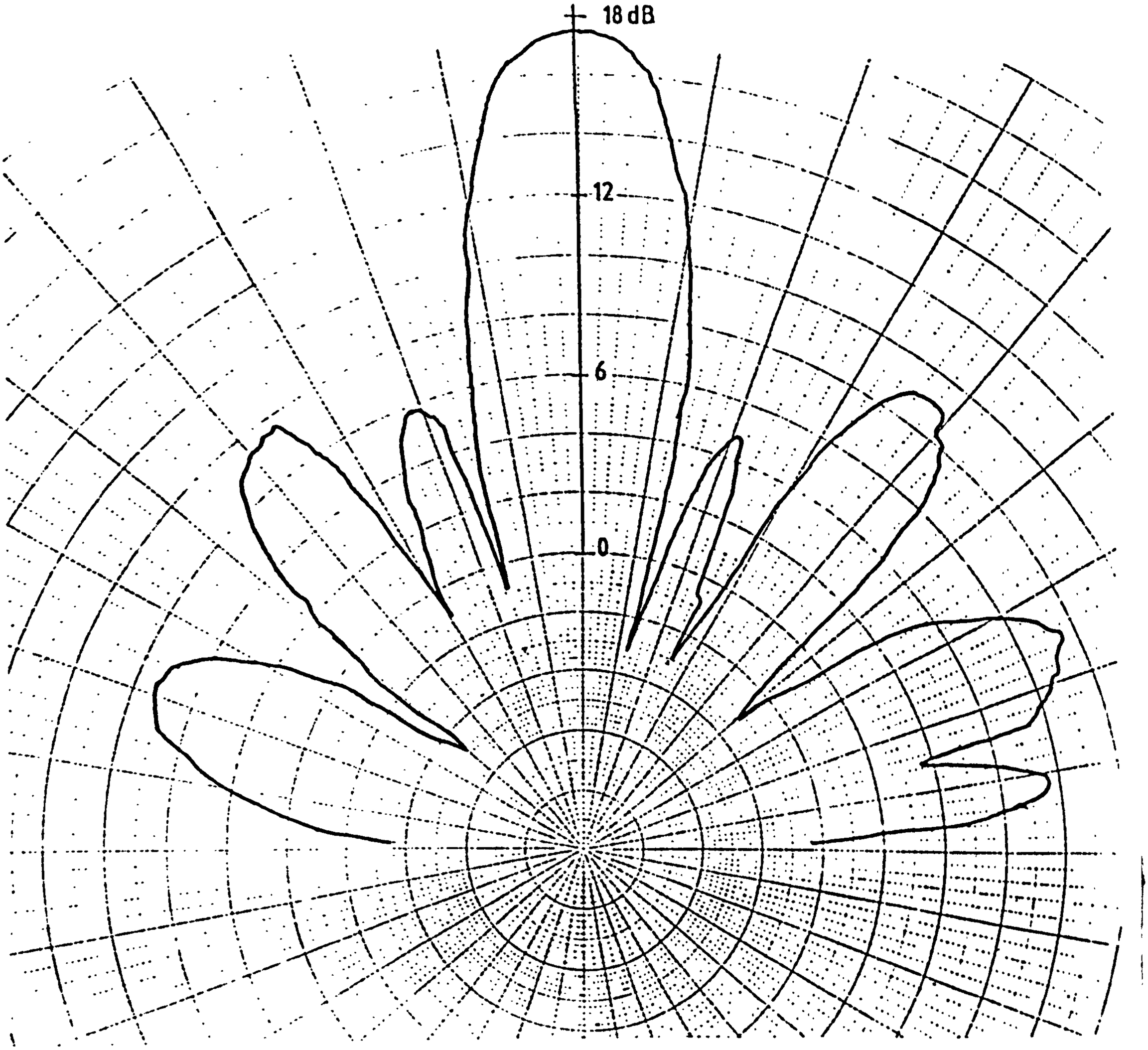

——— H plane radiation

Figure 5.12 (c). A 24 λ dipole array, fed by 4 balanced line feeders.

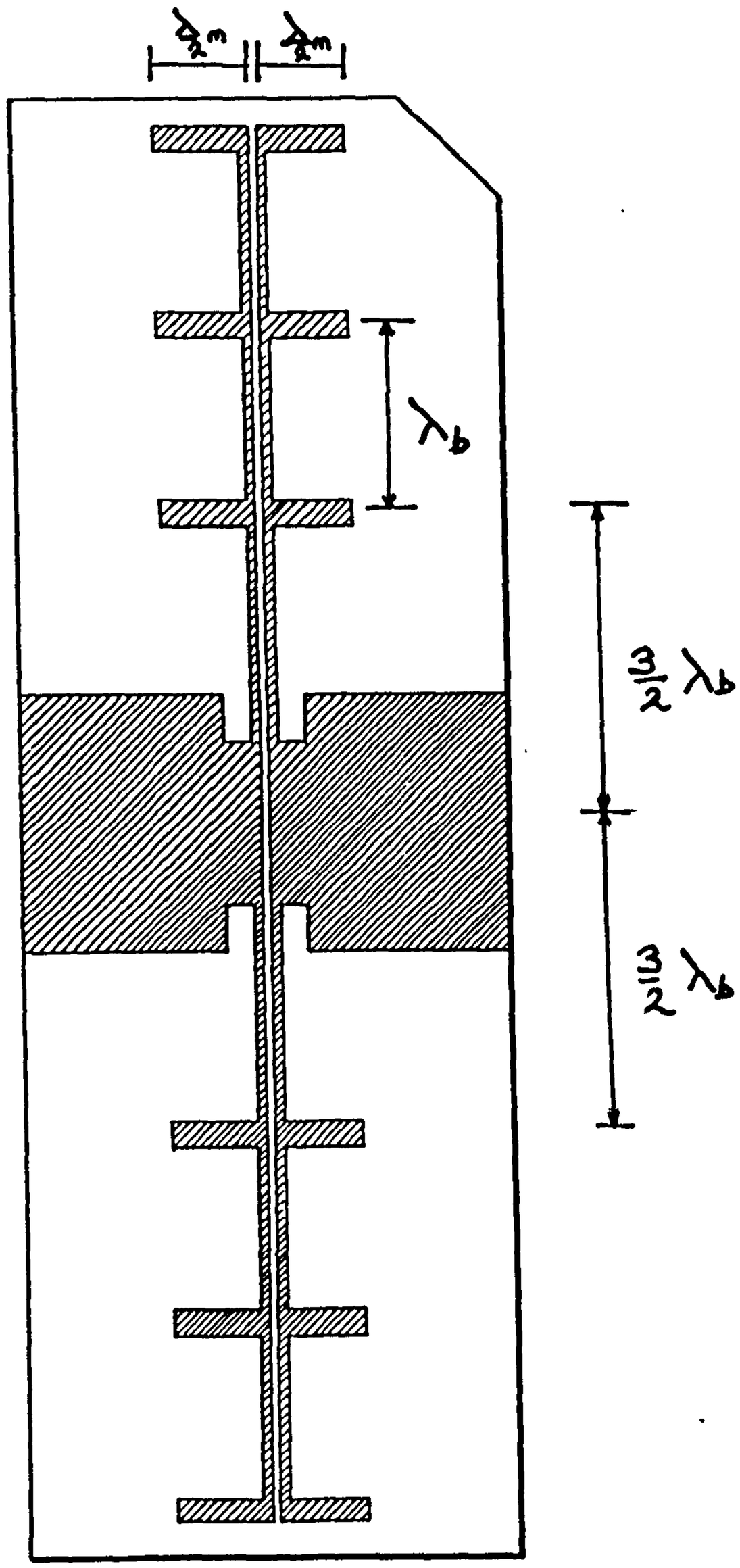

Figure 5.13(a) Centre fed balanced line antenna.

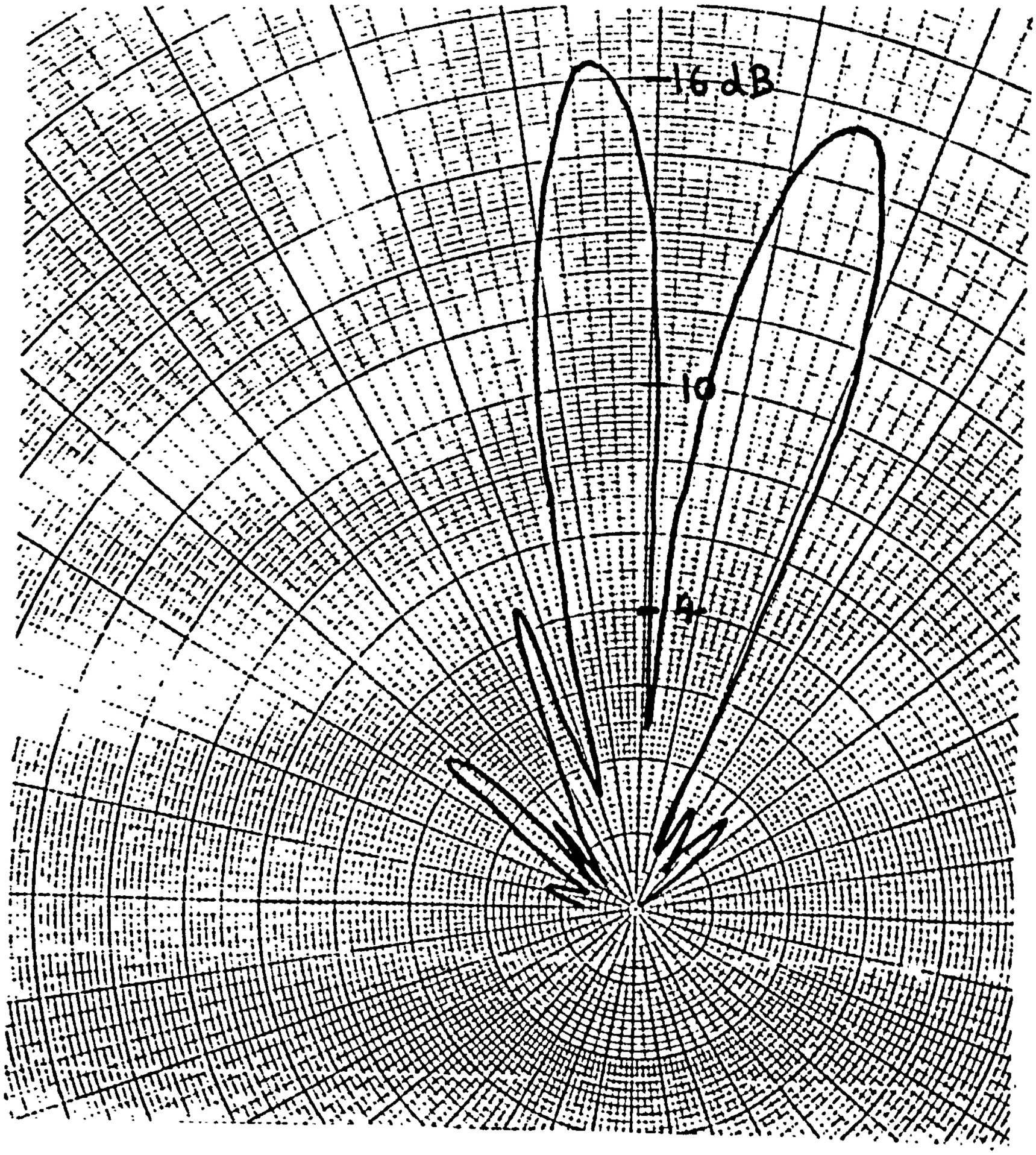

——— E field radiation

Figure 5.13 (b). Radiation pattern of a 6 λ dipole array, centre fed by a balanced line feeder.

This array radiated in the broadside direction with a main lobe gain of 16 dB and a beamwidth of 12^0 x 14^0. The side lobe levels were extremely high, with secondary lobe gains of 10dB. The cross polarisation was -4dB compared with a theoretical value of -18dB. A particular problem with centre feeding the array is that the feeder currents move in two different directions, hence the radiation from each end of the array has a different squint angle, which limits the bandwidth obtainable from this arrangement [4].

5.7 Conclusions.

Microstrip antenna suffer from considerable feed line radiation and it is evident that there is a cyclic variation of feeder radiation with length [5].

This radiation decreases as the feeder lines become longer. This effect is less noticeable with balance line antenna were feeder radiation is greatly suppressed, fig 5.14

The balanced line feeder requires the use of an unbalanced to balanced line converter (balun). This balun involves extra complexity and may lead to excessive antenna losses. For a balanced line antennas a microstrip to slot line transition can be used as the balun, with the slot line operating in a push-pull mode to drive the balanced line. Radiation from the open circuit microstrip was suppressed by the use of a below cut-off shield enclosure.

This enclosure physically changes the microstrip configuration with losses due to the presence of the enclosure. The physical structure of a suitable balun is investigated in chapter 6.

fig 5 .14 Summary of Microstrip Antennas.

No	Antenna Type	Gain (db)	fo Ghz)	B.W. MHz.	Beamwidths (degress)		Sidelobe level (dB)		Cross polar lobes (dB)		
					E plane	H plane	E	H	E	H	
1	Five Element Microstrip 	10.5	9.8	800	20	30	5	3	4	4	The loss within the feeder and radiating elements is an acceptable 1.5 dB.
2	Ten Element Microstrip 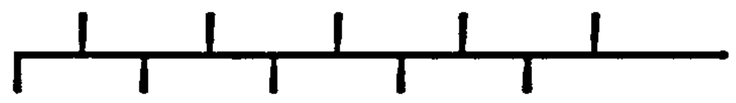	13.5	9.85	600	15	35	5	3	4	4	A Bore sight error of 1 was obtained, due to the measurement system.
3	2 x 10 Element (Suppressed Radiation). 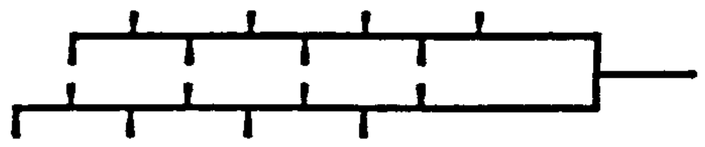	N/A	10	N/A	N/A	N/A	N/A		4	4	Cross polar radiation at + 45 (sections). End fire lobes due to travelling waves.
4	Corporate Feeds (a) U.C.N.W., Bangor 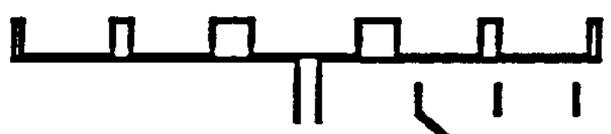 (b) Williams 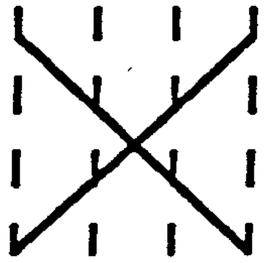	17	9.8	500	20	25	6	6	4	8	(A) High cross polar radiation in H plane due to co-planar radiation from the feeder sections. (B) Fig 5.9(b) and 5.9(c) show the two patterns obtained at + 45 and indicate the effect of feeder radiation.
		18	9.9	500	8	8.5	8	6	—	—	
5	Balanced line Feed 	13.2	10	400	14	35	6	6	- 6	- 6	Cross polar radiation is significantly reduced when compared with a similar microstrip fed antennas.
6	12 Element array (Balanced) 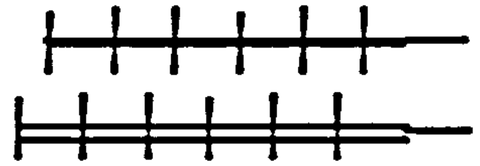	13.5	10.1	390	10	16	4	4	- 6	- 5	Theoretical cross polar radiation should be - 6 dB.
7	24 Element array (balanced) 	17	9.9	400	14	12	6	6	- 6	- 6	The theoretical cross polar radiation should be - 14 dB.
8	Centre fed Balanced line 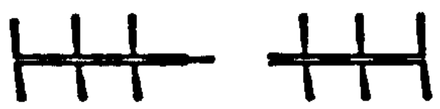	16	10	200	12	14	4	4	- 4	- 4	Since the feeder current moves in two directions the radiation from each end of the array has a different squint angle.

This array radiated in the broadside direction with a main lobe gain of 16 dB and a beamwidth of 12^0 x 14^0. The side lobe levels were extremely high, with secondary lobe gains of 10dB. The cross polarisation was -4dB compared with a theoretical value of -18dB. A particular problem with centre feeding the array is that the feeder currents move in two different directions, hence the radiation from each end of the array has a different squint angle, which limits the bandwidth obtainable from this arrangement [4].

5.7 Conclusions.

Microstrip antenna suffer from considerable feed line radiation and it is evident that there is a cyclic variation of feeder radiation with length [5].

This radiation decreases as the feeder lines become longer. This effect is less noticeable with balance line antenna were feeder radiation is greatly suppressed, fig 5.14

The balanced line feeder requires the use of an unbalanced to balanced line converter (balun). This balun involves extra complexity and may lead to excessive antenna losses. For a balanced line antennas a microstrip to slot line transition can be used as the balun, with the slot line operating in a push-pull mode to drive the balanced line. Radiation from the open circuit microstrip was suppressed by the use of a below cut-off shield enclosure.

This enclosure physically changes the microstrip configuration with losses due to the presence of the enclosure. The physical structure of a suitable balun is investigated in chapter 6.

REFERENCES FOR CHAPTER 5.

[1] Kardon B.,
Certify test stations for accurate antenna QA.,
Microwave & R.F., 1987 .

[2] Davies J.B. & Mirshekar-Syahkal D.,
Spectral domain solution of arbitrary coplanar line with multilayer substrate, IEEE trans. MTT-25, page 143, 1977 .

[3] Williams J.C.
Cross-fed printed aerials, Proc 7th European Microwave Conf. Copenhagen, page 292 - 296, 1977.

[4] James J.R., Hall P.S., Wood C.,
Microstrip antenna theory and design,
IEE Electromagnetic wave series 12, Peter Peregrinus ltd, 1984.

[5] Bahl I.J., Bhartia P.,
Microstrip antenna, 1980, Artech house.

CHAPTER 6.

6. Balun Design and Testing.

To successfully employ balanced line feeds driven from unbalanced line a balun is required. Several types of balun have been designed based on their coaxial counterparts. It would be attractive to fabricate the balun and the antenna array on a single coplanar substrate. Since broadside arrays are intrinsically narrow band a wide-band balun is not required. Experimental circuits have been designed using a $3\lambda/2$ hybrid ring as the balun [1] .

6.1 hybrid ring baluns.

A 12 element array consisting of six λ dipoles spaced at λ intervals along a feed line was fabricated. This balanced line was fed from a hybrid ring, fig 6.1, constructed using Manhattan Geometry. From radiation measurements on this array a broadside gain of 15dB with a beamwidth of $10^0 x 16^0$ was measured compared to a theoretical gain of 16dB. Thus indicating that there is an acceptable 1db of loss within the array. However the cross polarisation radiation was extremely high with an isotropic gain of 8dB being measured in both the E and H planes. The side lobe radiation is highly unsymmetrical, indicating that the travelling wave component of the feeder current is not negligible.

An antenna array consisting of 12 λ dipoles spaced at λ intervals and fed by two sets of balanced line driven by hybrid ring baluns was fabricated. The hybrid rings are connected in parallel by an unbalanced microstrip T section and quarter wave transformer to a 50Ω feed line and source.

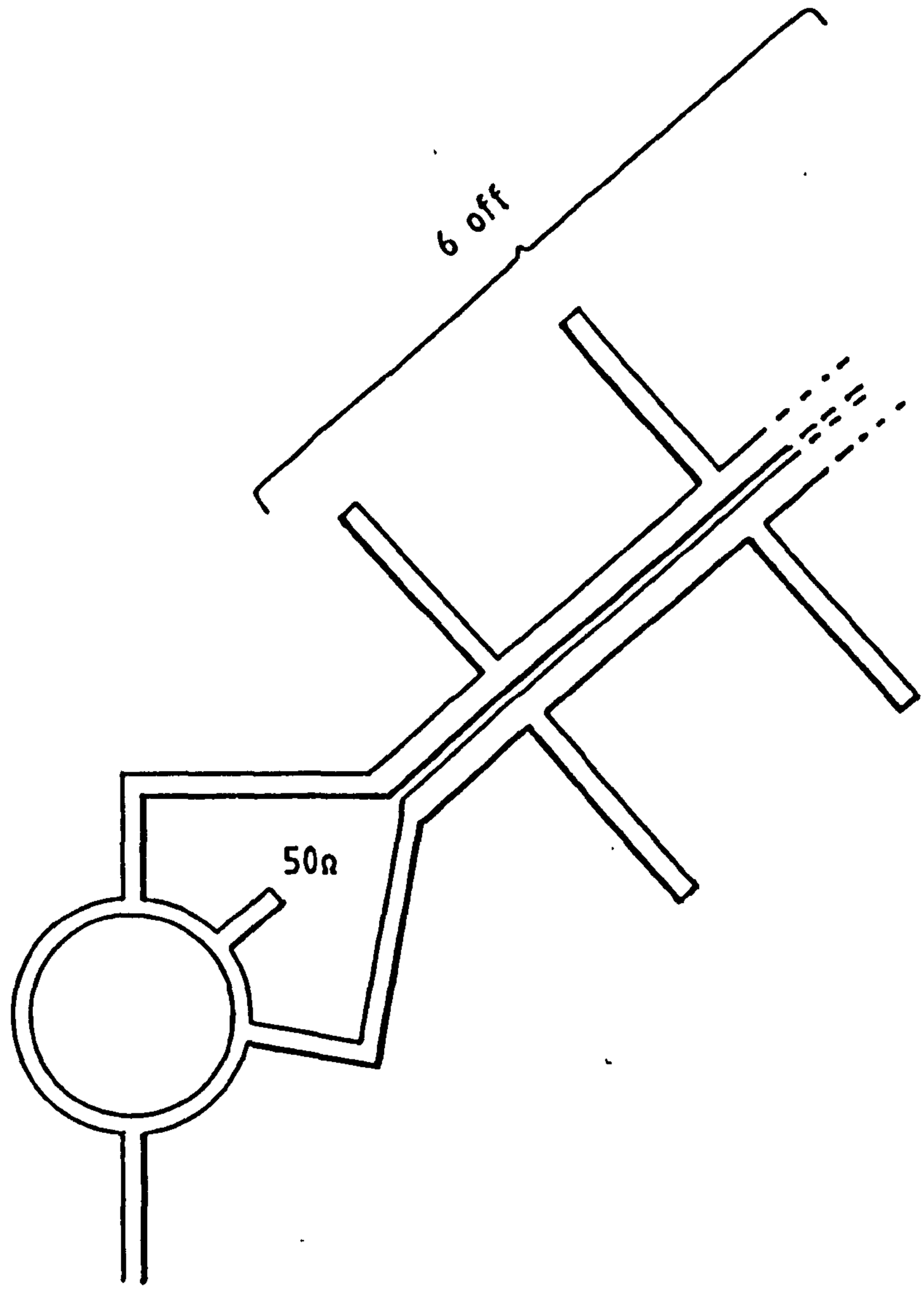

Figure 6.1. Six λ dipoles fed by a single hybrid ring balum.

A broadside antenna, fig 6.2 had a measured gain of 18dB for this array with a beamwidth of $12^0 \times 12^0$ which compares well with a theoretical gain of 18dB. Excessive cross polar radiation of 9dB in both the E and H planes was experienced for this array. Thus a balanced line fed antenna with a similar gain to a microstrip antenna can be fabricated. But a passive single substrate balanced line antenna requires the use of excessive unbalanced strip line leading to unrequired feed radiation. Shielding the hybrid ring reduced this feeder radiation by 3dB at the cost of increased complexity and leads to a major disruption of the radiation pattern.

6.2 Microstrip to slot line balun.

A more practical type of balun would require that the unbalanced microstrip line is shielded from the radiation suppressing balanced line. A slot line to microstrip transition can be used to drive the balanced line antenna while shielding the array from the strip line radiation. The fabrication of a slot line to microstrip transition can be easily included in the M.I.C fabrication routine.

The basic slot line configuration is shown in fig 6.3, and consists of a dielectric substrate with a narrow slot etched into the metallisation on one of the surfaces of the substrate. The other surface of the substrate is without metallisation. Slot line can be included in microstrip circuits by etching the slot line circuit in the ground plane of the microstrip circuit. In slot line the wave propagates along the slot with the major electric field components orientated along the slot in the ground plane. The mode of propagation is non T.E.M [2] and almost transverse electric in nature. The approximate field distribution is shown in fig 6.3 .

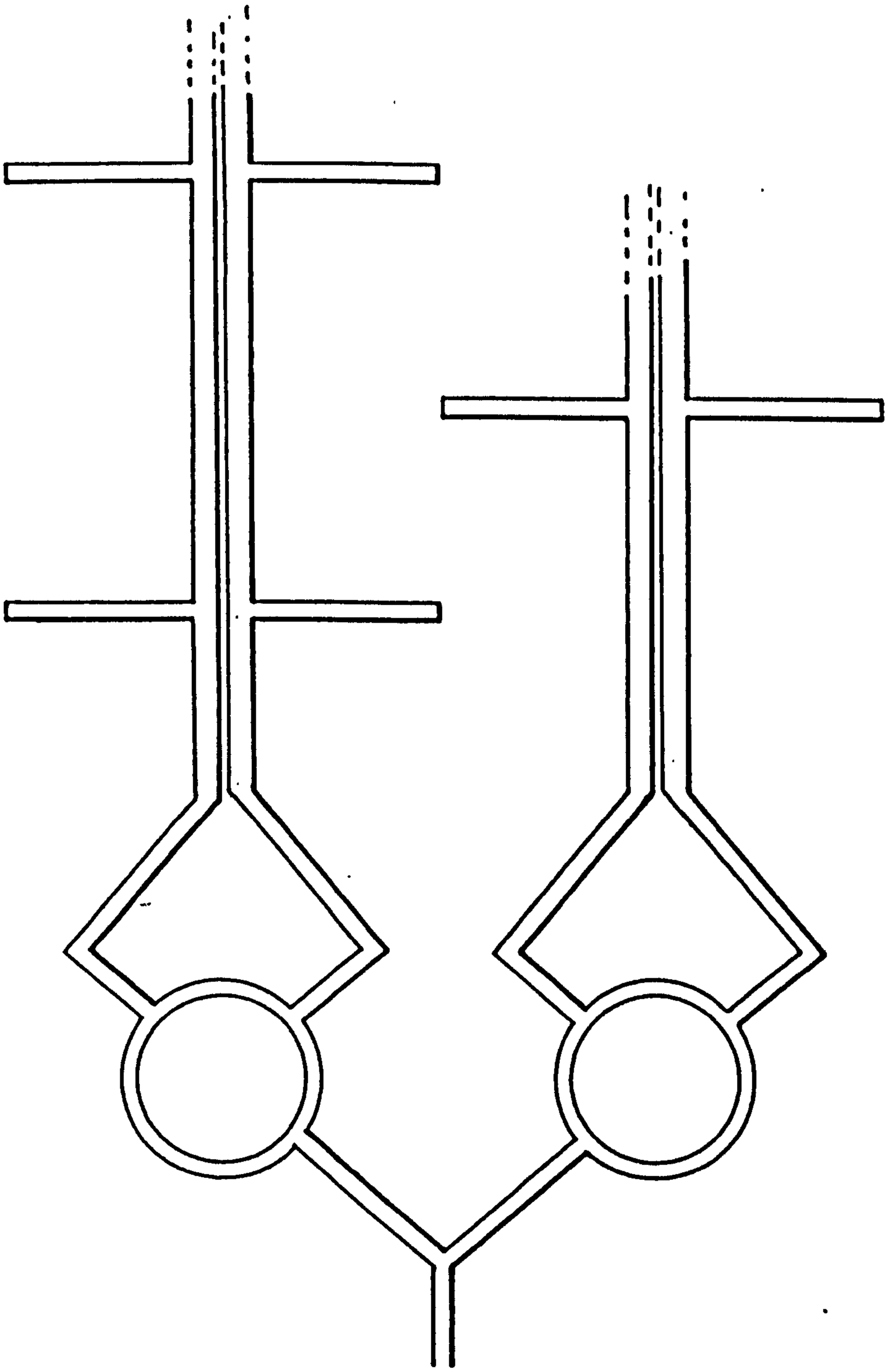

Figure 6.2. 12 λ dipoles fed by two hybrid rings.

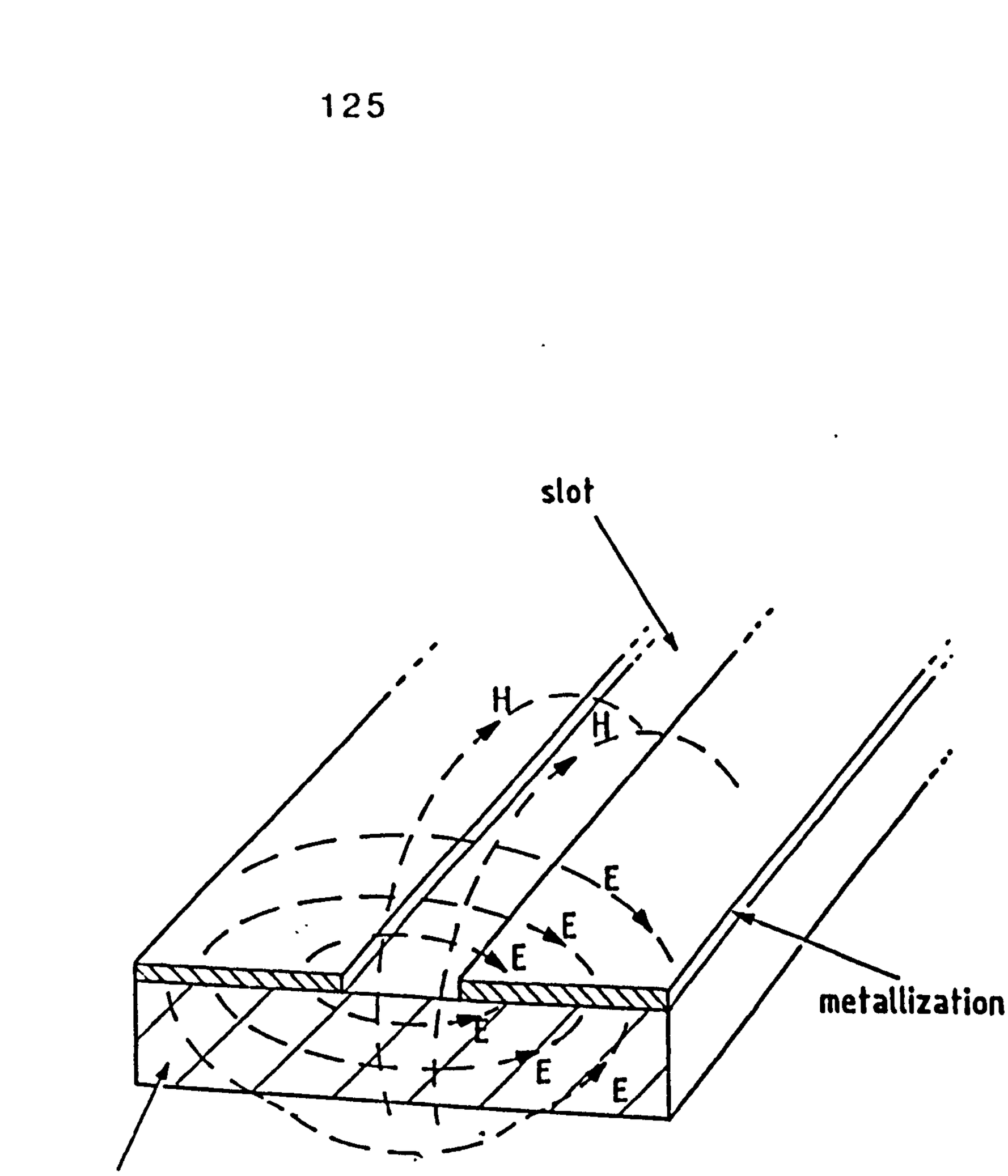

Figure 6.3. Field distribution in cross-section of slot line.

The transition from microstrip to slot line is achieved by placing microstrip on one side of the substrate and slot line on the other side. The slot line and microstrip line cross each other at right angles and extend from the crossing point for a quarter of a wavelength. The strip line is terminated in an open circuit while the slot line is terminated in a short circuit. Thus the microstrip line can be coupled to the slot line at the crossing point over a wide frequency range without loading the slot line. The microstrip to slot line transition has been rigorously analysed by Itoh et al [3] using a generalised transverse resonant technique for computing the resonant frequency of a resonator, created by enclosing the crossing with auxiliary perfect conducting walls.

For a specified frequency, resonant structures are found by adjusting the length of the strip and hence the resonator size. These structures are used for deriving the equivalent circuit parameters characterising the discontinuity. This approach requires the use of extensive computation and computer storage. A practical example of a planar balun utilising the microstrip to slot line transition is the Marchand Balun [4], fig 6.4 where the load impedance and bandwidth are specified in terms of the physical characteristics of the balun.

6.2.1 Marchand balun.

A 2nd order Marchand Balun was designed for a balanced line fed antenna feeding six λ dipoles operating at a centre frequency of 10 GHz, representing a load impedance of 150Ω to the slot line.

The characteristic impedance of the various sections of the balun were calculated from a set of design graphs to give:

$Z_{m1} = 70\Omega$

$Z_{m2} = 68\Omega$

$Z_{s1} = 120\Omega$

$Z_{s2} = 110\Omega$

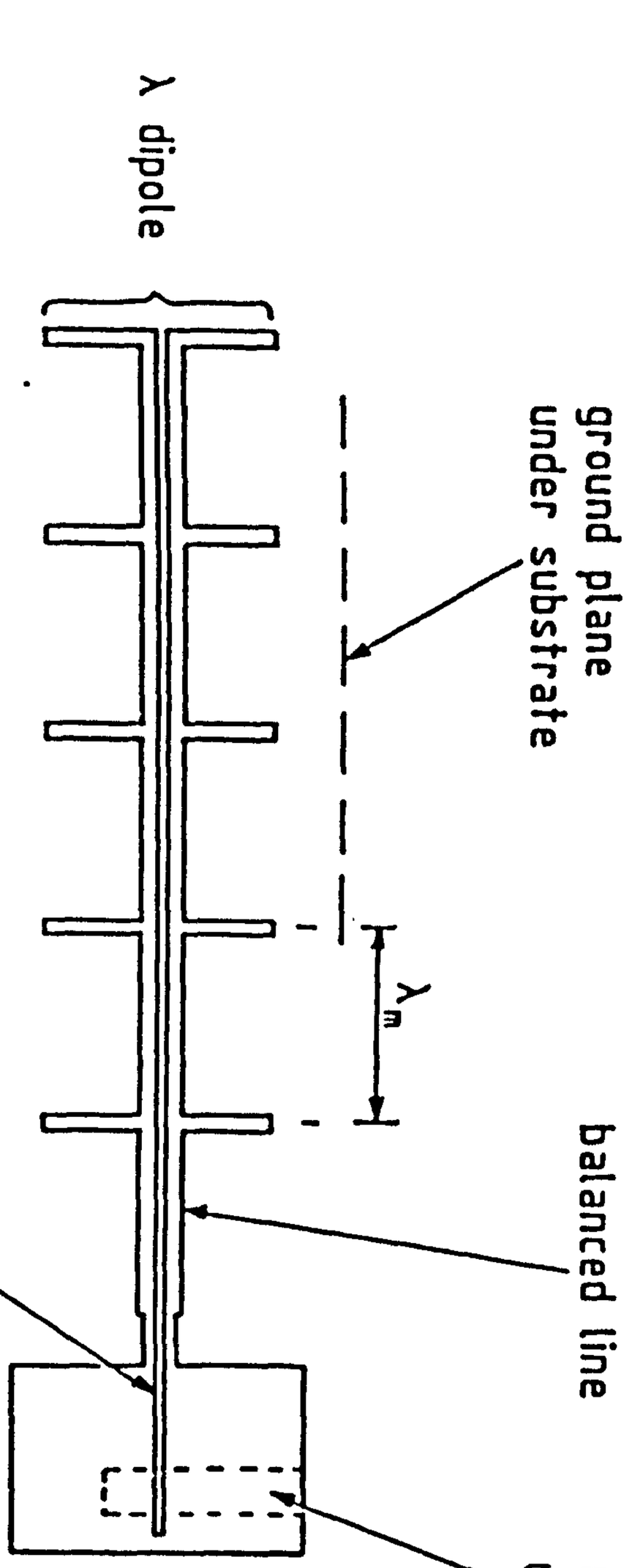

Figure 6.4. Marchand Balun connecting microstrip to slot line.

where,

Z_{m1} is the input microstrip feed line.

Z_{m2} is $\lambda/4$ open circuit microstrip.

Z_{s1} is $\lambda/4$ short circuit slot line section.

Z_{s2} is the output slot line.

Design graphs [5] were used for substrates with a permittivity of 2.55 to determine the characteristic impedance and propagation velocity of the slot line for a given slot line width and substrate thickness, fig 6.5 . For an antenna fabricated on a 1.6mm substrate the width of the slot for a characteristic impedance of 100Ω is 0.4 mm.

A network analyser was then used to obtain the S parameters for the microstrip to slot line transition and the transition from slot line to balanced line using a method described by Altman [6]. The slot line was short circuited at the crossing point using a highly polished aluminium sheet and a plastic clamp. Thus leaving the magnetic field in the slot line undisturbed. The effective end of the microstrip is then found by applying a frequency sweep and extending the reference plane to the open circuit termination of the microstrip. The reference plane is the shifted to the crossing point by moving the reference plane a $\lambda/4$ back towards the source. The short circuit is then placed at several points along the balanced line and the distance from the short circuit is measured using a travelling microscope. The value of the reflection coefficient was noted at each point.

The power loss in the balun was shown to be about 4dB. However from theoretical considerations the loss in the transition should be about 0.6dB. This additional loss is shown in section 6.3 to be due to the need for a good earth connector between the earth plane of the slot line and the earth plane of the balanced line.

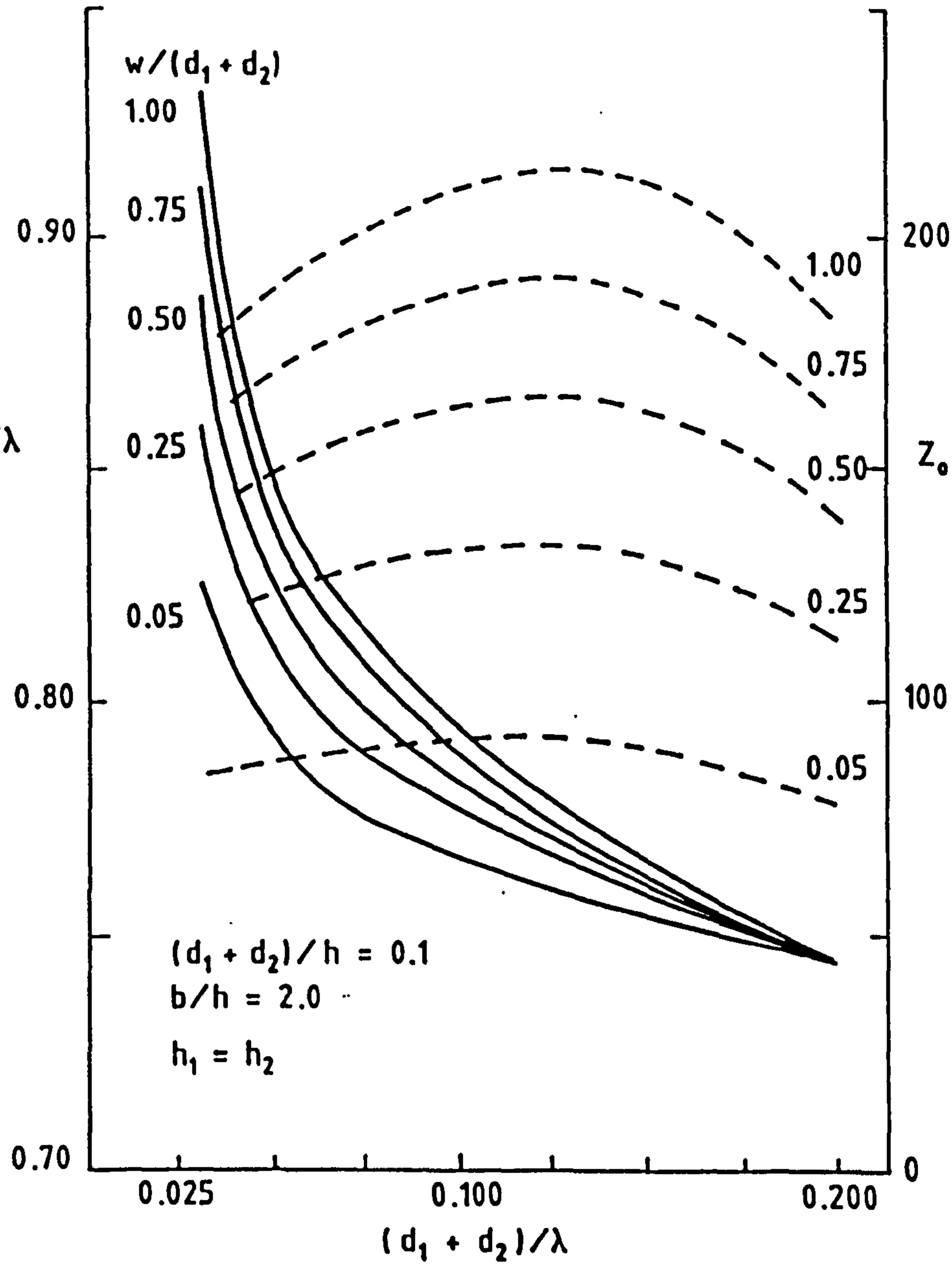

Figure 6.5. A design graph for characteristic impedance and propagation velocity in slot line.

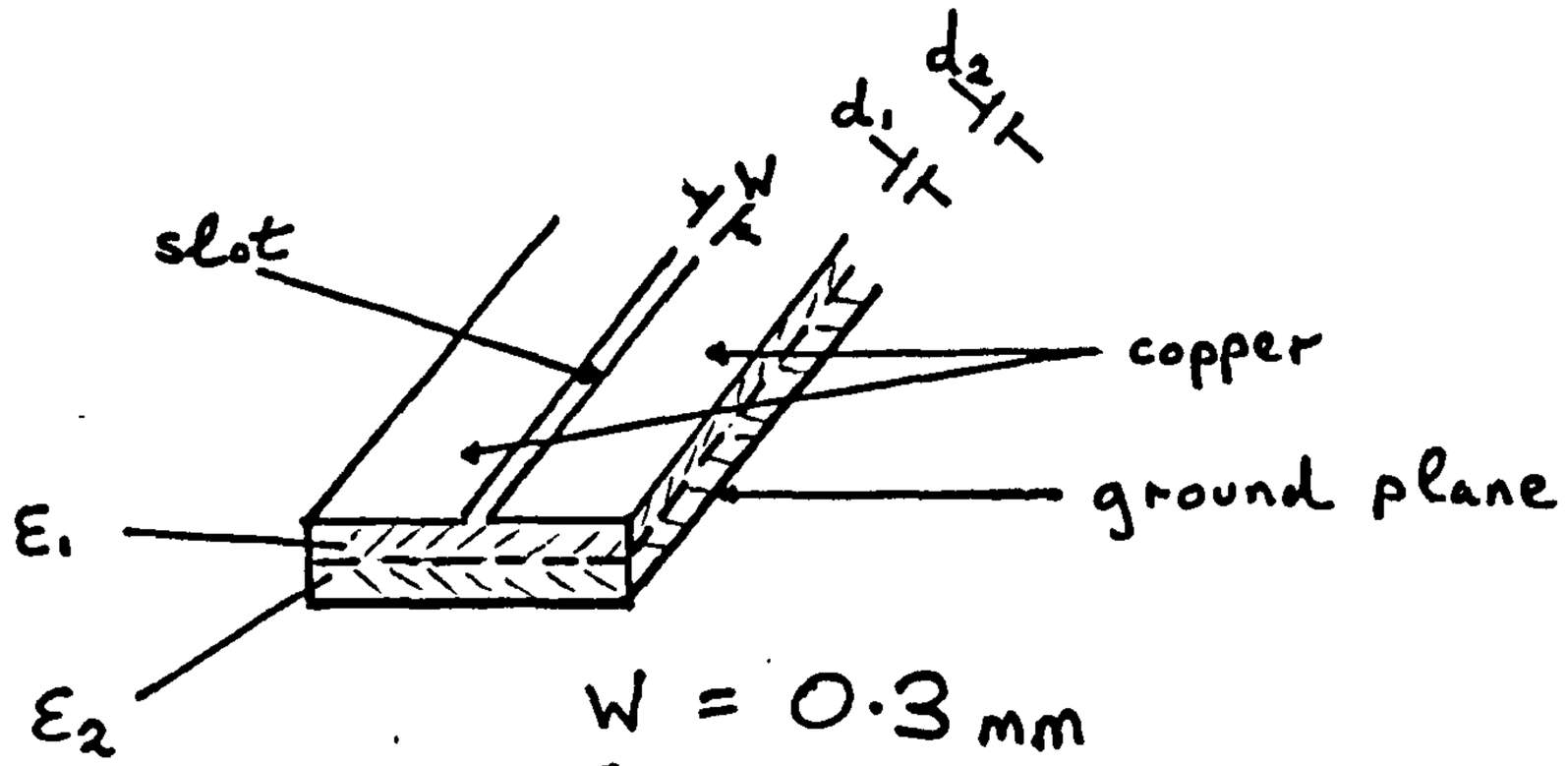

6.3 The slot line to balanced line transition.

Measurements of the E field and H fields at the transition from slot line to balanced line were undertaken at a frequency of 1 GHz on a scaled up easily fabricated model made from several layers of copper foil fixed to the substrate by adhesive. From the probe readings it could be seen that most of the E field is concentrated above the slot line, but that a standing wave pattern is set up between the transition from slot line to balanced line causing a 'quasi-slot' line propagation between the slot line earth plane and the balanced line earth plane leading to excessive antenna loss, fig 6.6 . The characteristic impedance of this line was calculated to be 180Ω leading to a 3dB loss in the transition from slot line to balanced line.

This problem was solved by placing shorting posts at $\lambda/4$ intervals from the balanced line, so that a high impedance is obtained at the slot line to balanced transition, fig 6.7(a,b) . These shorting posts 'tie' the two active ground planes together in order to suppress 'quasi-slot' propagation and radiation. The slot line ground plane was arranged so as not to overlap the balanced line ground plane. The power loss in the improved microstrip to slot line transition was then measured and shown to be approximately 0.5dB as expected.

6.4 Improvements in Balun Design.

A balanced line array utilising this improved balun was then fabricated. This array consisted of 6 λ dipoles spaced at λ intervals along the balanced line was fabricated. The balanced line feeder was then matched to an unbalanced microstrip feed line by the improved balun.

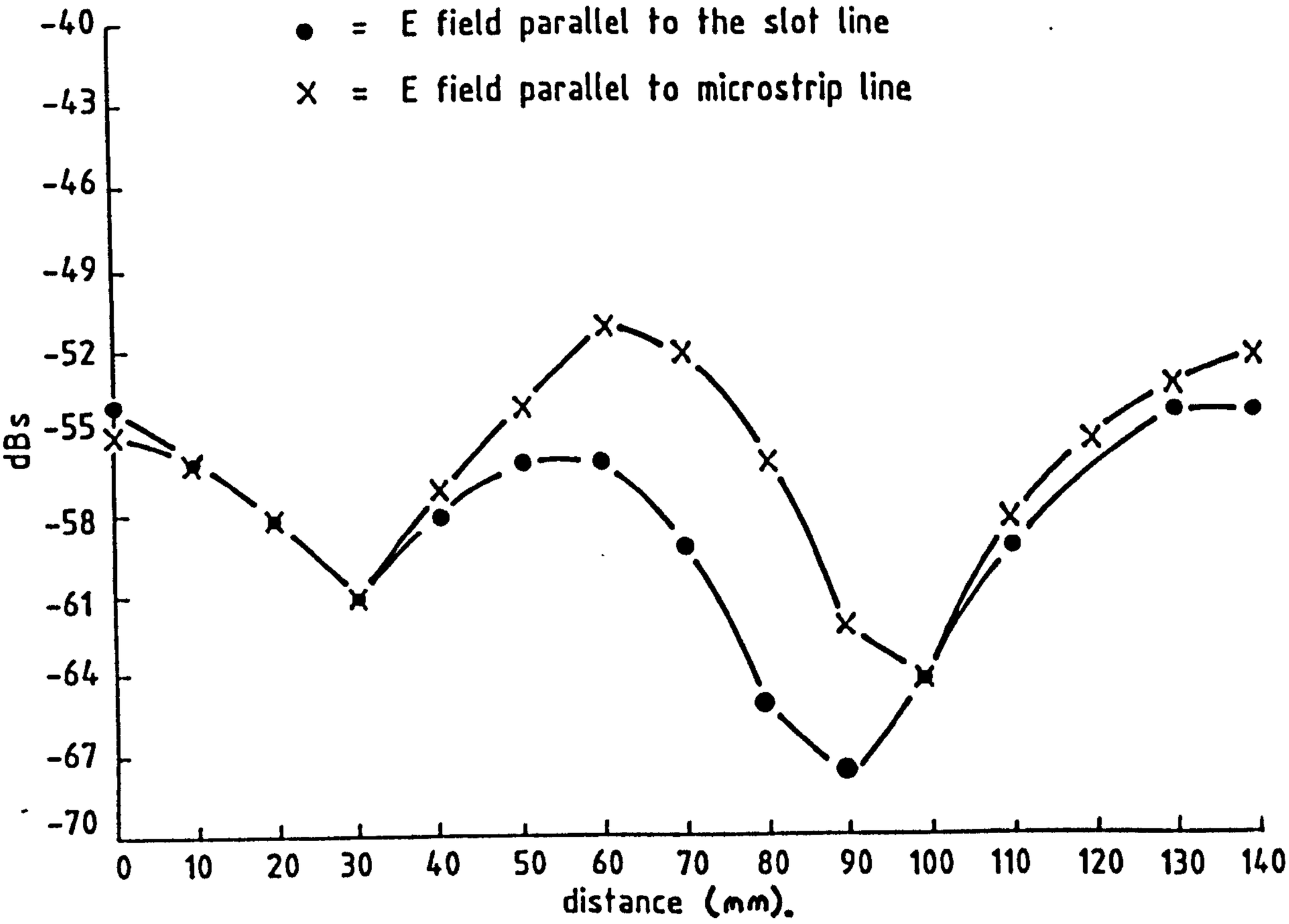

Figure 6.6. Transition from slot line to balanced line.

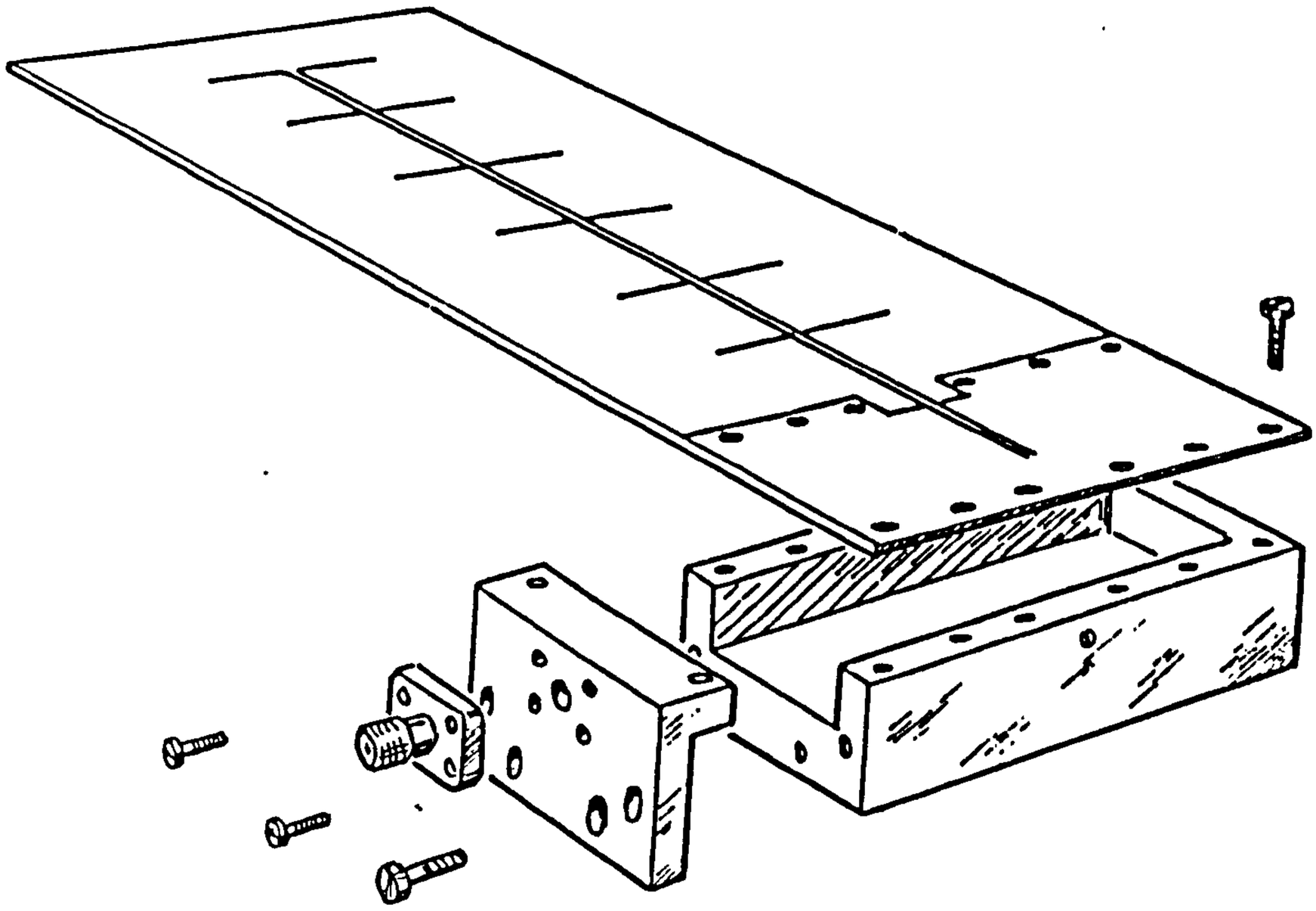

Figure 6.7 (a). Antenna assembly.

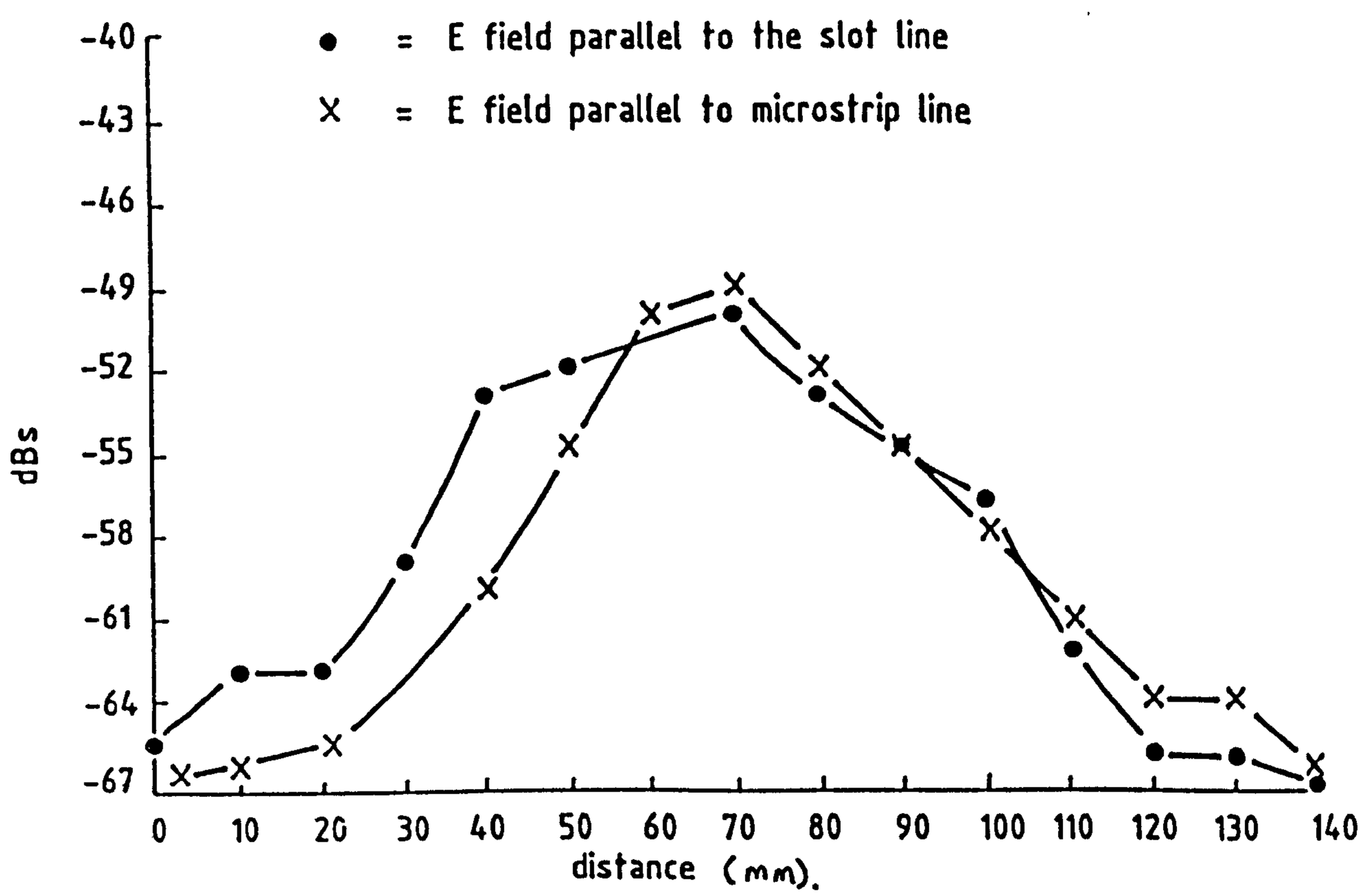

Figure 6.7(b). Transition from slot line to balanced line, with shorting post .

This balun consisted of overlapping balanced line and slot line ground planes shorted together at $\lambda/4$ intervals from the slot line to balanced line transitions, fig 6.8 . In order to present a very high impedance at the balanced line to any 'quasi-slot' modes. Radiation from the microstrip section was suppressed by a shielded enclosure taking into account balun characteristics.

This antenna array gave very promising results with a broadside antenna gain of 15dB and a 3dB beamwidth of 12^0x15^0. The side lobes were symmetrical with gains of 3dB and 2dB at $\pm 18^0$ respectively, fig 6.8(a). The cross polarised radiation in the E and H planes was only 10db. The theoretical gain calculated for this array is 16dB. Thus an acceptable 1db is lost within the feeder balun structure, while the cross polar radiation has been reduced by -14dB when compared with a similar microstrip antenna.

6.5 Conclusions.

In this chapter it has been successfully demonstrated that a balanced line antenna driven by a carefully designed baluns, can greatly reduce feeder radiation while providing similar antenna gains to microstrip antenna, with only a slight increase in antenna complexity and power loss.

During the course of this work only passive baluns have been investigated. The use of an active balun may further improve the performance of balanced line fed antennas. The feasibility of designing an active balun using two differential F.E.T. amplifiers to provide a balanced output from an unbalanced input signal has been demonstrated by Basset [7] and Sokolv [8].

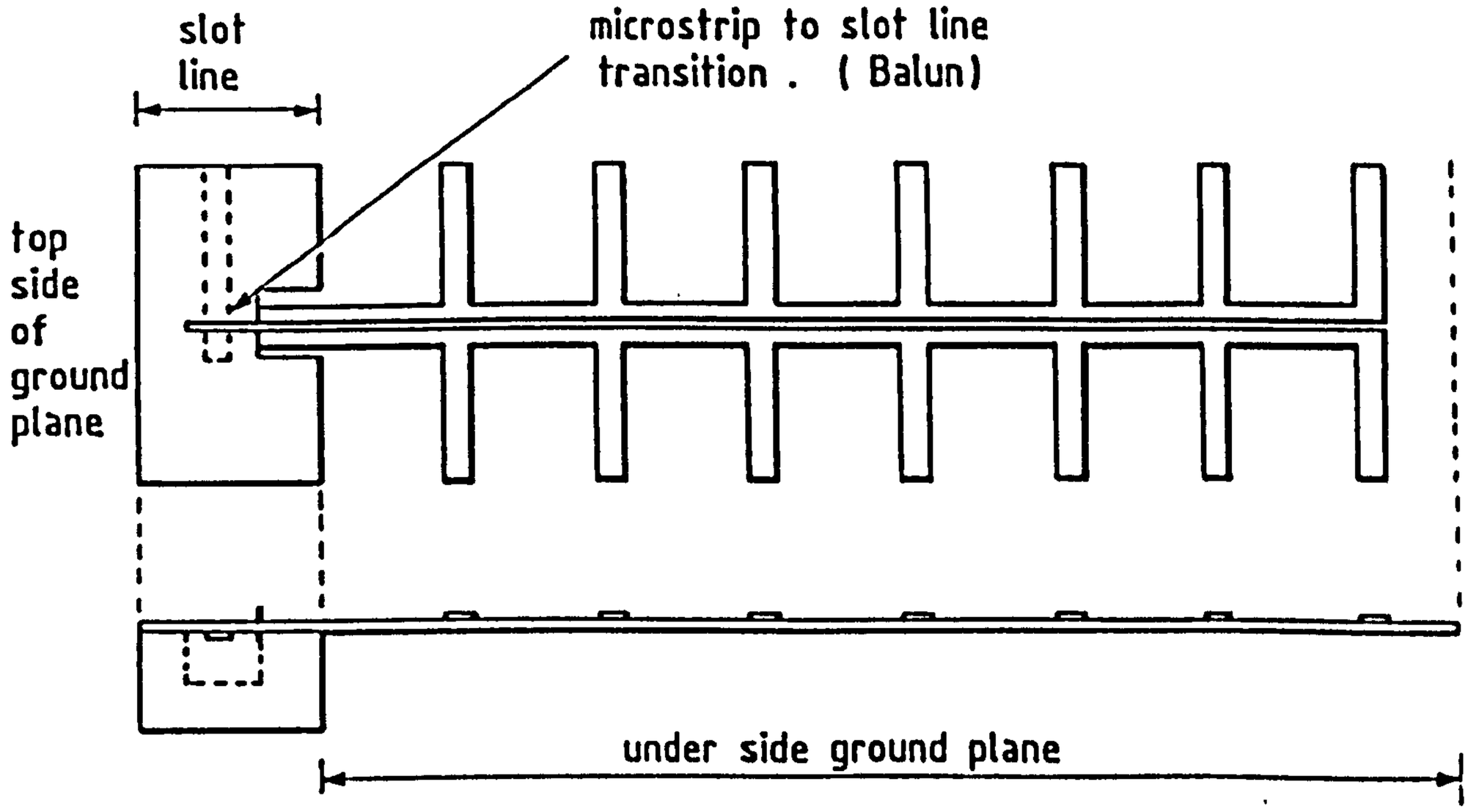

Figure 6.8(a)6 λ dipoles fed by a single balanced line.

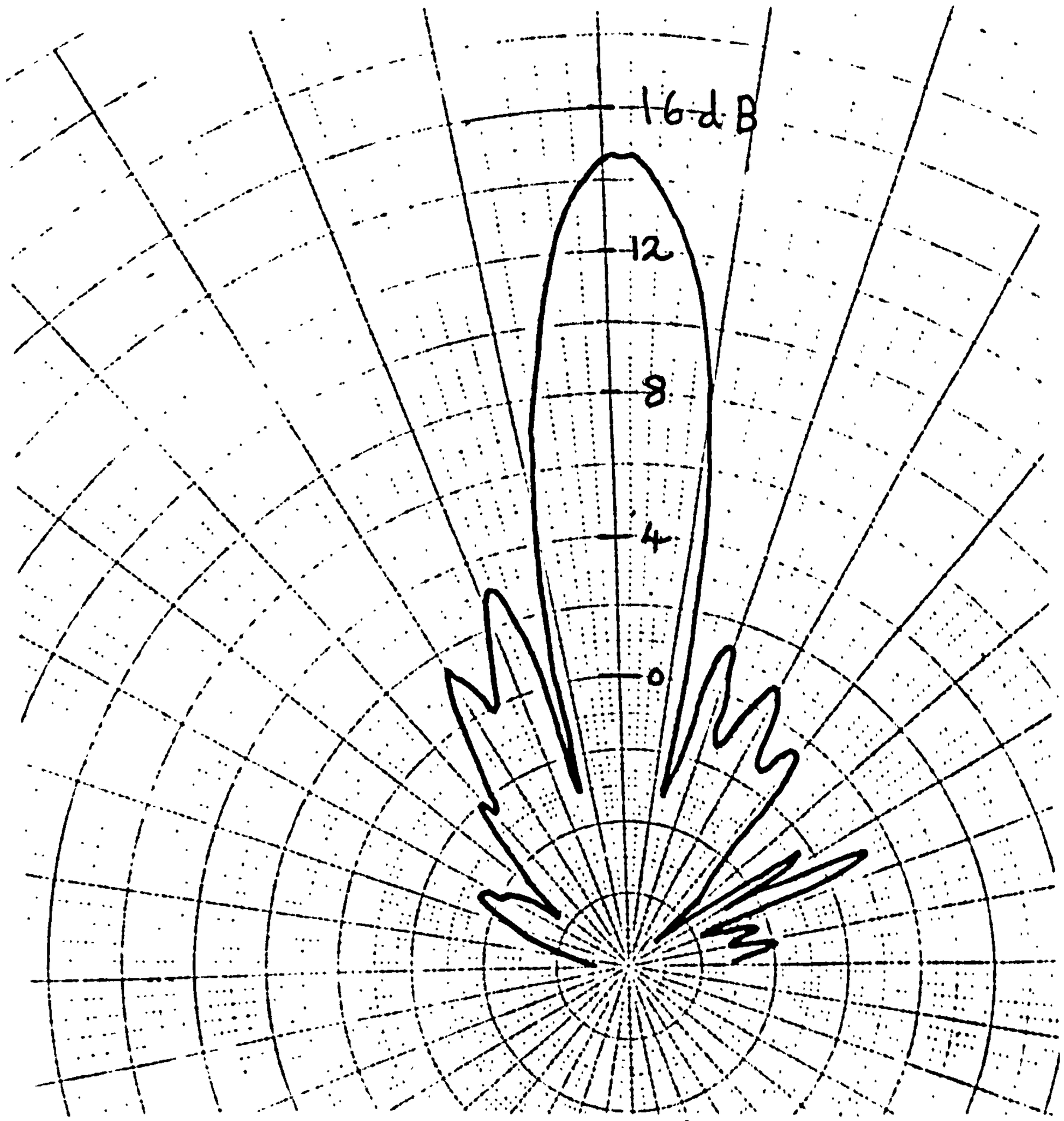

(E field).

Figure 6.8(b). Radiation pattern of a improved 6 λ dipole, balanced line fed antenna .

REFERENCES FOR CHAPTER 6.

[1] Fubini E.G.,
Airborne Instruments Laboratory Inc., Mineola N.Y., 1955 .

[2] Cohn S.B.,
Slot lines an alternate transmission medium for I.C's,
IEEE trans G - MTT, page 146 - 169, 1968 .

[3] Uwano T., Sorrentino S., Itoh T.,
Characterisation of microstrip-to-slot line transition discontinuities
by transverse analysis, European microwave conference 1987.

[4] Cloete J.H.,
Exact design of the Marchand Balun,
Microwave J., Vol 23, page 99 - 102, 1980.

[5] Simons R.,
Suspended slot line using double layer,
IEEE trans. MTT - 29, No 10, Oct 1981.

[6] Altman J.A.,
Microwave Circuits,
D. Van Nostrand Company Inc., 1961 .

[7] Basset R.,
TRW RF Semiconductors, Microwaves, July 1980.

[8] Sokolov.,
Development of GaAs monolithic Power amplifier in X band,
IEEE trans. on electronic devices, vol ED 27, No 6, July 1980.
Pg. 1164 - 1171

CONCLUSIONS 7.

Microstrip antennas have the potential to replace conventional antennas in many applications. At present a significant limitation of microstrip antennas is an incomplete understanding of the performance of the antenna and its feed structure. In particular, unwanted radiation from the feed structure can compromise antenna performance. In this thesis the radiation from both the nominal radiators and the feed lines has been calculated from an approximate current distribution, verifying the problems encountered when integrating the feeder and radiator onto a single substrate.

A continuing attraction of microstrip antennas is the possibility of fabricating the structure substantially onto the surface of a planar substrate which can be conformally mounted. Ideally low Q radiating elements should be fabricated on thick, low permittivity substrates for maximum radiation efficiency and bandwidth.

Since microstrip circuits and discontinuities radiate, it is obvious that the feeder network to the radiating elements will also radiate. The radiating elements should be fabricated on thick low permittivity substrates to maximise radiation efficiency, while conversely an above-ground feeder network needs to be fabricated on a thin, high permittivity substrate to minimise feeder radiation. In order to fabricate the radiating elements and a coplanar feed onto a single substrate of uniform thickness an alternate feed arrangement leading to a cancellation of feeder radiation was required.

For a microstrip feed line the current in the strip and its image are in anti-phase and this leads to some cancellation of feeder radiation. However, better cancellation will occur if two strip lines are configured as a balanced line. Since this configuration significantly reduces the unwanted feeder radiation while retaining the simplicity of a coplanar structure, reducing the separation distance between the two strip lines decreases feeder radiation but increases the attenuation of the balanced line.

The balanced line is fed by a slot line which is coupled to an unbalanced microstrip line on the underside of the board. This arrangement is attractive as it is compact with no unbalanced radiating elements on the upper surface of the board. A good balun is required to selectively excite odd mode propagation along the line. Significant problems were encountered in the design of the balun due to 'quasi-slot' modes of propagation along the slot line balanced line transition. These problems were solved by the careful positioning of the two earth planes with shorting pins placed at $\lambda/4$ intervals along the transition boundary. A successful balanced line antenna utilising this improved balun has been fabricated. This antenna has performance characteristics comparable to a similar microstrip antenna with greatly reduced feeder radiation. Thus an efficient balanced line fed antenna with reduced feeder radiation has been demonstrated.

APPENDIX 1.

NUMERICAL INTEGRATION USING SIMPSONS RULE.

Following the method described by Roberts [a] a computer programme was written, based on a numerical method of evaluating the definite integral by Morton [b].

$$\int_{x=a}^{x=b} f(x)\,\partial x \qquad (A1.1)$$

The function f(x) is calculated at an even number of sub-intervals of the whole interval (a,b), the size of the sub interval being chosen to give the required accuracy. The value of the integral is given by Simpson Rule as

$$\int_{x_0}^{(x_0 + 2nh)} f(x)\,\partial x = \frac{1}{3} h\,(f_o + 4f_1 + 2f_2 + 4f_3 + 2f_4 + \ldots\ 4f_{2n-1} + f_{2n}) \qquad (A1).$$

Double integrals can also be evaluated using Simpsons Rule as follows, fig a.1 :-

$$\int_{-h}^{h}\int_{-h}^{h} f(x,y)\,\partial x\,\partial y = \int_{-h}^{h}\left[\int_{-h}^{h} f(x,y)\right]\partial y = \int_{-h}^{h} f(y)\,\partial y \qquad (A1.3)$$

$$= \frac{1}{9} h^2 \left[f_{11} + f_{-11} + f_{-1-1} + f_{1-1} + 4f_{10} + 4f_{01} + 4f_{-10} + 4f_{0-1} + 16f_{00}\right] \qquad (A1.4)$$

To evaluate the double integral concerned between the limits θ_1, θ_2 and φ_1, φ_2 the function is first calculated for all points of a two dimensional array in θ and φ then equation (A1.4) is applied in turn to each sub of 'four squares' and the results summed to give the total value of the integral. The size of the array is chosen to give the required accuracy.

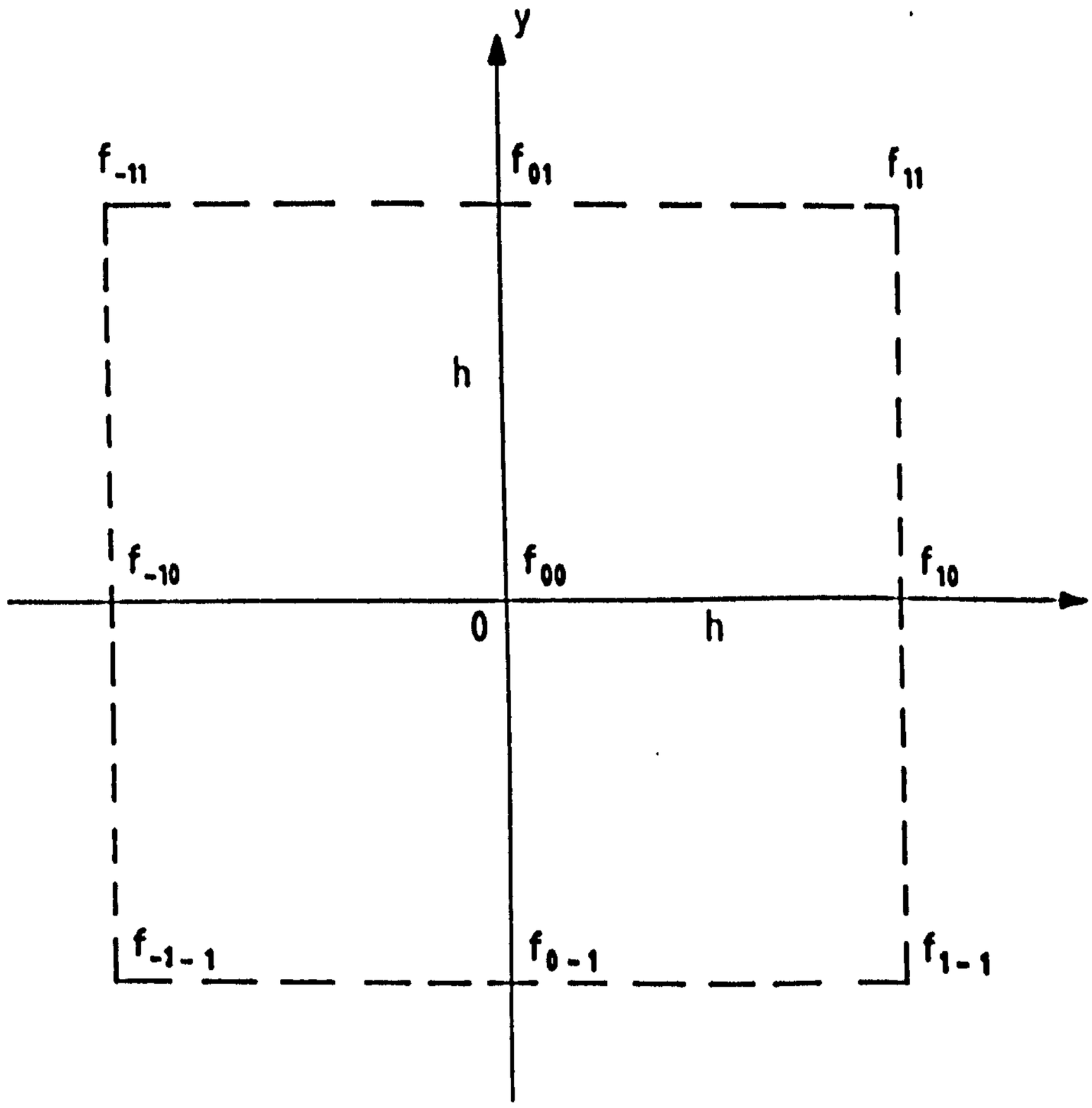

Figure a.1. Coordinates of double integral.

PROGRAM:

A computer program to calculate the radiation from microstrip feed lines and resonators.

```
C
      REAL THE,PHI,ETA,ETAR
      REAL IF,FREQ,NEW,IMAX,SFUNC(90,90)
      REAL H,K,B,L,LAMDA,FUNC
      REAL MAXA,MAXV,THEV,PHIV
C     INTEGER N,M,P,Q,SWITCH,CONT,MODE  C
      REAL NTHE,NPHI  C
      COMMON H,K,B,L,ETA,ETAR,LAMDA,NEW,PI,W
      COMMON /BLOCK/N,M,THE,PHI,SFUNC
      COMMON /IDIOT/SFUN,MODE  20   CONTINUE
      OPEN(UNIT=20,FILE='DATA1.OUT')
       N=40       M=N       WRITE(20,*)N,M
      FREQ=10
      PI=4*ATAN(1.0)
      LAMDA=0.3/FREQ
      K=2*PI/LAMDA
      ETA=2.55
      B=K*SQRT(ETA)
      ETAR=ETA
      H=1.6E-3
      W=.4E-3
C
      L=15E-3
      NEW=120*PI
C
```

```
      WRITE(5,305)
305   FORMAT(1H 'INPUT FREQ,ETA,ETAR,H,W  ?'$)
C
      READ(5,*)FREQ,ETA,ETAR,H,W
C
      H=H*1E-3
      W=W*1E-3
C     LAMDA=0.3/FREQ
      K=2*PI/LAMDA
      B=K*SQRT(ETA)
C
       WRITE(5,*)FREQ,ETA,ETAR,H,W
      WRITE(5,*)'SWITCH=1  FOR  SINGLE STRIP LAMDA/2 SECTION'
      WRITE(5,*)'SWITCH=2  FOR  SINGLE  STRIP  LAMDA  SECTION '
       WRITE(5,*)'SWITCH=3  FOR BALANCED LINE LAMDA/2 SECTION'
      WRITE(5,*)'SWITCH=4  FOR  BALANCED  LINE LAMDA   SECTION'
      WRITE(5,320)  320   FORMAT(1H ,'INPUT SWITCH ? '$)  C
      READ(5,*)SWITCH  330
      FORMAT(1H1 ,I1)
      WRITE(5,*)SWITCH  C
      WRITE(5,*)'  '
      WRITE(5,*)'INPUT MODE -1,0,1'
      READ(5,*)MODE
      WRITE(5,*)MODE
      DO 200 P=2,(N+2),1
      DO 100 Q=2,(N+2),1  C
      THE=(P-2)*PI/N
      PHI=(Q-2)*PI/N
C
```

```
      IF(SWITCH.EQ.1)CALL SUBA(THE,PHI,NTHE,NPHI,FUNC)
      IF(SWITCH.EQ.2)CALL SUBB(THE,PHI,NTHE,NPHI,FUNC)
      IF(SWITCH.EQ.3)CALL SUBC(THE,PHI,NTHE,NPHI,FUNC)
      IF(SWITCH.EQ.4)CALL  SUBD(THE,PHI,NTHE,NPHI,FUNC)
      SFUNC(P,Q)=FUNC  C
          IF(MAXV.GT.SFUN)GOTO 123
C
          MAXA=FUNC
          MAXV=SFUN
          THEV=THE
          PHIV=PHI
C
 123
          CONTINUE
C
          100   CONTINUE
          200   CONTINUE
C
          CALL SUBINT
          WRITE(5,*)MAXA,MAXV,THEV,PHIV
          CLOSE(UNIT=20,FILE='DATA1.OUT')
          WRITE(5,*)'CONTINUE (INPUT 1) ?'
          READ(5,*)CONT
          IF (CONT.EQ.1)GOTO 20
C
          STOP
          END
C
```

```
      SUBROUTINE SUBA(THE,PHI,NTHE,NPHI,FUNC)
      REAL THE,PHI,IF,FUNC,IMAX
      REAL H,K,B,L,ETA,ETAR,LAMDA
      REAL A1,B1,C1,D1,E1,PI,NEW  C
      REAL RNTHE,INTHE,RNPHI,INPHI
      REAL EX1,EX2  C
      REAL RNTHEA,RNTHEB,RNPHIA,RNPHIB
      REAL INTHEA,INTHEB,INPHIA,INPHIB
      COMMON H,K,B,L,ETA,ETAR,LAMDA,NEW,PI,W
      COMMON /IDIOT/SFUN,MODE  C
      PT=1.0
      IMAX=1.0   C
      A1=4*IMAX*SIN(K*H*SIN(THE)*SIN(PHI))*COS(PI*COS(THE)
     1/(2*SQRT(ETA)))
     1/(K*(ETA-(COS(THE)^2)))
C
        B1=4*H*IMAX*SQRT(ETA)*((ETAR-1)/ETAR)
     1*COS(THE)*COS(PI*COS(THE)/(2*SQRT(ETA)))
     1/(   (ETA-(COS(THE)^2)))
C
        INTHEA=A1*(-SIN(THE))
        INTHEB=B1*COS(THE)*SIN(PHI)
C
          INPHIA=0.0
          INPHIB=B1*COS(PHI)
C
          RNTHEA=0
         RNTHEB=0
         RNPHIA=0
```

```
      RNPHIB=0 C
      INTHE=INTHEA+INTHEB
      RNTHE=RNTHEA+RNTHEB
C
      INPHI=INPHIB+INPHIA
      RNPHI=RNPHIB+RNPHIB
C
      D1=NEW*SIN(THE)/(8*(LAMDA^2))
C
      FUNC=D1*(RNTHE^2+INTHE^2+RNPHI^2+INTHE^2)  C
      SFUN=FUNC
      WRITE(20,*)THE,PHI,FUNC
C
      WRITE(5,*)RNTHEA,RNTHEB,RNPHIB,FUNC
C
      RETURN
      STOP
      END
      SUBROUTINE SUBB(THE,PHI,NTHE,NPHI,FUNC)
      C
      REAL THE,PHI,IF,FUNC,IMAX
      REAL H,K,B,L,ETA,ETAR,LAMDA
      REAL A1,B1,C1,D1,E1,PI,NEW
C
      REAL RNTHE,INTHE,RNPHI,INPHI
      REAL EX1,EX2
C
      REAL RNTHEA,RNTHEB,RNPHIA,RNPHIB
```

```
      REAL INTHEA,INTHEB,INPHIA,INPHIB
      COMMON H,K,B,L,ETA,ETAR,LAMDA,NEW,PI,W
      COMMON /IDIOT/SFUN,MODE
C
      PT=1.0
        IMAX=1.0
        A1=-4*IMAX*SIN(K*H*SIN(THE)*SIN(PHI))
     1*SQRT(ETA)*SIN(PI*COS(THE)/SQRT(ETA))
     1/(K*(ETA-(COS(THE)^2)))
C
        B1=4*H*((ETAR-1)/ETAR)*IMAX*SQRT(ETA)
     1*SIN(PI*COS(THE)/SQRT(ETA))*COS(THE)
     1/(   (ETA-(COS(THE)^2)))
C
        RNTHEA=A1*(-SIN(THE))
C
        RNTHEB=COS(THE)*SIN(PHI)*B1
C
        RNPHIA=0.0  C
        RNPHIB=COS(THE)*B1
        INTHEA=0
        INTHEB=0
        INPHIA=0   ;   INPHIB=0
C       INTHE=INTHEA+INTHEB
        RNTHE=RNTHEA+RNTHEB
        INPHI=INPHIB
        RNPHI=RNPHIB
        D1=NEW*SIN(THE)/(8*(LAMDA^2))
        FUNC=D1*(RNTHE^2+INTHE^2+RNPHI^2+INTHE^2)
```

```
      SFUN=FUNC
C
      WRITE(20,*)THE,PHI,FUNC
C
      WRITE(5,*)RNTHEA,RNTHEB,RNPHIB,FUNC
C
      RETURN
      STOP
      END
      SUBROUTINE SUBC(THE,PHI,NTHE,NPHI,FUNC)
C
      REAL THE,PHI,IF,FUNC,IMAX
      REAL H,K,B,L,ETA,ETAR,LAMDA
      REAL A1,B1,C1,D1,E1,PI,NEW
C
      REAL RNTHE,INTHE,RNPHI,INPHI
      REAL EX1,EX2
C
      REAL RNTHEA,RNTHEB,RNPHIA,RNPHIB
      REAL INTHEA,INTHEB,INPHIA,INPHIB
      COMMON H,K,B,L,ETA,ETAR,LAMDA,NEW,PI,W
      COMMON /IDIOT/SFUN,MODE
C
        PT=1.0
        IMAX=1.0
        A1=4*IMAX*SIN(K*H*SIN(THE)*SIN(PHI))*COS(PI*COS(THE)
     1/(2*SQRT(ETA)))
     1/(K*(ETA-(COS(THE)^2)))
        IF(MODE.LT.0.0)A1=A1*2*SIN(K*W*SIN(THE)*COS(PHI))
```

```
      IF(MODE.GT.0.0)A1=A1*2*COS(K*W*SIN(THE)*COS(PHI))
C
      B1=4*H*IMAX*SQRT(ETA)*((ETAR-1)/ETAR)
     1*COS(THE)*COS(PI*COS(THE)/(2*SQRT(ETA)))
     1/(    (ETA-(COS(THE)^2)))
     IF(MODE.LT.0.0)
     B1=B1*2*SIN(K*W*SIN(THE)*COS(PHI))
     IF(MODE.GT.0.0)B1=B1*2*COS(K*W*SIN(THE)*COS(PHI))
     INTHEA=A1*(-SIN(THE))
     INTHEB=B1*COS(THE)*SIN(PHI)
     RNTHEA=0
     RNTHEB=0
     RNPHIA=0
     RNPHIB=0
      INTHE=INTHEA+INTHEB
      RNTHE=RNTHEA+RNTHEB
      INPHI=INPHIB+INPHIA
      RNPHI=RNPHIB+RNPHIB
C
      D1=NEW*SIN(THE)/(8*(LAMDA^2))
      FUNC=D1*(RNTHE^2+INTHE^2+RNPHI^2+INTHE^2)
C
       SFUN=FUNC
     WRITE(20,*)THE,PHI,FUNC
     WRITE(5,*)RNTHEA,RNTHEB,RNPHIB,FUNC
     RETURN
     STOP
     END
```

```
      SUBROUTINE SUBD(THE,PHI,NTHE,NPHI,FUNC
      REAL THE,PHI,IF,FUNC,IMAX
      REAL H,K,B,L,ETA,ETAR,LAMDA
      REAL A1,B1,C1,D1,E1,PI,NEW
C
      REAL RNTHE,INTHE,RNPHI,INPHI
      REAL EX1,EX2
C
      REAL RNTHEA,RNTHEB,RNPHIA,RNPHIB
      REAL INTHEA,INTHEB,INPHIA,INPHIB
      COMMON H,K,B,L,ETA,ETAR,LAMDA,NEW,PI,W
      COMMON /IDIOT/SFUN,MODE
C
      PT=1.0
      IMAX=1.0
      A1=-4*IMAX*SIN(K*H*SIN(THE)*SIN(PHI))
     1*SQRT(ETA)*SIN(PI*COS(THE)/SQRT(ETA))
     1/(K*(ETA-(COS(THE)^2)))
      C
      IF(MODE.LT.0.0)A1=A1*2*SIN(K*W*SIN(THE)*COS(PHI))
      IF(MODE.GT.0.0)A1=A1*2*COS(K*W*SIN(THE)*COS(PHI))
      B1=4*H*((ETAR-1)/ETAR)*IMAX*SQRT(ETA)
     1*SIN(PI*COS(THE)/SQRT(ETA))*COS(THE)
     1/(  (ETA-(COS(THE)^2)))
      IF(MODE.LT.0.0)B1=B1*2*SIN(K*W*SIN(THE)*COS(PHI))
      IF(MODE.GT.0.0)B1=B1*2*COS(K*W*SIN(THE)*COS(PHI))
      RNTHEA=A1*(-SIN(THE))
      RNTHEB=COS(THE)*SIN(PHI)*B1
      RNPHIA=0.0
```

```
RNPHIB=COS(THE)*B1
INTHEA=0
INTHEB=0
INPHIA=0
INPHIB=0
INTHE=INTHEA+INTHEB
RNTHE=RNTHEA+RNTHEB
INPHI=INPHIB
 RNPHI=RNPHIB
D1=NEW*SIN(THE)/(8*(LAMDA^2))
FUNC=D1*(RNTHE^2+INTHE^2+RNPHI^2+INTHE^2)
SFUN=FUNC
WRITE(20,*)THE,PHI,FUNC
WRITE(5,*)RNTHEA,RNTHEB,RNPHIB,FUNC
RETURN
STOP
END
SUBROUTINE SUBINT
REAL FUNC,MULT,DINT,A,SFUNC(90,90)
REAL THE,PHI
INTEGER N,M,P,Q,MODE
COMMON /BLOCK/N,M,THE,PHI,SFUNC
      A=0.0
      PI=4*ATAN(1.0)
      DO 300 P=2,(N+2),1
      DO 400 Q=2,(N+2),1
      WRITE(5,*)THE,PHI,SFUNC(P,Q)
400   CONTINUE  300  CONTINUE
      DO 500 Q=3,(N+1),2
```

```
      DO 600 P=3,(N+1),2
C     Begin
      MULT=SFUNC((P+1),(Q+1))+SFUNC((P-1),(Q+9))+SFUNC((P-1),(Q-1))
      MULT=MULT+SFUNC((P+1),(Q-1))
      MULT=MULT+4*(SFUNC((P+1),Q)+SFUNC(P,(Q+1))+SFUNC((P-1),Q)
     1+SFUNC(P,(Q-1)))    MULT=MULT+16*(SFUNC(P,Q))
        DINT=(PI^2/(9*N^2))*MULT
        A=DINT+A
        WRITE(5,*)P,Q,DINT,A
C
 600    CONTINUE
 500     CONTINUE
        WRITE(5,*)A,INT
   10   CONTINUE
        RETURN
        END
```

REFERENCES [a]

[a] Roberts J.R.,
An investigation into the application of microwave integrated circuits - Microstrip Resonators, Ph.D. thesis, U.C.N.W., Bangor, 1971 .

[b] Morton B.R.,
Numerical Approximation, Rutledge & Regan Paul, 1964, Chapters 4 & 5

APPENDIX 2.

Computation of the shielded microstrip and coupled microstrip parameters in suspended and conventional form.

These computer programs can compute effective dielectric constant, characteristic impedance, dielectric losses and conductor losses of shielded microstrip and coupled microstrip for the two different conditions of suspended or conventional substrates.

Language : Fortran IV

Authors : Mirshekar-Syahkal, D. and Davies, J.B

Description :

The method of computation is based on the spectral domain approach [a,b]. 'ZERO1' and 'ZERO2' are zero order solutions which can be used in most practical cases. The problems being solved can be seen by considering fig a.2, which shows shielded microstrip on two layers of substrate. The same situation is seen in fig a.2 for coupled microstrip. Removing the first substrate (putting h=0) gives a conventional form of the shielded microstrip, or coupled microstrip, while letting h = 0 and $\varepsilon_1=\varepsilon_0$, gives shielded suspended substrate versions of microstrip or coupled microstrip.

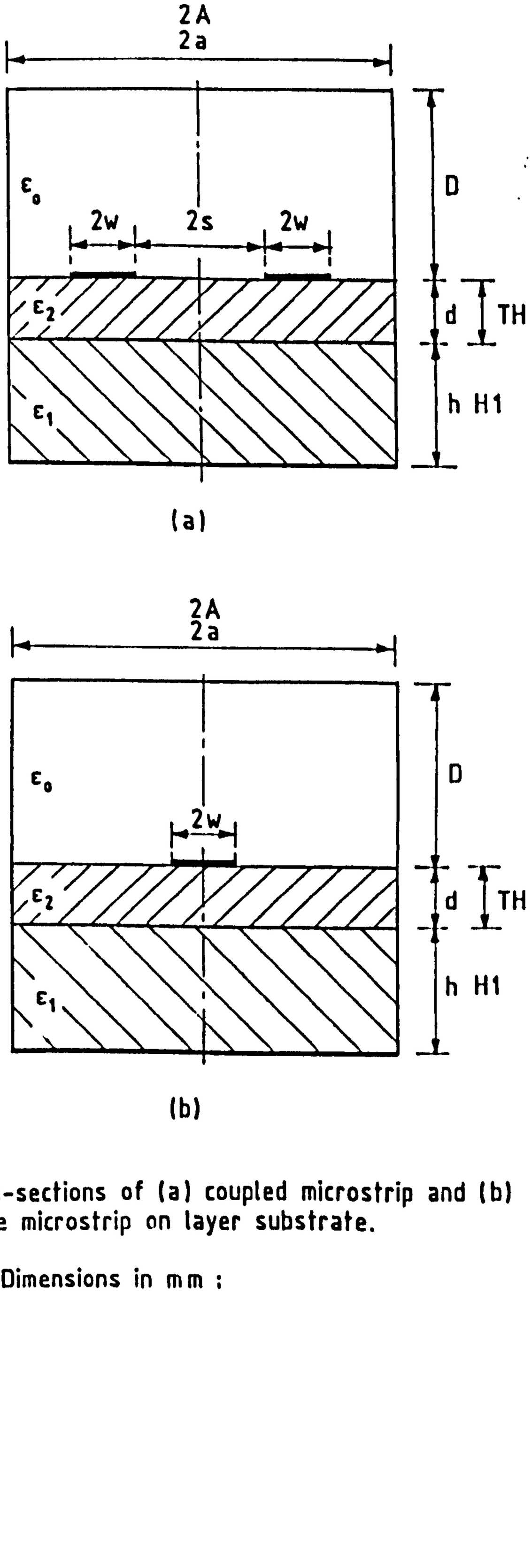

Figure a.2. Cross-sections of (a) coupled microstrip and (b) single microstrip on layer substrate.

N.B. Dimensions in mm ;

Program 'ZERO1' computes the effective dielectric constant and propagation constant of the line of interest. The method of the spectral domain gives a hybrid mode solution to these structures and hence the dispersive nature of them is properly dealt with [a,b]. 'ZERO2' computes characteristic impedance, conductor losses and dielectric losses, using a perturbation formula for low loss substrates. All the parameters are frequency dependent. By suitable choice of dimensions, an open version of the same structure can be effectively examined.

References :

a) Davies, J.B and Mirshekar-Syahkal, D.
"Spectral Domain Solution of Arbitrary Coplanar Transmission line with Multilayer Substrate", IEEE Trans. Microwave Theory Tech, Vol. MTT-25 (1977), page 143-146, feb. 1977 .

b) Itoh, T. and Mittra, R.
"A technique for computing Dispersion Characteristics of Shielded Microstrip Lines", IEEE Trans. Microwave Theory Tech., Vol MTT-22, 1974, page 896-898, Oct 1974 .

APPENDIX 3.

PUBLICATIONS.

1. Easter B., Richards O., Stephenson I.M.
Radiation from the feeder lines of Microstrip Antennas and a design approach offering a reduction; Fifth International Conference on Antennas and Propagation. ICAP 87. York